EERC
Energy & Environmental Research Center®
Putting Research into Practice

University of North Dakota
15 North 23rd Street, Stop 9018 • Grand Forks, ND 58202-9018 • P. 701.777.5000 • F. 701.777.5181
www.undeerc.org

January 29, 2016

Dr. Phil Gurney
Chief Executive Officer
Brown Coal Innovation – Australia
Level 27, 101 Collins Street
Melbourne, VIC 3000
AUSTRALIA

Dear Mr. Gurney:

Subject: Final Report Entitled "Demonstration of Pilot-Scale Hydrogen and CO_2 Separation Membrane Technology on North Dakota Coal-Derived Syngas" EERC Fund 20250

Attached please find the subject final report. If you have any questions, please contact me by phone at (701) 777-5087, by fax at (701) 777-5181, or by e-mail at jstanislowski@undeerc.org.

Sincerely,

Joshua J. Stanislowski
Principal Process Engineer
Energy Systems Development

JJS/bjr

Attachment

EERC
Energy & Environmental Research Center

DEMONSTRATION OF PILOT-SCALE HYDROGEN AND CO_2 SEPARATION MEMBRANE TECHNOLOGY ON NORTH DAKOTA COAL-DERIVED SYNGAS

Final Report

Prepared for:

Phil Gurney

Brown Coal Innovation – Australia
Level 27, 101 Collins Street
Melbourne, VIC 3000
AUSTRALIA

Fund: 20250

Prepared by:

Joshua J. Stanislowski
Scott G. Tolbert
Tyler J. Curran
Michael L. Swanson

Energy & Environmental Research Center
University of North Dakota
15 North 23rd Street, Stop 9018
Grand Forks, ND 58202-9018

2016-EERC-01-15

January 2016

UND University of North Dakota
Grand Forks

EERC DISCLAIMER

LEGAL NOTICE This research report was prepared by the Energy & Environmental Research Center (EERC), an agency of the University of North Dakota, as an account of work sponsored by the University of Wyoming, the North Dakota Industrial Commission, Dakota Gasification Company, Brown Coal Innovation of Australia, CSIRO, and the U.S. Department of Energy (DOE). Because of the research nature of the work performed, neither the EERC nor any of its employees makes any warranty, express or implied, or assumes any legal liability or responsibility for the accuracy, completeness, or usefulness of any information, apparatus, product, or process disclosed or represents that its use would not infringe privately owned rights. Reference herein to any specific commercial product, process, or service by trade name, trademark, manufacturer, or otherwise does not necessarily constitute or imply its endorsement or recommendation by the EERC.

DOE DISCLAIMER

This report was prepared as an account of work sponsored by an agency of the United States Government. Neither the United States Government, nor any agency thereof, nor any of their employees, makes any warranty, express or implied, or assumes any legal liability or responsibility for the accuracy, completeness, or usefulness of any information, apparatus, product, or process disclosed, or represents that its use would not infringe privately owned rights. Reference herein to any specific commercial product, process, or service by trade name, trademark, manufacturer, or otherwise does not necessarily constitute or imply its endorsement, recommendation, or favoring by the United States Government or any agency thereof. The views and opinions of authors expressed herein do not necessarily state or reflect those of the United States Government or any agency thereof.

NDIC DISCLAIMER

This report was prepared by the EERC pursuant to an agreement partially funded by the Industrial Commission of North Dakota, and neither the EERC nor any of its subcontractors nor the North Dakota Industrial Commission nor any person acting on behalf of either:

(A) Makes any warranty or representation, express or implied, with respect to the accuracy, completeness, or usefulness of the information contained in this report or that the use of any information, apparatus, method, or process disclosed in this report may not infringe privately owned rights; or

(B) Assumes any liabilities with respect to the use of, or for damages resulting from the use of, any information, apparatus, method, or process disclosed in this report.

Reference herein to any specific commercial product, process, or service by trade name, trademark, manufacturer, or otherwise does not necessarily constitute or imply its endorsement, recommendation, or favoring by the North Dakota Industrial Commission. The views and opinions of authors expressed herein do not necessarily state or reflect those of the North Dakota Industrial Commission.

DEMONSTRATION OF PILOT-SCALE HYDROGEN AND CO_2 SEPARATION MEMBRANE TECHNOLOGY ON NORTH DAKOTA COAL-DERIVED SYNGAS

PROJECT SUMMARY

The work at the Energy & Environmental Research Center (EERC) focused on the testing of Praxair's hydrogen separation membrane for purifying hydrogen from coal-derived syngas. Praxair provided a pilot-scale membrane that was tested on syngas produced in the EERC's pilot-scale transport reactor development unit. The goal of the project was to conduct a pilot-scale demonstration of coal-to-hydrogen production technology using warm-gas cleanup techniques and Praxair's hydrogen separation membrane. In addition to a Powder River Basin coal, high-sodium Freedom lignite from North Dakota was also tested on the unit, and it was found that the fuel could be fired successfully with the addition of kaolin as a sodium-gettering agent.

Hydrogen concentrations leaving the gasifier were as high as 15% and were further increased to 20% on a dry basis after the water–gas shift reactor. It was determined that operation of the sour shift catalyst near 400°C provided the highest level of shift, and CO was able to be reduced below 1%. Regenerable RVS-1 sulfur sorbent was shown to be able to reduce sulfur concentrations from nearly 4000 to below 5 ppm in one reactor. A hot-side syngas compressor was successfully demonstrated to raise the pressure of the syngas from 120 to over 450 psi while maintaining the temperature above 450°F.

The membrane was operated on syngas over two separate test campaigns. As expected, the membrane flux was maximized when the highest partial pressure of hydrogen was delivered to the system at high-flow conditions and 425°C. Membrane performance did not appear to signficantly change with time during the campaigns. A modeling effort showed that hydrogen membranes have the potential to improve the efficiency of a 550-MW power plant with carbon capture from 31.7% to 35.7% when using Selexol as a base case for CO_2 capture. Additional optimization of the membrane technology is needed to achieve these goals.

TABLE OF CONTENTS

Continued. . .

TABLE OF CONTENTS (continued)

LIST OF FIGURES

Continued. . .

LIST OF FIGURES (continued)

Continued. . .

LIST OF FIGURES (continued)

LIST OF TABLES

Continued. . .

LIST OF TABLES (continued)

NOMENCLATURE

AGFC	advanced gasification fuel cell
AHT	advanced high temperature
ASU	air separation unit
bby	billion barrels per year
bcc	body-centered cubic
BTX	benzene, toluene, and xylene
CEM	continuous emission monitor
CF	capacity factor
CGEs	cold-gas efficiencies
COE	cost of electricity
DOE	U.S. Department of Energy
EERC	Energy & Environmental Research Center
fcc	face-centered cubic
FMEA	failure modes and effects analysis
GC	gas chromatograph
HAZOP	hazardous operations
HGFV	hot-gas filter vessel
HHV	higher heating value
HRSG	heat recovery steam generator
HT	high temperature
i.d.	inner diameter
ICEV	internal combustion engine vehicle
IGCC	integrated gasification combined-cycle
IGFC	integrated gasification fuel cell
ITM	ion transport membrane
Kn	Knudsen number
LGA	laser gas analyzer
MAF	moisture- and ash-free
MF	moisture-free
NETL	National Energy Technology Laboratory
NGCC	natural gas combined cycle
o.d.	outer diameter
P&ID	piping and instrumentation diagram
pc	pulverized coal
PHEV	plug-in hybrid electric vehicle
PRB	Powder River Basin
PSA	pressure swing adsorption
SOP	standard operating procedure
TGTU	Tail gas treatment unit
TPC	total plant cost
TRDU	transport reactor development unit
TRIG	transport reactor integrated gasification
UND	University of North Dakota
WGCU	warm-gas cleanup
WGS	water–gas shift
XRFA	x-ray fluorescence analysis

DEMONSTRATION OF PILOT-SCALE HYDROGEN AND CO_2 SEPARATION MEMBRANE TECHNOLOGY ON NORTH DAKOTA COAL-DERIVED SYNGAS

INTRODUCTION

In order to facilitate the use of hydrogen in integrated gasification combined-cycle (IGCC) applications or as a transportation fuel, hydrogen-from-coal technologies that are capable of managing carbon will be needed. Many technologies are under development for the separation of hydrogen from coal-derived syngas, and among the most promising are hydrogen separation membranes. Studies indicate a significant IGCC plant efficiency increase can be realized if warm-gas cleanup and hydrogen separation membranes are used in the place of conventional technologies. These membranes provide the potential to produce hydrogen while simultaneously separating carbon dioxide at system pressure. Membrane development activities need to take into account the impact of coal-derived impurities. Gasification syngas typically has many impurities that, if not removed, will poison most hydrogen separation materials. In order to commercialize this promising technology, scale-up to bench- and pilot-scale gasifiers is required so that the impact of impurities can be evaluated.

The work at the Energy & Environmental Research Center (EERC) focused on the testing of Praxair's hydrogen separation membrane for purifying hydrogen from coal-derived syngas. Praxair provided a pilot-scale membrane that was tested on syngas produced in the EERC's pilot-scale transport reactor development unit (TRDU). The goal of the project was to conduct a pilot-scale demonstration of coal-to-hydrogen production technology using warm-gas cleanup techniques and Praxair's hydrogen separation membrane. Four separate tasks were performed to enable the demonstration of the technology. Tasks 1 and 2 consisted of membrane acquisition and installation and making modifications to the TRDU and warm-gas cleanup systems to facilitate the test runs. The testing occurred in Task 3, and the data derived were used to support Praxair's efforts in developing a techno-economic analysis and a modeling effort performed by the EERC in Task 4 of the project.

OBJECTIVES

The overall goal of the project was to demonstrate the performance of Praxair's pilot-scale hydrogen separation membrane on coal-derived syngas and provide data for scale-up to demonstration scale. Specific project objectives consisted of the following:

- Setup and installation of the membrane modules on the EERC's TRDU.
- Setup and installation of a warm-gas cleanup train for the TRDU.
- Production of a stream of syngas from the TRDU using Wyoming coal and suitable for application to hydrogen separation membrane technology.

- Performance of up to 400 hours of testing of the hydrogen separation membranes using coal-derived syngas to determine optimum performance conditions.

- A final report detailing the results of the gasification test issued to the project sponsors.

TECHNICAL INFORMATION

Five main types of membranes are currently under development: dense polymer, microporous ceramic, porous carbon, dense metallic, and dense ceramic (1). Of these types, dense metallic and dense ceramic have the highest hydrogen selectivity. Dense metallic membranes also have very high hydrogen flux rates, making them potential candidates for large-scale commercial application if poisoning issues can be overcome. Palladium is the typical base metal for metallic membranes, and alloy combinations such as Pd–Cu, Pd–Au, and Pd–Ag have been tested. Many other formulations exist, but most are closely guarded trade secrets.

Two main applications for hydrogen separation membranes employed at large scale are envisioned. Large-scale hydrogen production facilities could provide fuel for fuel cell vehicles. Power generation facilities with CO_2 capture could employ hydrogen separation membranes to reduce the cost of separation. Both scenarios are likely to employ coal gasification to produce the hydrogen.

Membranes for Hydrogen Production for Transportation Applications

The U.S. Department of Energy (DOE) views hydrogen as an energy carrier of the future because it can be derived from domestic resources that are clean and abundant and because hydrogen is an inherently clean fuel. According to DOE, the deployment of hydrogen technologies could lead to the creation of 675,000 green jobs in the United States (2). Coal gasification plants can separate hydrogen from the synthesis gas, purify the carbon for storage, and burn the hydrogen to produce power in an IGCC configuration. In this type of configuration, the only major emission from the plant is water. Hydrogen can also play a key role as a transportation fuel. If all vehicles in Los Angeles were converted to hydrogen, the urban smog problems would be virtually eliminated. Hydrogen fuel cell technologies have undergone rapid development over the past decade, and the technology exists today to produce commercial hydrogen fuel cell vehicles that have a transportation range of up to 280 miles (3). The main challenges that remain today are the economical production of hydrogen; the economical production of fuel cell vehicles; and the development of hydrogen transportation, storage, and dispensing infrastructure.

The National Hydrogen Association views hydrogen as the best pathway to both reduce oil consumption in the United States and reduce transportation-based CO_2 emissions. Figure 1 compares three different vehicle market penetration scenarios for light-duty vehicles (4). The bar on the left represents 100% gasoline internal combustion engines, the middle bar represents market penetration for plug-in hybrid electric vehicles, and the bar on the right represents hydrogen fuel cell vehicles. Each scenario is compared to the annual oil consumption for that time period. It can

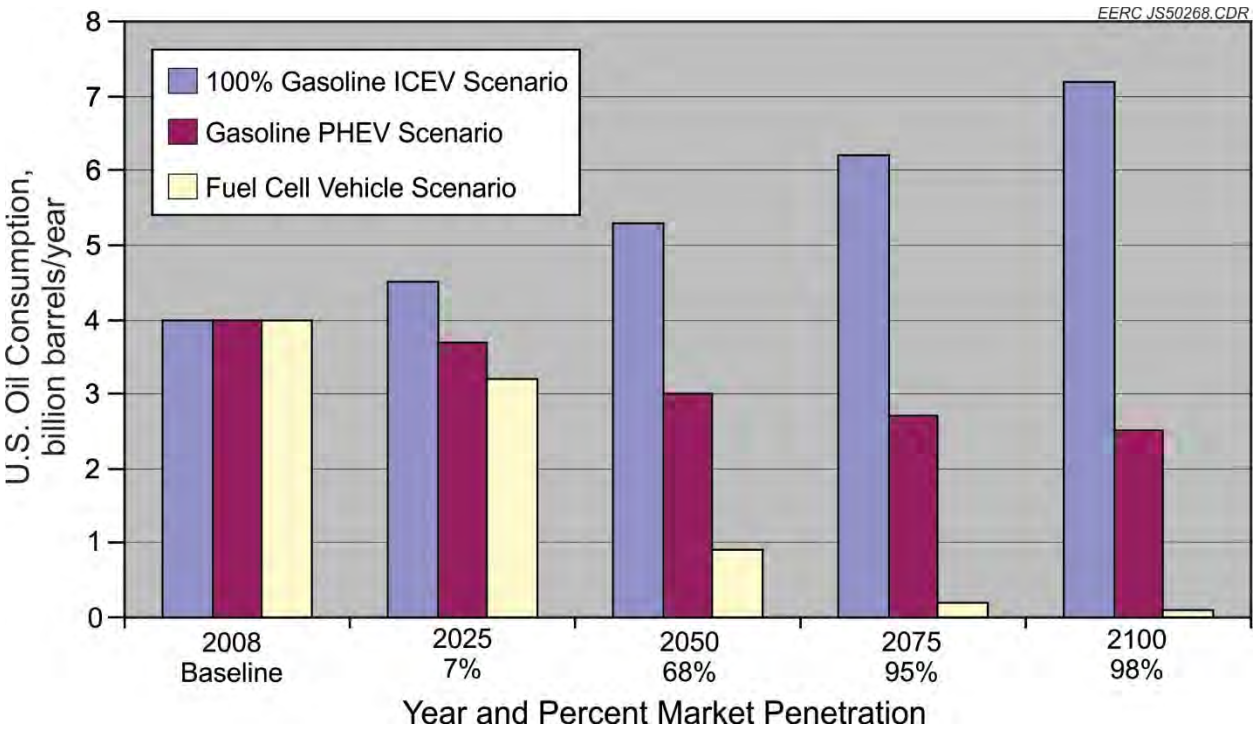

Figure 1. U.S. oil consumption for various vehicle scenarios (4) (ICEV is internal combustion engine vehicle, and PHEV is plug-in hybrid electric vehicle).

be seen that if nothing changes and the United States continues to rely solely on gasoline-powered vehicles, the annual oil consumption is predicted to increase from 4 billion barrels per year (bby) to over 7 bby by the year 2100. With a significant market penetration of plug-in hybrid vehicles, oil consumption can be reduced to about 2.5 bby by 2100. However, with 98% market penetration of fuel cell vehicles, dependence on oil is virtually eliminated. While the future of transportation will certainly be a mix of several technologies, this graph illustrates that hydrogen is one of the only pathways toward eliminating the use of oil.

Figure 2 shows a similar set of scenarios but compares the market penetration with annual CO_2 emissions from vehicles (4). It should be noted that the study assumes hydrogen production is occurring with carbon capture and storage or hydrogen is supplied from a renewable source. The graph shows that CO_2 emissions from vehicles will almost double by the year 2100 if gasoline vehicles are continued to be used exclusively. A reduction in CO_2 emissions is achieved if the course of plug-in hybrid vehicles is followed. However, with the fuel cell vehicle scenario, CO_2 emissions are reduced by over 80% in the year 2100. This illustrates that hydrogen is a potential fuel pathway in a carbon-constrained world. Increased production of natural gas and coal will be needed to meet these targets, and the data assume that the hydrogen production facility is equipped with carbon capture technology.

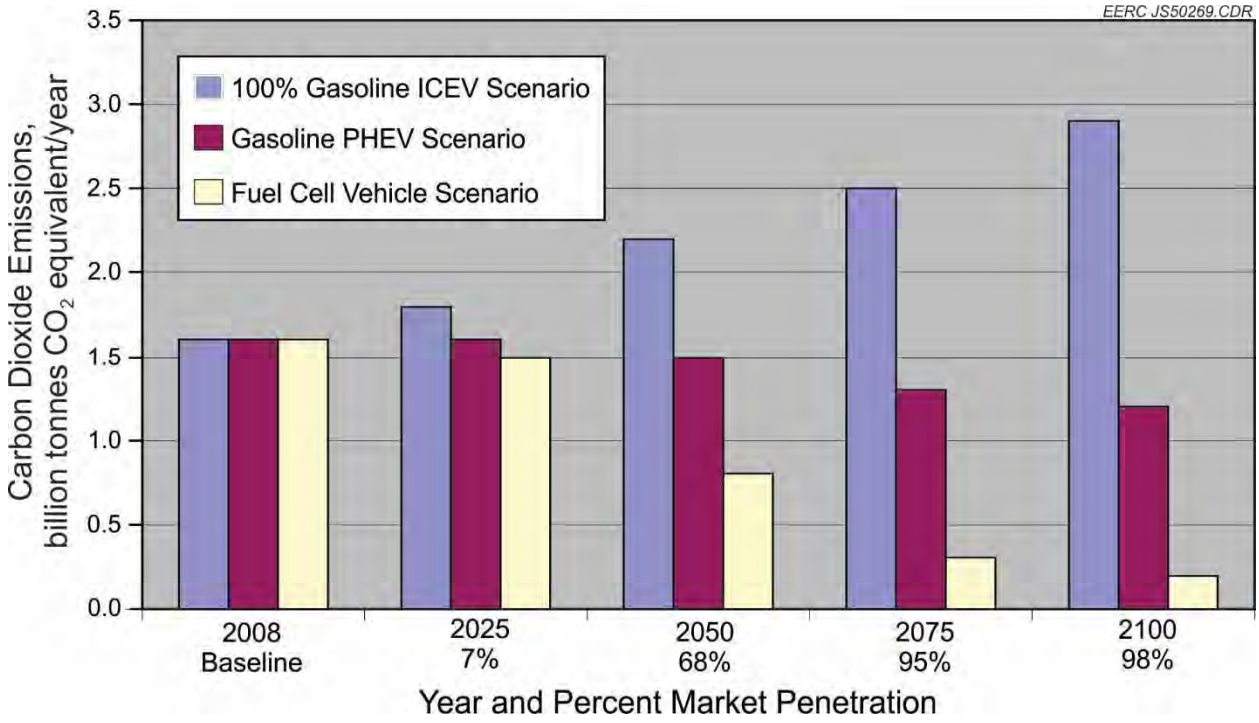

Figure 2. CO_2 emissions for various vehicle scenarios (4).

Membranes Integrated with Power Systems

Coal gasification is of significant interest to the future of power generation in the United States because it can be performed more efficiently and with fewer emissions than conventional combustion. IGCC systems fire the syngas produced directly in a gas turbine and recover the heat produced, resulting in more efficient conversion of energy to electricity than a conventional steam cycle. Currently, gasification systems produce electricity at a higher cost than conventional combustion systems. One significant advantage of gasification over combustion is the ability to capture CO_2 at a much lower cost and energy penalty. The CO_2 in gasifier syngas streams is at much higher concentration and typically at elevated pressure; therefore, less energy is required to perform the separation. When the cost of CO_2 capture is considered in the overall capital and operating cost of a power system, gasification units can have advantages in the cost of electricity over conventional combustion. Figure 3 compares the cost of electricity for gasification versus conventional power systems with and without CO_2 capture (5). The figure shows that for conventional power systems, the cost of electricity is significantly less if CO_2 capture is not required. In the cases where CO_2 capture is needed, the IGCC plant produces electricity at a lower cost than the pulverized coal (pc) systems. The cost of natural gas combined cycle (NGCC) is heavily dependent on the price of natural gas. With recent natural gas prices as low as $2/MMBtu, the current cost of NGCC is significantly lower than competing technologies.

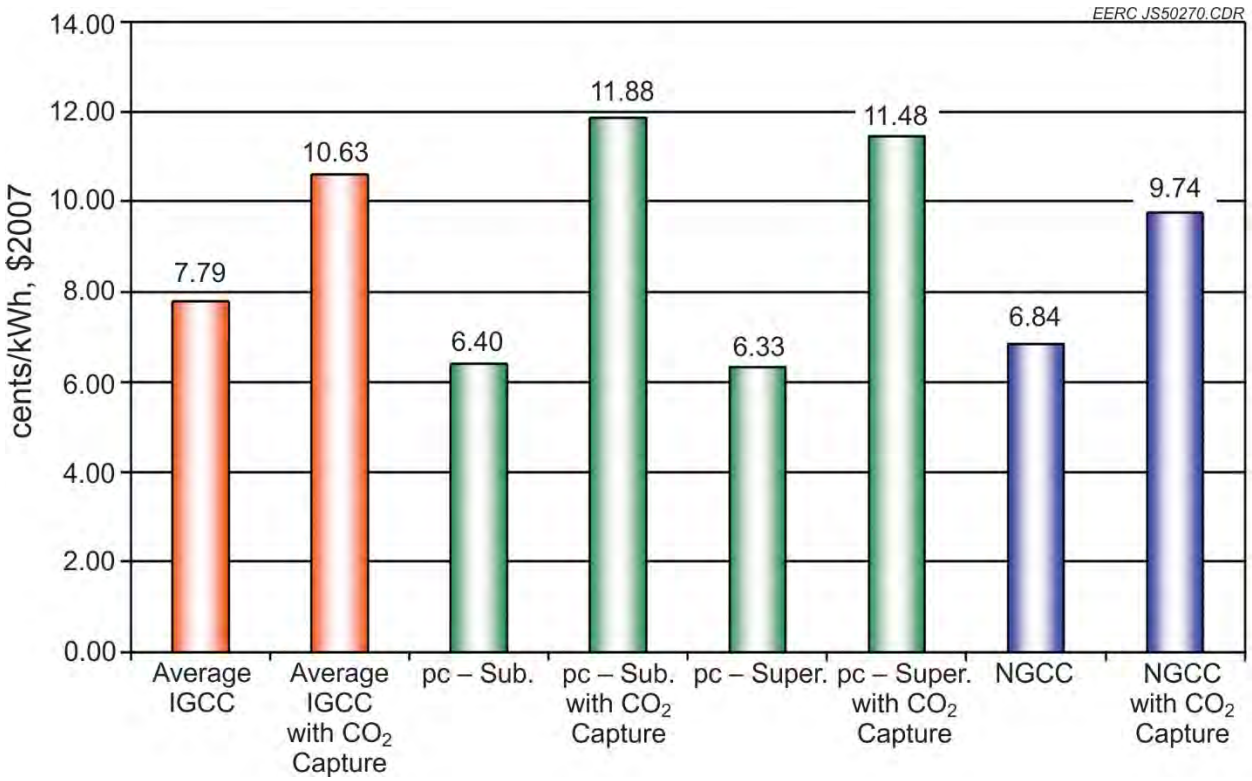

Figure 3. Comparison of the cost of electricity for gasification vs. conventional systems with and without CO_2 capture (5).

The cost of gasification with CO_2 capture utilizing technologies that are commercially available today is still relatively high compared to the cost of electricity production with no capture. Advanced technologies are needed to further reduce the costs of capture and improve the overall efficiency of the plants. Several critical research pathways and technologies have been identified by DOE's National Energy Technology Laboratory (NETL) that will greatly improve the efficiency of gasification-based power systems. Figure 4 depicts the technology advancements and the incremental increase in net plant efficiency if each technology is implemented (6). The figure indicates that the technology with the highest potential for reducing the cost of gasification systems is hydrogen and CO_2 separation using hydrogen selective membranes. According to NETL, the implementation of membrane technology can result in a nearly 3% efficiency point increase for a gasification system over using a conventional Selexol™ process. If all of the advanced pathway technologies are realized, the efficiency of an IGCC system with hydrogen separation membrane technology and CO_2 capture and compression could reach 40%. Advanced gasification fuel cell (AGFC) technologies could push the efficiency over 50%.

FERC JS50271.CDR

Case Title	Efficiency (% HHV)	Delta* Efficiency (% points)	TPC** (S/kW)	Delta* TPC** ($/kW)	20-yr Leveraged COE (¢/kWh)	Delta* COE (¢/kWh)
Reference IGCC	30.4	0	2718	0	11.48	0
Adv. "F" Turbine	31.7	1.3	2472	-246	10.64	-0.84
Coal Feed Pump	32.5	0.8	2465	-7	10.54	-0.10
85% CF	32.5	0.0	2465	0	10.14	-0.40
WGCU/Selexol	33.3	0.8	2425	-40	10.00	-0.14
WGCU/H_2 Membrane	36.2	2.9	2047	-378	8.80	-1.20
AHT-1 Turbine	38.0	1.8	1855	-192	8.14	-0.66
ITM	38.3	0.3	1724	-131	7.74	-0.40
AHT-2 Turbine	40.0	1.7	1683	-41	7.61	-0.13
90% CF	40.0	0.0	1683	0	7.36	-0.25
IGCC Pathway		+9.6% pts (+32%)		-1035 (-38%)		-4.12 (-36%)
Advanced IGFC	56.3	+26% pts +85%	1759	-959 (-35%)	7.45	-4.03 (-35%)

* Delta shown is the incremental change as each new technology is added to previous case configuration.
** TPC is reported in January 2007 dollars and excludes owner's costs.

Figure 4. Advanced gasification pathways toward improving efficiency and reducing the cost of electricity for IGCC systems (6) TPC is total plant cost, COE is cost of electricity, CF is capacity factor, WGCU is warm-gas cleanup, AHT is advanced high temperature, ITM is ion transport membrane, and IGFC is integrated gasification fuel cell.

Coal Gasification Fundamentals

Coal gasification is a process in which coal is reacted with steam and oxygen at temperature and pressure to form H_2 and carbon monoxide. Pressures can range from atmospheric pressure to 1200 psi, and temperatures can range from about 1200° to over 2900°F. Besides the typically desired products, H_2 and CO, many other by-products are formed during gasification such as CO_2, CH_4, H_2S, COS, HCl, NH_3, higher hydrocarbons, tars and oils, and particulate matter. The biggest challenge with any gasification system is dealing with the inorganic components in the coal and matching gasifier design to fuel-specific properties and desired end products. Gasifiers are typically configured as fixed beds, fluidized beds, moving beds, or entrained flow. Each gasifier type has strengths and weaknesses depending on the fuel used and the desired end products.

Entrained-flow gasifiers operate at very high temperatures and pressures, usually exceeding 2700°F and 600 psig. Systems are either upfired or downfired, and the gasifier operates like a plug flow reactor, with the pulverized solids entrained in the gas stream. Residence times are on the order of seconds. The main advantage of entrained-flow gasifiers is that the high temperature results in the destruction of heavy organic materials, light aromatics, and hydrocarbons, including

methane. Carbon conversions of low-reactivity high-rank coals and petroleum coke can exceed 99%, and most entrained-flow gasifiers are designed for high-rank fuels. The inorganic components are melted in the high-temperature environment and flow out of the gasifier as liquid slag. The elevated temperature results in lower cold-gas efficiencies (CGEs) with entrained-flow gasifiers, and most gasifiers average near 80% CGE. Entrained-flow gasifiers are commercially available today and are backed by large companies such as Shell, GE, Siemens, and CB&I.

Fluid-bed gasifiers operate with a fluidized bed of unconverted carbon and inorganic particles, typically sized to approximately 0.075 in. Solids residence times are typically 0.5 to 2 minutes. The temperature of the system is kept below the ash-melting point, usually below 1600°F, and the systems typically operate at elevated pressure. These systems are well suited for high-reactivity, low-rank fuels. Fluid beds can produce high levels of tars and organic materials and can achieve CGEs of 90% and carbon conversions over 95%. Commercial systems include the High-Temperature Winkler offered by ThyssenKrupp and the U-Gas technology developed by the Gas Technology Institute and licensed to Synthesis Energy Systems.

Fixed-bed gasifiers operate with a bed of larger coal particles, ranging from 0.5 to 2 in. in size. Both slagging and nonslagging fixed beds have been developed. Depending on the operating conditions, fixed beds can produce high levels of tars, organics, and methane. The low temperature and relatively simple operation of nonslagging systems can lead to high CGEs and low-cost operation. The Lurgi gasifier offered by Air Liquide is currently deployed commercially at Sasol in South Africa and the Great Plains Synfuels Plant in North Dakota.

For the purposes of this test program, syngas was produced from a small pilot-scale entrained-flow gasifier and fluid-bed gasifier. These systems were chosen because they are commercially available and tend to produce less methane than fixed-bed gasifiers. While methane is not expected to harm membrane materials, elevated levels in syngas reduce the overall capture efficiency of an IGCC facility.

Coal gasification had taken on a renewed interest in recent years because of the rising price of oil and pending carbon legislation. Falling natural gas and oil prices over the last 2 years have made recent deployment and financing of gasification technologies more difficult. Historically, studies have shown that if carbon capture and storage are required, IGCC plants will have a significant cost advantage over conventional pc boilers with retrofit carbon capture (7, 8). However, the most recent studies have stated that the costs may be similar between the two technologies, especially when considering ultrasupercritical boilers (9–11). At this point, it is difficult to accurately estimate the cost of carbon capture from a pc power plant because no commercially available technology exists. Therefore, these studies must be reevaluated once technologies are commercially available.

Gas Cleanup Fundamentals

Conventionally, cold-gas cleanup methods have been employed to remove contaminants from coal gasification syngas streams. Methods such as Rectisol® or Selexol are commercially available and do a very good job removing contaminants but are also very costly from a capital and operational perspective. Significant economic benefits can be realized by utilizing warm- or

hot-gas-cleaning techniques. DOE has stated thermal efficiency increases of 8% over conventional techniques can be realized by integrating warm-gas cleanup technologies into IGCC plants (7). Hydrogen separation membranes typically operate at warm-gas cleanup temperatures, so they are a good match for IGCC projects looking to employ warm-gas cleanup and carbon capture.

Work has been performed at the EERC in conjunction with DOE to develop methods to remove contaminants from syngas to levels suitable for a hydrogen separation membrane. The warm-gas cleanup train is capable of removing sulfur, particulate, chlorine, and trace metals including mercury at temperatures above 400°F. All of the technologies utilized are considered either commercial or near-commercial in development. One such test involved gasification of Texas lignite in the EERC's TRDU, with a slipstream of gas being sent to the warm-gas cleanup train (12). Figure 5 shows the test setup and a sampling of the results from the test.

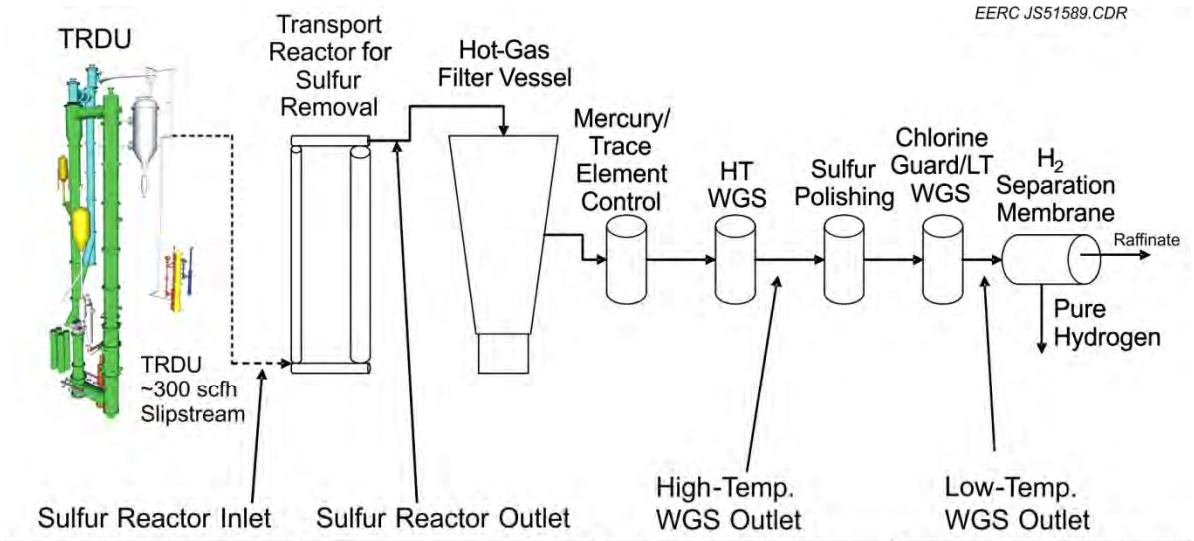

Component	Concentration	Unit
H_2	8.3	%
CO	4.8	%
CO_2	15.0	%
N_2	69.1	%
CH_4	1.7	%
H_2S	3455	ppm
H_2/CO	1.7	ratio

Component	Concentration	Unit
H_2	7.7	%
CO	4.4	%
CO_2	133.8	%
N_2	72.3	%
CH_4	1.5	%
H_2S	4.4	ppm
H_2/CO	1.8	ratio

Component	Concentration	Unit
H_2	10.9	%
CO	1.0	%
CO_2	16.7	%
N_2	68.6	%
CH_4	1.5	%
H_2S	3.0	ppm
H_2/CO	11.0	ratio

Component	Concentration	Unit
H_2	13.3	%
CO	0.1	%
CO_2	18.4	%
N_2	65.5	%
CH_4	1.6	%
H_2S	0	ppm
H_2/CO	98.3	ratio

Figure 5. Gasification and gas cleanup process diagram with test results (12). HT WGS is high-temperature water–gas shift.

Sulfur in the form of hydrogen sulfide and carbonyl sulfide was removed in a transport-style gas–solid contactor at temperatures between 600° and 1000°F. The system was capable of reducing sulfur to single-digit ppm levels in the syngas. Particulate was removed in a hot-gas filter vessel (HGFV) that provided near-absolute filtration using candle filters. Mercury and trace elements were removed with a proprietary sorbent. A high-temperature WGS catalyst significantly increased the hydrogen concentration in the gas stream, while reducing CO. A sulfur-polishing bed removed hydrogen sulfide to concentrations below 0.2 ppm. A chlorine guard bed was used

in front of the low-temperature WGS catalyst to prevent poisoning. CO was reduced to 0.1% in a low-temperature shift bed, and hydrogen was maximized. If the system were run under oxygen-fired conditions, the resulting syngas would have had combined H_2 and CO_2 levels greater than 90%. After passing through the cleanup train, the syngas was ready for hydrogen and CO_2 separation in a hydrogen separation membrane.

Conventional Hydrogen Separation Processes

The most commonly employed method used today for hydrogen separation is a process called pressure swing adsorption (PSA). PSA technology is based on an adsorbent bed that captures the impurities in the syngas stream at higher pressure and then releases the impurities at low pressure. Multiple beds are utilized simultaneously so that a continuous stream of hydrogen may be produced. This technology can produce hydrogen with purity greater than 99.9% (13). Temperature swing adsorption is a variation on PSA, but is not widely used because of the relatively long time it takes to heat and cool sorbents. Electrical swing adsorption has been proposed as well but is currently in the development stage. Cryogenic processes also exist to purify hydrogen but require extremely low temperatures and are, therefore, very expensive (14).

Principles of Hydrogen Separation Membranes

Most hydrogen separation membranes operate on the principle that hydrogen selectively penetrates through the membrane because of the inherent properties of the material. The mechanism for hydrogen penetration through the membrane depends on the type of membrane in question. Most membranes rely on the partial pressure of hydrogen in the feed stream as the driving force for permeation, which is balanced with the partial pressure of hydrogen in the permeate stream. Kluiters has categorized membranes into five main types that are commercial or appear to have commercial promise: dense polymer, microporous ceramic, porous carbon, dense metallic, and dense ceramic (1). Each membrane type has advantages and disadvantages, and research organizations and companies continue to work to develop better versions of each (15). Figure 6 illustrates the basic operating principles of hydrogen separation membranes for use in coal-derived syngas (12). This figure shows a dense metallic tubular membrane, but plate-and-frame-style membranes have also been developed. The “syngas in” stream refers to the feed gas into the membrane module. The permeate stream has permeated through the membrane wall and, in this case, is made up of mostly hydrogen. The raffinate stream is what is left of the feed stream once the permeate is separated. A sweep gas such as nitrogen may be used on the permeate side to lower the partial pressure of hydrogen and enable more hydrogen to permeate the membrane.

The mechanisms for hydrogen transport through each membrane type are different. However, the performance of each membrane is gauged by two main principles: hydrogen selectivity and hydrogen flux. Hydrogen selectivity is defined by Equation 1 (1):

$$\alpha_{A/B} = \frac{y_A / y_B}{x_A / x_B} \qquad \text{[Eq. 1]}$$

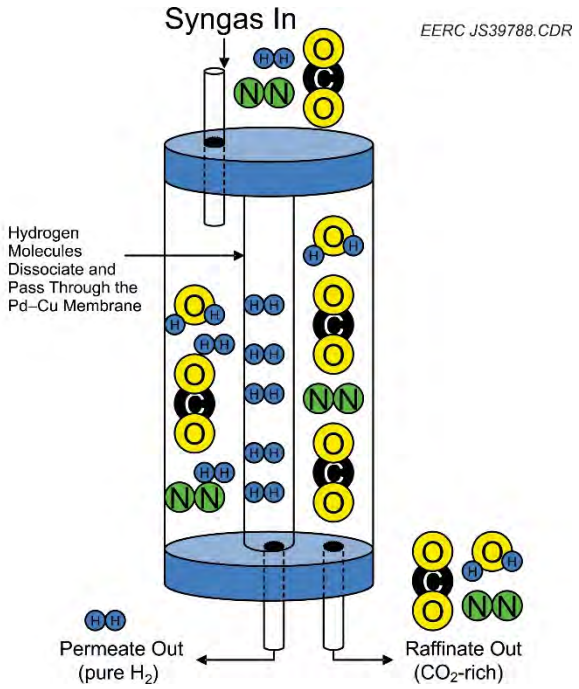

Figure 6. Illustration of the operating principle of hydrogen separation membranes (12).

where α is the selectivity factor of component A over component B in the mixture, y_A and y_B are the fractions of those components in the permeate, and x_A and x_B are the fractions of those components in the feed. Components A and B are usually defined so that a higher selectivity factor refers to better membrane performance. A selectivity factor of 1 means there is no component separation.

Hydrogen flux is a measure of the rate of permeation of hydrogen through a membrane wall. The general equation for flux is shown by Equation 2 (1, 14):

$$J_x = \frac{P(p^n_{x,\,feed} - p^n_{x,\,permeate})}{t} \qquad \text{[Eq. 2]}$$

where J_x represents the flux of species x, P_x represents the permeability of species x, $p_{x,feed}$ and $p_{x,permeate}$ are the partial pressures of species x in the feed and permeate streams, t is the membrane thickness, and n is the partial pressure exponent. The value of n is usually between 0.5 and 2 and, like the value of P, depends on the transport mechanism assumed. When n = 1, the equation is called Fick's law. For hydrogen transport through a metal membrane, the value of n is usually 0.5, and the equation reduces to what is referred to as Sievert's law. Sievert's law is a useful way of measuring membrane performance because it takes into account the membrane thickness and the partial pressure of hydrogen on each side of the membrane.

Since most membranes operate on a partial pressure differential, there will always be some hydrogen left behind in the raffinate stream. Therefore, an additional measurement of performance is the recovery or yield, as shown by Equation 3 (1):

$$S = \frac{q_p}{q_f} \qquad \text{[Eq. 3]}$$

where S is the yield, q_p is the permeate flow, and q_f is the feed flow. There are numerous other ways to quantify the yield, including calculating the volume reduction in the raffinate or the percentage hydrogen recovery from the feed.

The five basic types of membranes mentioned earlier each have inherent advantages and disadvantages, depending on the desired operating conditions and necessary product specifications. With data presented by Kluiters (1) and modified with Adhikari and Fernando (14) and Ockwig and Nenoff (16), Table 1 compares, in general, the relative operational performance of these five membrane types. Typical operational temperature will vary by specific membrane type, but it can be seen that the dense polymer membranes are only applicable at low temperature. Dense ceramic and dense metallic membranes have the highest hydrogen selectivity, and hydrogen flux is highest with dense metallic or microporous ceramic membranes. While dense metallic membranes seem to have the best performance relative to hydrogen, they are also very susceptible to poisoning from many compounds found in syngas, and metal alloys can be very expensive. Dense ceramic membranes also have high potential for commercial applications. They are less susceptible to poisoning than metallic membranes and, depending on the material, can be significantly less inexpensive. Development work is under way with each of these membrane types to increase the resistance to poisoning and reduce cost.

Table 1. Properties of Five Hydrogen-Selective Membranes (1, 14, 16)

	Dense Polymer	Microporous Ceramic	Dense Ceramic	Porous Carbon	Dense Metallic
Temperature Range	<100°C	200°–600°C	600°–900°C	500°–900°C	300°–600°C
H_2 Selectivity	Low	Moderate	Very high	Low	Very high
H_2 Flux	Low	High	Moderate	Moderate	High
Known Poisoning Issues	HCl, SO_x, CO_2		H_2S	Organics	H_2S, HCl, CO
Example Materials	Polymers	Silica, alumina, zirconia, titania, zeolites	$SrCeO_{3-\delta}$, $BaCeO_{3-\delta}$	Carbon	Palladium Alloys, Pd–Cu, Pd–Au
Transport Mechanism	Solution/ diffusion	Molecular sieving	Solution/ diffusion	Surface diffusion, molecular sieving	Solution/ diffusion

Hydrogen Transport Mechanisms

For porous membranes, four types of diffusion mechanisms can effect hydrogen separation: Knudsen diffusion, surface diffusion, capillary condensation, and molecular sieving. Knudsen diffusion occurs when the Knudsen number, Kn defined by Equation 4, is large (16):

$$Kn = \frac{\lambda}{L} \qquad \text{[Eq. 4]}$$

where λ represents the mean free path of the gas molecules and L is the pore radius. At Knudsen numbers larger than 10, Knudsen diffusion becomes significant. Surface diffusion refers to gas molecules that are absorbed on the pore wall and migrate along the surface to the other side. Surface and Knudsen diffusion can occur simultaneously. Capillary condensation occurs if a partially condensed phase fills the pores and does not let other molecules penetrate. Molecular sieving occurs when the pores are so small that only the smaller molecules can fit through. Selectivity toward hydrogen is greatest with molecular sieving and is least with the Knudsen diffusion mechanism (1, 16).

This work focuses on palladium-based dense metallic membranes, which rely on a solution/diffusion mechanism to transport hydrogen. The solution/diffusion mechanism is somewhat more complex than the porous diffusion mechanisms, although relatively straightforward in nature. Ockwig and Nenoff (16) have presented a seven-step mechanism in which 1) the hydrogen mixture moves to the surface of the membrane, 2) dissociation of the H_2 molecules into H^+ ions and electrons, 3) adsorption of the ions into the membrane bulk, 4) diffusion of the H^+ ions through the membrane, 5) desorption of the H^+ ions from the membrane, 6) recombination of the H^+ ions and electrons back to H_2 molecules, and 7) diffusion of the H_2 from the surface of the membrane. In the case of metal membranes, only hydrogen undergoes the solution/diffusion mechanism; therefore, the membranes are considered 100% selective to hydrogen.

Figure 7 illustrates the mechanism of separation in a 7-step process that depicts hydrogen transport through dense metallic membranes as atoms. The mechanism is very similar to that proposed by Ockwig and Nenoff in the case of ion transport membranes. Key points for the mechanism of separation are the catalytic dissociation of hydrogen on the membrane surface and absorption of H atoms into the alloy structure. Both of these key steps can be hindered by the presence of sulfur on the surface of the membrane, reducing the overall flux rate. Sulfur could also be present on the reassociation side of the membrane if a significant leak in the material were ever present during operations. Diffusion of the hydrogen away from the surface is also an important point because under normal operating conditions, the gas is pure hydrogen; therefore, the partial pressure of hydrogen can be high. In IGCC cases, a sweep gas of nitrogen would be employed to improve the overall efficiency of the separation, temper the combustion flame in the gas turbine, and provide additional mass to drive the turbine.

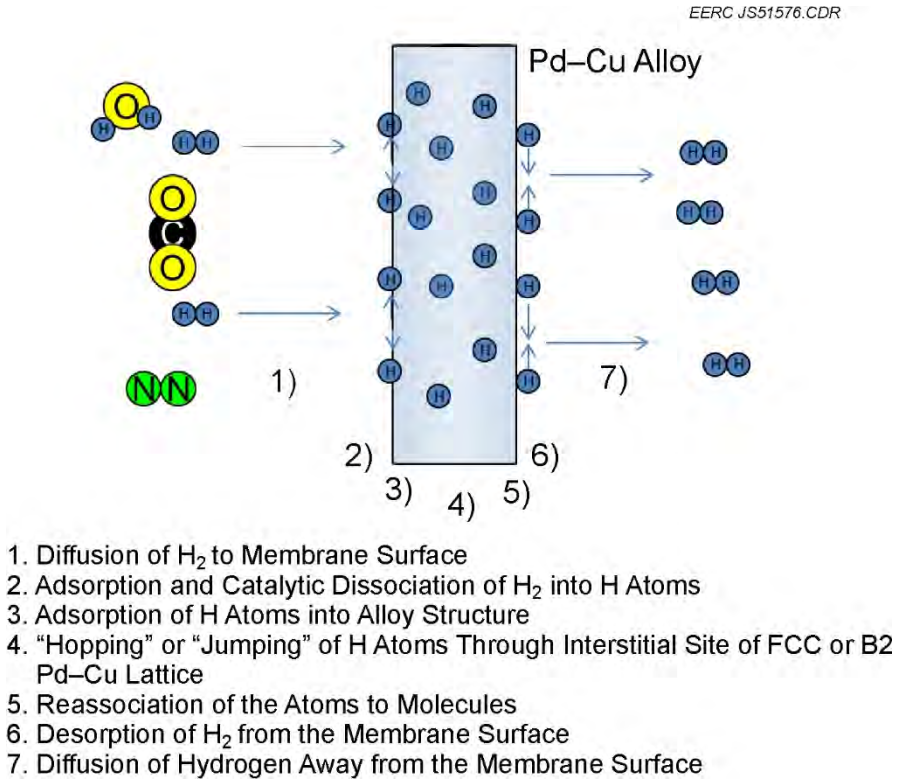

Figure 7. Seven-step mechanism of hydrogen separation through dense metallic membranes.

Impact of Pd–Cu Crystalline Structure and Sulfur on Membrane Performance

Dense metallic Pd–Cu-based membranes are of great interest to researchers because they hold properties of high selectivity and high flux rates and have shown the potential to have resistance to sulfur poisoning (17, 18). The nature of the Pd–Cu structure is of great importance when it comes to the permeation of hydrogen through the membrane. Pd–Cu either forms a body-centered cubic (bcc or b2) structure or a face-centered cubic (fcc) structure. Figure 8 depicts the crystalline structure of each. The bcc structure contains copper atoms at each of the eight corners of the cubic matrix, with a palladium atom at the center of the cube. The fcc structure also contains eight copper atoms at the corners, but also a palladium atom at the center of each face of the cube.

As shown in Figure 9, the type of crystalline structure formed depends on both the composition and temperature of the material (17, 19, 20). The bcc structure is encountered in the widest temperature range at a concentration of 53 wt% Pd and 47 wt% Cu. It is for this reason that many studies have evaluated this particular composition. Studies also indicate that the bcc structure has higher hydrogen permeability but lower resistance to sulfur than the fcc structure. Rothenberger et al. reported that performance degradations of an order of magnitude were observed when exposing bcc structures to 1000-ppm H_2S, but performance degradations of less than 20% were observed when exposing fcc–crystalline-phase materials to the same conditions (17).

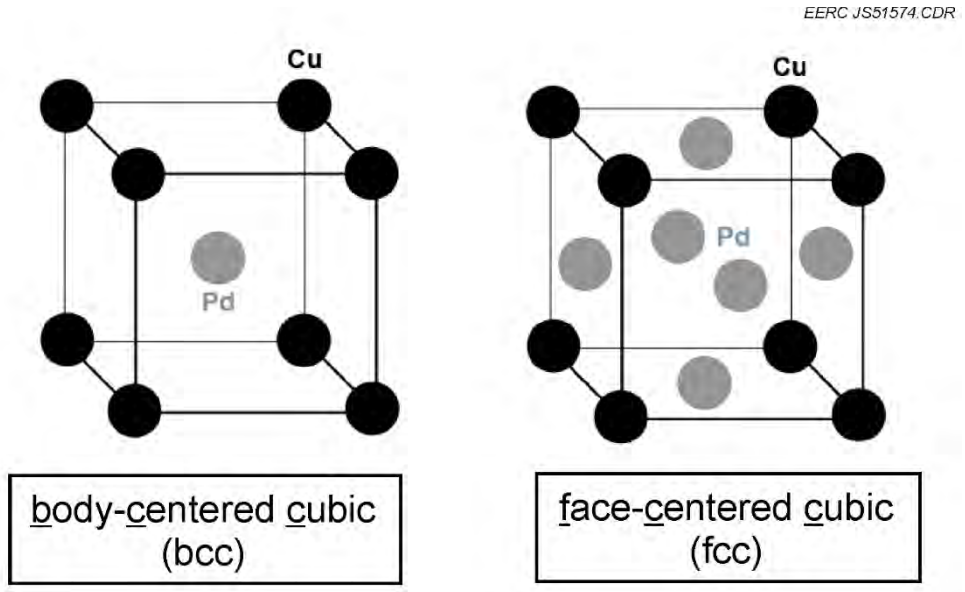

Figure 8. Pd–Cu crystalline structure in bcc and fcc orientations (17).

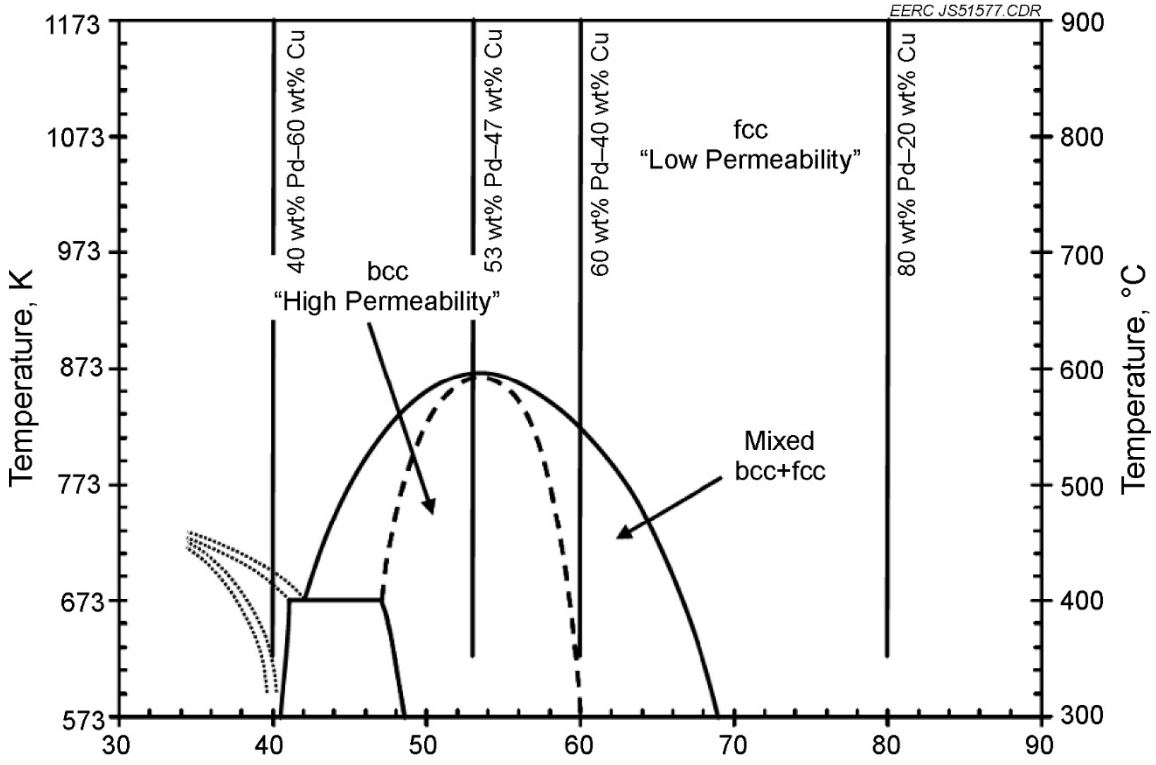

Figure 9. Pd–Cu phase diagram (17, 19, 20).

The diffusion of hydrogen through a palladium membrane or a palladium copper alloy has been described in detail by a number of authors (21–23) in an attempted to understand and predict the energies required for hydrogen atoms to diffuse through Pd–Cu lattices. Figure 10 depicts possible positions for H atoms to exist in bcc Pd–Cu. Sholl described the movements to and from tetrahedral sites and determined the activation energy required for each of these movements (22). Understanding of the first principles of hydrogen diffusion through metal materials can lead to breakthroughs in development of new materials and crystal arrangements. Kamakoti and Sholl have also studied the impact of ternary alloys on hydrogen diffusion (24) and have undertaken a number of studies involving novel metals and amorphous materials for hydrogen separation (25–27).

Sulfur poisoning is known to impact the flux rate of hydrogen through Pd and Pd–Cu alloys. O'Brien (28) theorized that hydrogen transport across a membrane is impacted by sulfur poisoning in two manners: 1) by producing a thin sulfide film on the surface of the membrane with low hydrogen permeability and 2) by blocking Pd from catalyzing the hydrogen dissociation reaction and, therefore, slowing the rate of dissociation. O'Brien's permeation experiments and H_2–D_2 experiments showed that both mechanisms indeed impact hydrogen flux rates through Pd–Cu membranes. The study also showed that at elevated temperature (900 K), H_2S has no impact on hydrogen permeation through $Pd_{47}Cu_{53}$ alloys.

Studies by Gabitto and Tsouris (29) concluded that $Pd_{60}Cu_{40}$ alloys represent the best combination of high hydrogen flux and sulfur resistance. Studies by Ma et al. have shown that sulfur poisoning of a thin membrane of fcc $Pd_{81}Cu_{19}$ was completely reversible if the sulfur was exposed to the membrane above 450°C (30). If the sulfur was exposed at 400°C, the original membrane performance could not be reestablished. Yang et al. evaluated the performance of a $Pd_{60}Cu_{40}$ membrane covered with a thin coating of nickel to promote resistance to H_2S (31). The results of this study indicated that the H_2S poisoning was reversible and that the membrane shows little performance degradation when operated above 573 K.

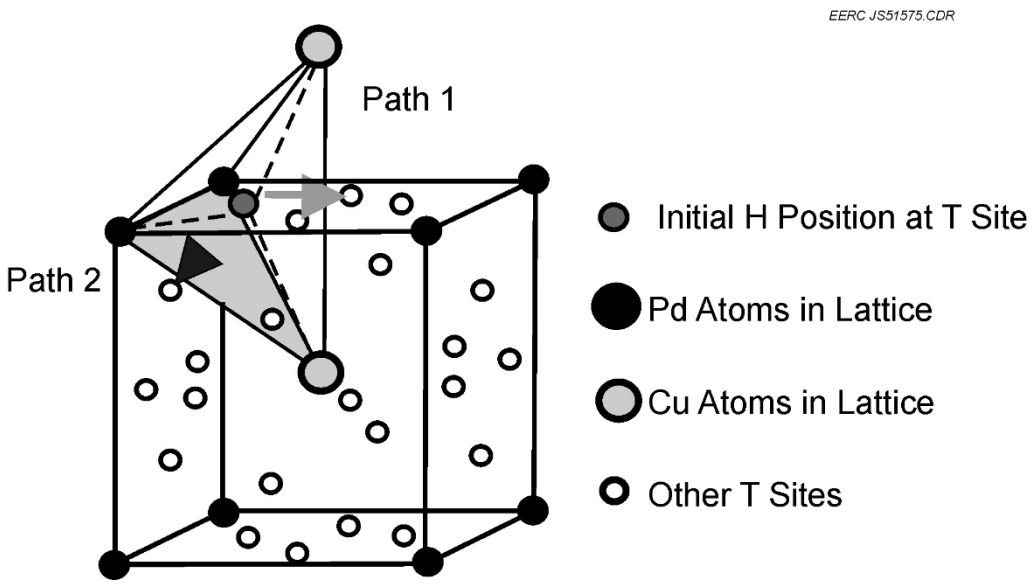

Figure 10. Possible pathways for H motion in bcc Pd–Cu (23).

METHODS

This section describes equipment that existed at the EERC prior to the start of the project. Equipment installation and modification were major parts of this project, and newly installed equipment will be described in the Results section.

TRDU

The TRDU system at the EERC, shown in Figure 11, is a pilot-scale fluidized-bed gasifier located at the EERC in Grand Forks, North Dakota. This system operates in the near-pneumatic transport regime of gas–solid particle flow, provides excellent gas–solid contacting of relatively small particles to promote high gasification rates, and also provides the highest coal throughput per unit cross-sectional area of any gasifier, thereby, reducing the capital cost of the gasification island. The system can fire nominally at a rate of 200–500 lb/hr using combinations of coal and opportunity fuels and is rated at approximately 1 MW_{th}. A slipstream can be pulled from the system between the HGFV and the thermal oxidizer that can be used for testing warm-gas cleanup, shift reactions, and fuel production. The size of the system enables the gasification reactions to be self-sustaining, but it is still small enough that several different operating conditions can be evaluated in a single day. Over 4000 hours of operation on more than a dozen different fuels ranging from bituminous to lignite coals, petroleum coke, shale gas, coal–biomass blends, and 100% biomass have been accomplished in this unit. The EERC has established an extensive database on the operation of these various fuels in both air-blown and oxygen-blown modes utilizing a pilot-scale transport reactor gasifier. This database has been useful in determining the effectiveness of design changes on an advanced transport reactor gasifier and for determining the performance of various feedstocks in a transport reactor.

While firing at about 400 lb/hr of subbituminous coal, the EERC's TRDU can produce about 400 scfm of syngas when using air (250 scfm in oxygen-blown mode). The gasifier system generates a fuel gas, or "produced" gas, with heating values ranging from 105 to 128 Btu/scf in air-blown mode, while heating values of 200 to 240 Btu/scf on a dry basis have been achieved in oxygen-blown mode. Carbon conversions up to 97% have also been attained and are highly dependent on the oxygen/coal ratio. Higher-reactivity (low-rank) coals appear to perform better in a TRDU system than the less reactive bituminous coals. Factors that affect TRDU system product gas quality appear to be fuel type, temperature, and air/fuel ratios.

The TRDU has an exit gas temperature of up to 980°C (1800°F), a gas flow rate of 325 scfm (0.153 m^3/s), and an operating pressure of 120 psig (9.3 bar). It can be divided into three sections: the fuel feed section, the TRDU proper, and the product recovery section. The TRDU proper (Figure 11) consists of a riser reactor with an expanded mixing zone at the bottom, a disengager, and a primary cyclone and standpipe. The standpipe is connected to the mixing section of the riser by an L-valve transfer line. All of the components in the system are refractory-lined and designed mechanically for 150 psig (11.4 bar) and an internal temperature of 1090°C (2000°F). The TRDU is equipped with a HGFV for particulate removal and a thermal oxidizer to convert the combustibles before venting to the stack. A slipstream can be pulled from the system between the HGFV and the thermal oxidizer that can be used for testing warm-gas cleanup, shift reactions, and fuel production.

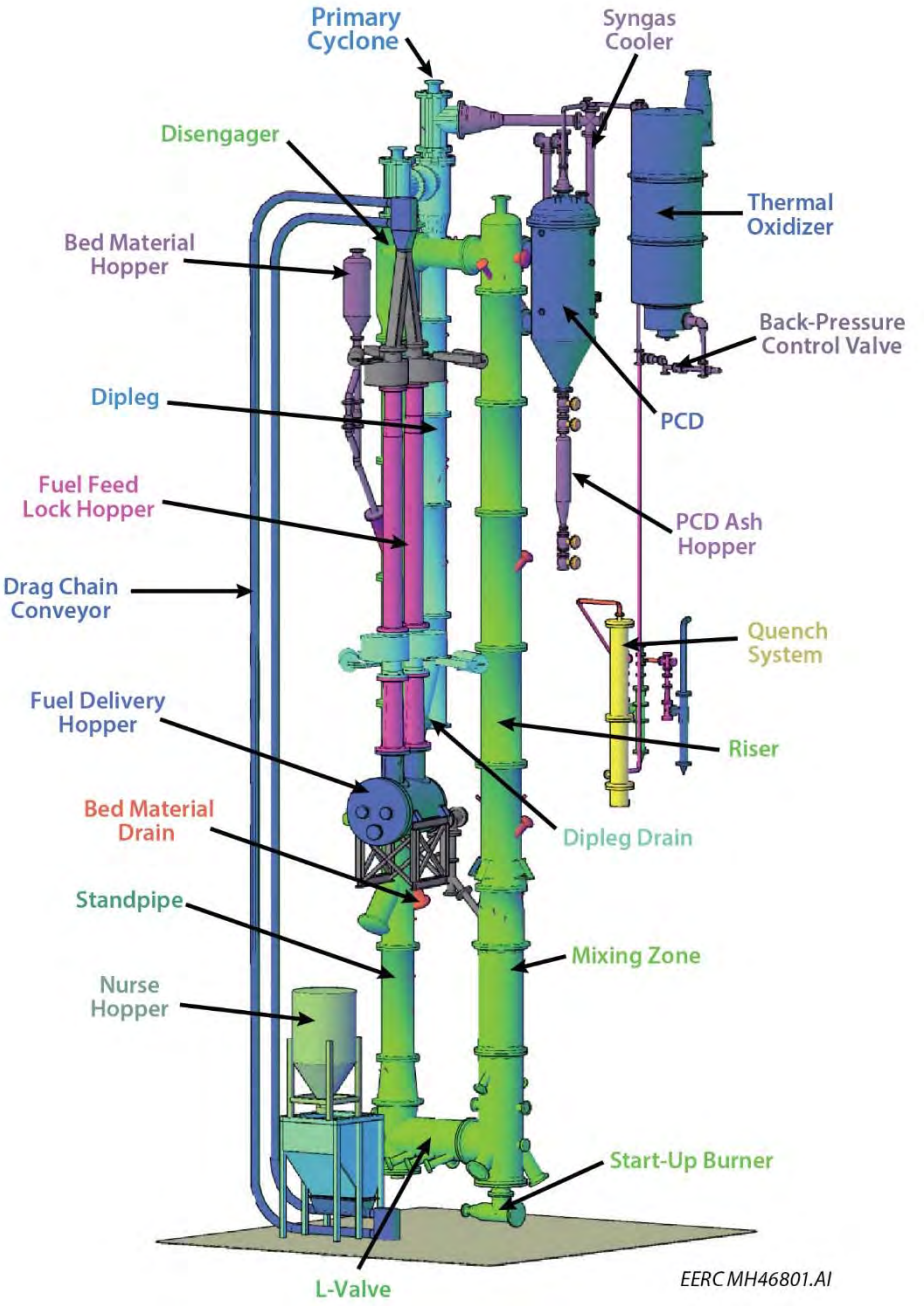

Figure 11. TRDU system located at the EERC.

The feeder system consists of dual lock hoppers with a diverging vessel design, and a high-capacity drag chain conveyor is used to refill the lock hoppers that can be isolated. The ambient-temperature pneumatic transport gas consists of 100% nitrogen or a blend of air and nitrogen. Steam can also be injected through the annulus of the fuel injection pipe, which serves to help depress the swelling tendencies of known high-swelling, high-rank fuels.

Oxidant and steam are fed to the reactor through two pairs of nozzles at varying elevations within the mixing zone. Hot solids from the standpipe are circulated into the mixing zone, where they come into contact with the nitrogen, air, and the steam being injected into the L-valve. This feature enables spent char to contact steam prior to the fresh coal feed, allowing for staged gasification to occur where the steam and oxidant partially oxidize the recirculating char and the fresh fuel feed enters into an oxygen-deficient gas stream. Fuel will then devolatilize, crack, and reform the volatile matter into syngas. Gasification or combustion reactions are carried out in the riser as fuel and oxidant (with steam for gasification) flow up the reactor. The solids circulation into the mixing zone is controlled by fluffing gas in the standpipe, L-valve aeration flows, and the solids level in the standpipe.

The bulk of entrained solids leaving the riser separates from the gas stream in the disengager and circulates back to the riser via the standpipe. Gas exiting the disengager enters a primary cyclone where finer recovered solids are recirculated back to the standpipe through the dipleg crossover. Gas exiting the primary cyclone enters a series of jacketed-pipe heat exchangers before entering a HGFV. The cleaned syngas leaving the HGFV (see Figure 11) is depressurized and combusted in a thermal oxidizer. The HGFV for the TRDU testing was a hot-gas particulate collection device able to handle all of the gas flow from the TRDU at its expected operating conditions. Detailed design criteria and a comparison to actual operating conditions on the design coal are given in Table 2.

The unit is well instrumented for controlling and monitoring the system and recording all system data, including parameters such as gas composition. The EERC uses a high-speed data acquisition and control system based on National Instruments LabVIEW. The central system is highly reconfigurable to meet specific testing needs.

HGFV

The HGFV, as shown in Figure 12, is designed to handle all of the gas flow from the TRDU at its expected operating conditions. The vessel has an approximately 48-in. i.d. (121.9 cm) and is 185 in. (470 cm) long. It is designed to handle gas flows of approximately 325 scfm at temperatures up to 815°C (1500°F), with a pressure of 120 psig (8.3 bar). The refractory has a 28-in. (71.1-cm) i.d., with a shroud diameter of approximately 22 in. (55.9 cm). The vessel is sized such that it could handle candle filters up to 2.0 m long; however, 1.5-m iron aluminide metal candle filters were utilized in these reported gasification tests. Candle filters are 2.375-in. (6-cm) o.d., with a 4-in. (10.2-cm) center line-to-center line spacing. The filter design criteria are summarized in Table 3.

Table 2. Summary of TRDU Design and Operation on Design Coal

Parameter	Design[1]	Actual
Coal	Illinois No. 6	Illinois No. 6
Moisture Content, %	5	8.5
Pressure, psig	120 (9.3 bar)	120 (9.3 bar)
Steam/Coal Ratio	0.34	0.34
Air/Coal Ratio	4	2.3
Ca/S Ratio, mol	1.5	2
Air Inlet Temperature, °C	427	180
Steam Preheat, °C	537	350
Coal Feed Rate, lb/hr	198 (89.9 kg/hr)	220 (99.9 kg/hr)
Gasifier Temperature, maximum °C	1010	950
ΔT, maximum °C	17	60 to 100
Carbon Conversion,[2] %	>80	76.5
HHV of Fuel Gas, Btu/scf (corr.[3])	100	110
Heat Loss as Coal Feed, %	19.5	13[4]
Riser Velocity, ft/s	31.3	25
Heat Loss, Btu/hr	252,000	450,000[3]
Standpipe Superficial Velocity, ft/s	0.1	0.38

[1] KBR design specifications.
[2] Carbon conversion = (wt carbon feed − wt carbon removed)/wt carbon feed × 100.
[3] Corrected.
[4] Higher coal feed rate and lower air and steam preheat resulted in lower percent heat loss but higher net heat loss.

The total number of candles that can be mounted in the current geometry of the HGFV tube sheet is 13. This enables filter face velocities as low as 2.0 ft/min to be tested using 1.5-m candles. Higher face velocities are achieved by using fewer candles. The majority of testing has been performed at a face velocity of approximately 4.0 ft/min by using 13 candle filters. These recent tests have utilized the Pall iron aluminide metal candle filters exclusively. Previous candles tested in the program included granular SiC candles from Pall Advanced Separation Systems Corporation.

A preheat natural gas burner attached to a lower inlet nozzle on the HGFV can be used to preheat the HGFV separately from the TRDU. The hot gas from the burner enters the vessel via a nozzle inlet separate from the dirty gas.

The high-pressure nitrogen backpulse system is capable of backpulsing up to four sets of four or five candle filters with ambient-temperature nitrogen in a time-controlled sequence. The pulse length and volume of nitrogen displaced into the HGFV is controlled by regulating the pressure (up to 600 psig [42 bar]) of the nitrogen reservoir and controlling the solenoid valve pulse duration. Figure 12 also shows the HGFV location and process piping in the EERC gasifier tower. HGFV operating filter temperatures around 260°C (500°F) to 300°C (575°F) were tested during this campaign.

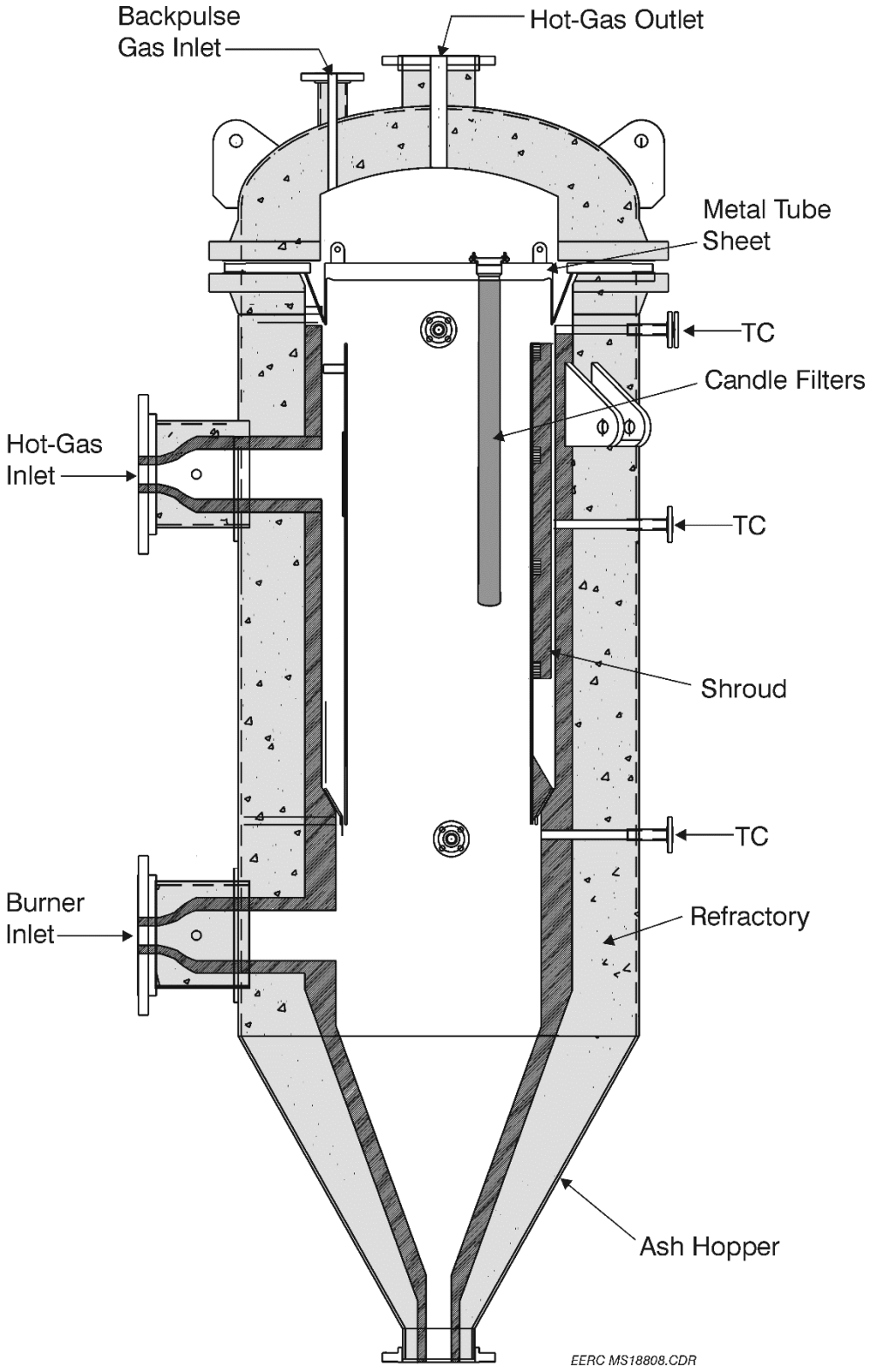

Figure 12. Schematic of HGFV design with internal refractory, tube sheet, and shroud.

Table 3. Design Criteria and Actual Operating Conditions for Pilot-Scale HGFV

Operating Conditions	Design	Actual
Inlet Gas Temperature	540°C	280°–305°C
Operating Pressure	150 psig	120 psig
Volumetric Gas Flow	325 scfm	360–420 scfm
Number of Candles	19 (1 or 1.5 m)	13 (1 m)
Candle Spacing	4 in. ℄ to ℄	4 in. ℄ to ℄
Filter Face Velocity	2.5–10 ft/min	4–4.5 ft/min
Particulate Loading	<10,000 ppmw	<38,000 ppmw
Temperature Drop Across HGFV	<30°C	25°C
Nitrogen Backpulse System Press	up to 600 psig	210 psig
Backpulse Valve Open Duration	up to 1 s	0.5 s

Ports for obtaining hot high-pressure particulate samples both upstream and downstream of the HGFV are part of the filter system piping.

The ash letdown system consists of two sets of alternating high-temperature valves with a conical pressure vessel to act as a lock hopper. HGFV solids discharge from the lock hopper to a barrel sitting on an electronic weigh scale.

Hot-Side Syngas Compressor

While capable of generating a slipstream that would expose test membranes to a range of conditions, the TRDU has a maximum operating pressure of 120 psig, which is substantially less than the desired +400-psi pressures of commercial gasifiers. To address this limitation, the EERC modified the TRDU downstream equipment to include a compressor capable of providing a stream of about 250 scfm at more than 500 psig for periods of more than 8 hours. The compressor is installed at the EERC and is operational. Of the syngas stream, more than 90 scfm can be sent to the membrane for separation to produce 200 lb/d of hydrogen, with the remainder returned to the gasifier to satisfy purge requirements. Figure 13 displays a block diagram of the system. While the modified system does not attain the harshest conditions projected by DOE for future commercial gasifiers (such as +800-psi syngas product pressure), its 500-psia design pressure places it in the range of existing gasifiers. It should be noted that the compressor can be modified to achieve +800-psi exhaust pressure merely by the addition of a single stage, if such pressures are desired in the future.

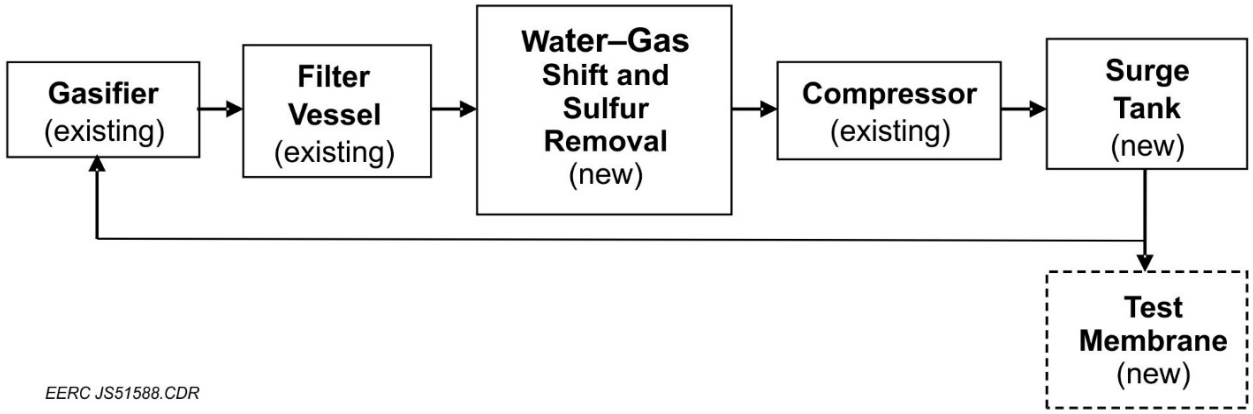

Figure 13. Block diagram of the system.

Ultimately, the modified TRDU system can perform cold- or warm-gas (up to 450°F) cleanup with or without WGS to produce a synthesis gas product stream of more than 45 scfm containing more than 100 lb/d of hydrogen at pressures up to 500 psig. Compressor specifications are listed as follows:

- Suction pressure: 135–140 psig
- Discharge pressure: 500 psig
- Capacity: 250 scfm
- Suction temperature: 450°–500°F from gasifier, 60°–80°F from quench system
- Site elevation: 830 feet
- Ambient temperature: 100°F (assuming indoor location)
- Interstage temperature: must be kept at or above 450°F
- Driver: electric, 208 V, 3Ø, 60 Hz
- HazLoc rating: Class I, Division II, Group B (in accordance with the requirements of National Fire Protection Association 70)
- Corrosives: H_2S up to 7500 ppm, NH_3 up to 3600 ppm, HCl up to 5 ppm

Gas Analysis

All of the gasification testing, shift, and hydrogen separation included the continuous analysis of gas constituents. In these cases, a slipstream of dry quenched syngas was fed to laser gas analyzers (LGAs) and gas chromatographs (GCs) for online analysis of major gas components

and sulfur species. The EERC has three Atmosphere Recovery, Inc., LGAs for use at various sample points. The LGAs employ lasers with Raman detectors to stimulate sample gas and emit distinct light spectra that are picked up by the detectors. The LGAs use designations LGA35, LGA39, and LGA106. The LGAs are each capable of measuring the real-time concentrations of eight gases at once. Seven of those gases are H_2, CO, CO_2, N_2, H_2S, CH_4, and total hydrocarbons. LGA39 is capable of measuring O_2 in addition to the aforementioned suite of gases. A Yokogawa GC capable of measuring H_2, CO, CO_2, N_2, O_2, H_2S, COS, CH_4, ethane, ethene, propane, and propene is also used for syngas analysis. The Yokogawa has high-level H_2S measurement capabilities and provides a measurement of the syngas stream every 10 minutes.

In addition, a continuous emission monitor (CEM) analyzer bank continuously samples the outlet of the TRDU. The analyzers consist of dual Rosemount 880s for CO and CO_2 compositions, a Teledyne thermal conductivity analyzer for hydrogen, a Teledyne Model 731R infrared for total hydrocarbons, and an Ametek Western Research Series 900 ultraviolet analyzer for H_2S. The TRDU is also equipped with a Beckman Model 755 paramagnetic analyzer for oxygen to discern when the TRDU is in either gasification or combustion mode.

The analyzers are calibrated prior to the start of each test program. Sample gas streams can be manually switched via selector valves, although a single port was used for this testing. Sample gas tubing from sample ports to the analyzers is polyethylene, with no line longer than 50 feet. Sample gas transit times to the analyzers are estimated to be less than 1 minute, depending on the individual sample gas flow rate. Gas is cooled and quenched using indirectly cooled quench pots before transport to the analyzers, so measurements are on a dry basis. For the testing conducted, all sampling was from the back end of the quench pots, just upstream of the back-pressure control valve.

In addition to analyzer sampling from various points throughout the system, Dräger tubes are used to sample gases that cannot be detected by the online analyzers. H_2S, HCl, HCN, NH_3, and other trace gases can be checked to supplement or verify low-to-mid-level H_2S chromatograph data.

RESULTS AND DISCUSSION

The results section is divided into four main sections. The first section provides a high-level overview of the membrane test system in order to set the stage for the detailed equipment installation activities that occurred in Tasks 1 and 2. The second section describes the acquisition and installation of the membranes (Task 1). The third section describes the modifications to the TRDU system required for the membrane testing (Task 2). The fourth section describes the testing that was conducted and results of the testing (Task 3).

Overview of Membrane Testing Setup

Systems and equipment were added to the TRDU in order to enable testing of Praxair's hydrogen separation membrane at the EERC. A high-level overview of the test system is shown in Figure 14. It should be noted that the analyzer sampling locations moved periodically during testing. Approximately 50% of the syngas exiting the TRDU was sent to the warm-gas cleanup and compression train. The remainder of the syngas was sent directly to the thermal oxidizer. The CEM bank was used to measure the composition of the major gas components exiting the gasifier, including H_2S. An existing pressure vessel (referred to as the carbonizer) was converted to a fixed-bed WGS reactor. The reactor was filled with a sour shift catalyst called Katalco K8-11, supplied by Johnson Matthey. The syngas was analyzed after the shift bed by LGA39 to determine the effectiveness of the shift process. After shifting, the syngas was sent to the hot-syngas compressor in order to pressurize the stream from approximately 120 up to 500 psig. The temperature of the syngas was kept above 450°F throughout the compression process in order to prevent condensation of tars and moisture. A portion of the compressed syngas was recycled back to the TRDU to provide necessary transport gas and offset nitrogen purging. The remainder of the syngas was sent to a two-bed regenerable system for desulfurization using RVS-1 sorbent produced by Clariant. One of the beds was used for sulfur removal of the syngas stream while the other was being regenerated. Upon saturation with sulfur, the newly regenerated bed would be brought online, and the other bed would be regenerated. Syngas with a H_2S concentration of less than 5 ppm was then sent to the hydrogen membrane separator. The hydrogen (or permeate) stream was measured with LGA35, and the CO_2 (or retentate) stream was measured with LGA106 and the Yokogawa GC. Both streams were sent to the thermal oxidizer to convert the syngas species to flue gas before venting in the TRDU stack. Detailed descriptions of each of the systems follow in the next two sections.

Task 1 – Acquisition and Installation of Pilot-Scale Hydrogen Separation Membranes

Praxair constructed the membrane module at its laboratory facilities in Tonawanda, New York, and tested it on bottle-derived mixtures of hydrogen and N_2. After this baseline performance was established, the membrane was disassembled and shipped to the EERC as a separate pressure vessel and set of tubes. Praxair also shipped a furnace box to the EERC to heat the membrane module. Prior to arrival of the membrane, the EERC procured and installed preheat modules, syngas piping, and a membrane test stand.

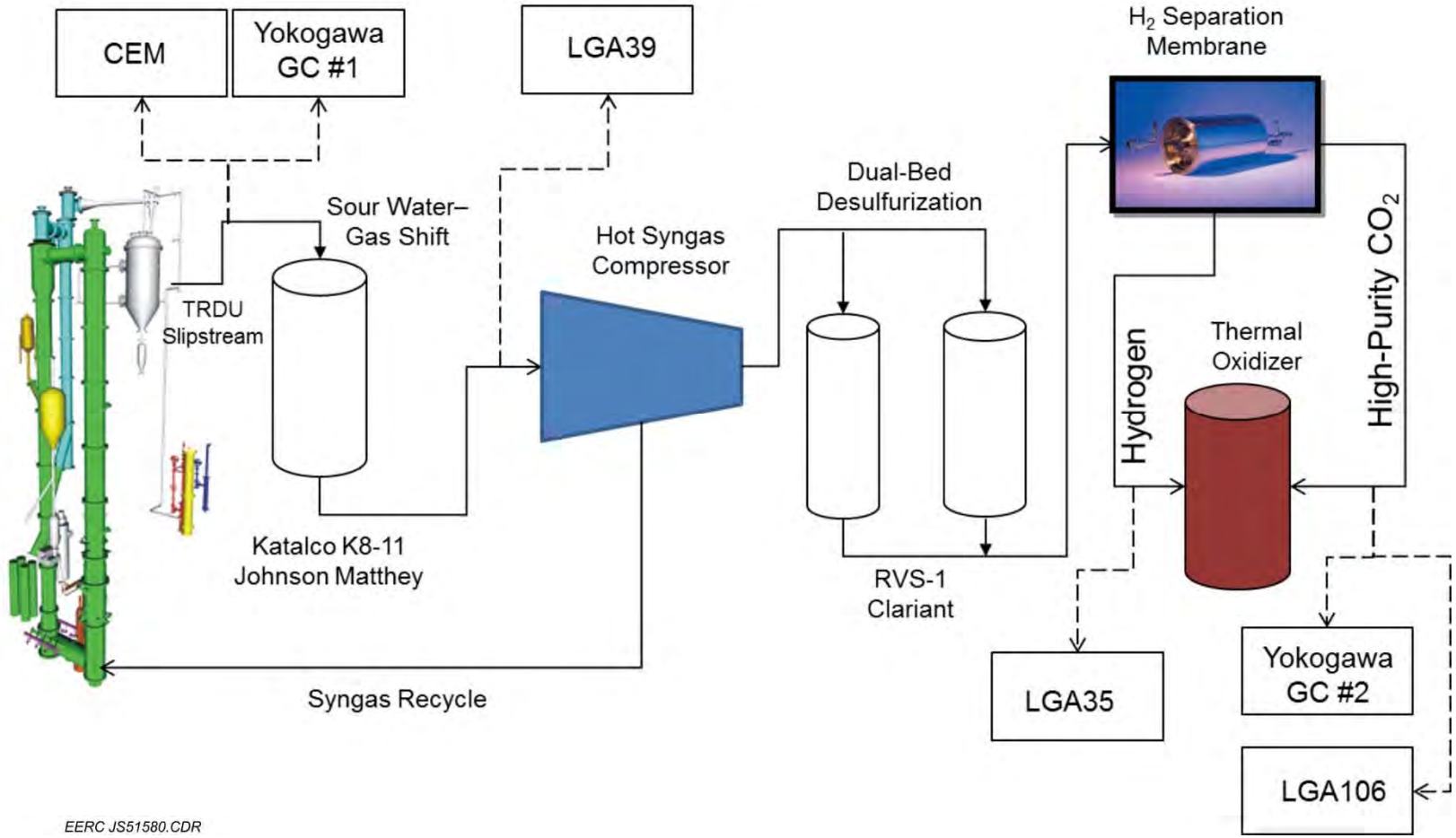

Figure 14. High-level overview of membrane test setup.

The specifications for the design of the membrane assembly were provided by Praxair and reviewed by the EERC. The supporting systems at the EERC were designed to meet the testing requirements specified by Praxair. After a detailed review, it was decided that the first floor of the seven-floor gasification tower was the best location for installing the membrane to ensure a short distance for the feed gas piping. This would also mean that piping runs would need to be run to the seventh floor of the gasification tower in order to send the exhaust to the thermal oxidizer. Piping components and flow control and measurement devices for the permeate and retentate streams were procured and installed. Piping up to the thermal oxidizer on the seventh floor was completed and insulated. Figure 15 shows the piping runs in the gasification tower. The two pipe runs include an orifice (permeate) and Coriolis meter (retentate) and control valves. This enabled flow control on the retentate and feed streams and back-pressure control on the permeate stream. Sample ports were also installed on the permeate and retentate streams so that the gas compositions could be measured on a continuous basis. Small quench pots were installed on the sample lines to knock out moisture and tars prior to sending the gas streams to the analyzers.

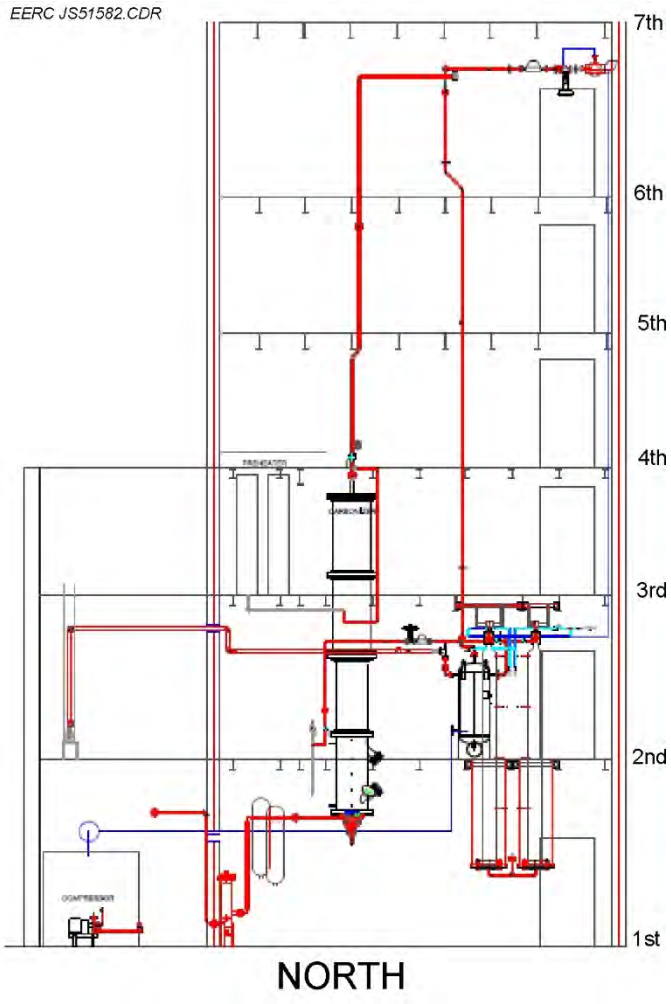

Figure 15. Piping runs installed in the gasification tower as viewed from the north side of the tower.

It was determined that preheat would be needed in order to take the syngas from the operating temperature of the sulfur removal bed at about 300°C to the maximum desired membrane temperature of 500°C. Ideally, this would be accomplished with a heat recovery heat exchanger in a commercial system, but for this scale, it was determined that an electric preheater would be adequate. Heat-transfer analysis was completed, and preheaters were designed and constructed to Class I, Division II, Group B specifications. Two preheaters were used in series, which consisted of wound coils of tubing inside of electric, three-phase clamshell heaters. Specifications for Praxair's electrical furnace for the main membrane module were reviewed to determine the requirements to integrate the furnace with the electrical and control systems in the TRDU tower at the EERC. Electrical wiring was completed in advance of receiving the furnace to speed up installation upon arrival.

Based on the location of the operating membrane system, it was determined that the membrane module would be housed on a movable skid. This allowed the tubes to be installed in the crane well, and then the system could be moved to its final location and not hinder fuel refill operations. The movable skid to mount the membrane vessel and preheaters was constructed prior to the arrival of the membranes.

National Instruments control software was written for the data acquisition system, and instrumentation and control wiring was run to the specified membrane location in the TRDU tower. The control computer for the membrane system was placed in the control room near the control center for the gasifier. This enabled continuous communications between the gasifier control room operator and the personnel running the membrane skid. Figure 16 shows the control systems page for the membrane system.

A preliminary hazardous operations (HAZOP) review was conducted in September 2014. The main finding from the review regarding the membrane module was concern about the potential for a leak of relatively pure hydrogen which could result in an invisible flame. It was determined that a flame detector would be needed for the system that could warn operators and potentially shut the system down if a leak was detected. A basic flame detector rated for the environment was procured and installed. A formal HAZOP review of the TRDU and separation membranes was held January 14, 2015, and it was determined that the risks associated with the membranes were adequately addressed.

The pressure vessel for the membrane tubes was received at the EERC in June 2015. The EERC fabricated the stand to mount the vessel and placed it in the gasification tower next to the sulfur removal beds. Upon receipt of the membrane pressure vessel, the system was positioned, and the final connections to the module were field-fit and welded. The heater box for heating the membrane was also received at the EERC, installed, and connected to existing controllers.

The membrane tubes were received during the week of June 22, just prior to the first test run. Prior to tube installation, a dry run of the membrane installation and positioning was conducted to ensure smooth setup of the vessel with minimal risk for damaging tubes during the install. Praxair personnel worked directly with the EERC to determine the best method for moving

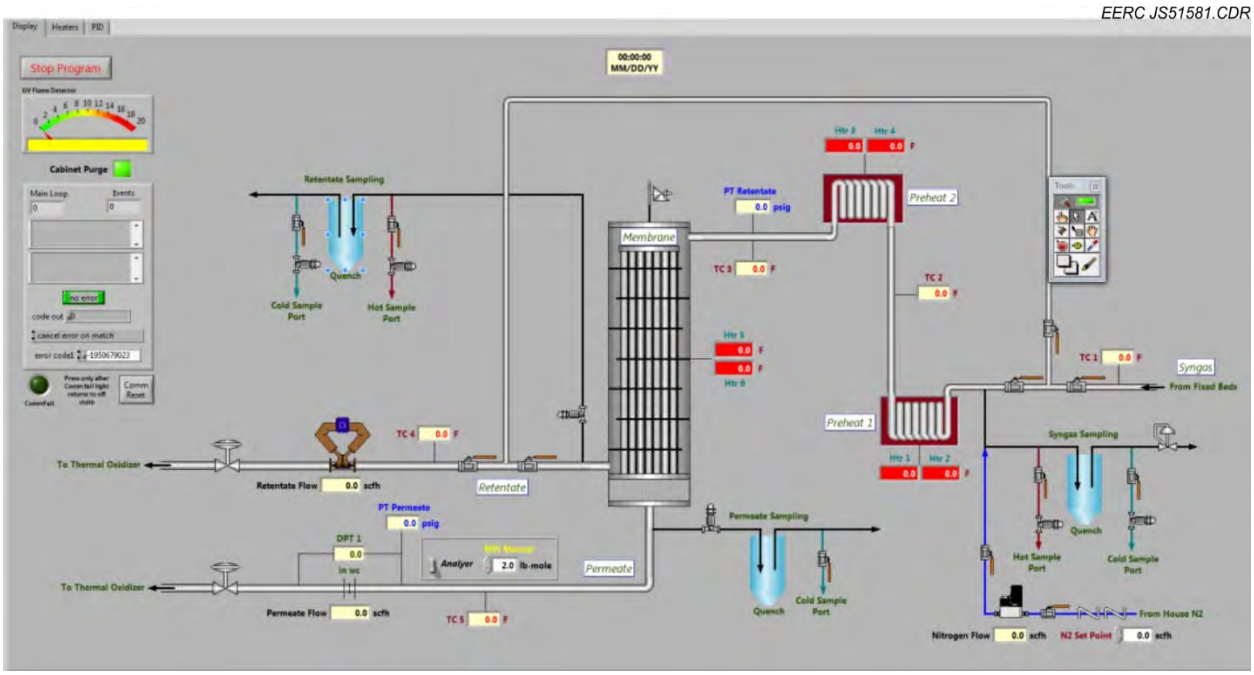

Figure 16. National Instruments membrane control screen.

the module once the tubes were installed. The module was moved back to the crane well, and the tubes were installed under the guidance of Praxair personnel during the week of June 29, 2015. After tube and flange installation was complete, the vessel was carefully put in place without incident. Figure 17 is a photo of the installed membrane module, which is surrounded by the furnace box. The preheat modules are also shown to the left of the membrane. The heaters were bumped, and the system was ready for the first week of operation on July 6, 2015.

Task 2 – Modification of the Transport Reactor System for Membrane Testing

Overview and Piping and Instrumentation Diagrams (P&IDs)

Several modifications to the TRDU tower were needed in order to prepare the system for membrane testing. WGS reactor and sulfur removal beds needed to be installed, and piping and interconnections were needed between each piece of equipment. An existing reactor system called the carbonizer that was already located in the TRDU tower was converted to a fixed-bed WGS reactor. Modifications were needed for the existing compressor system for cooling and also for syngas recycle. An additional guard filter was put in place upstream of the compressor to protect it from particulate. A pressure surge tank was installed downstream of the compressor to ensure consistent pressure delivery to the membranes and eliminate rapid pressure swings. Bypass systems were also needed for each of the major pieces of the equipment to enable operational flexibility as well as allow for the membrane to be brought online in a controlled manner.

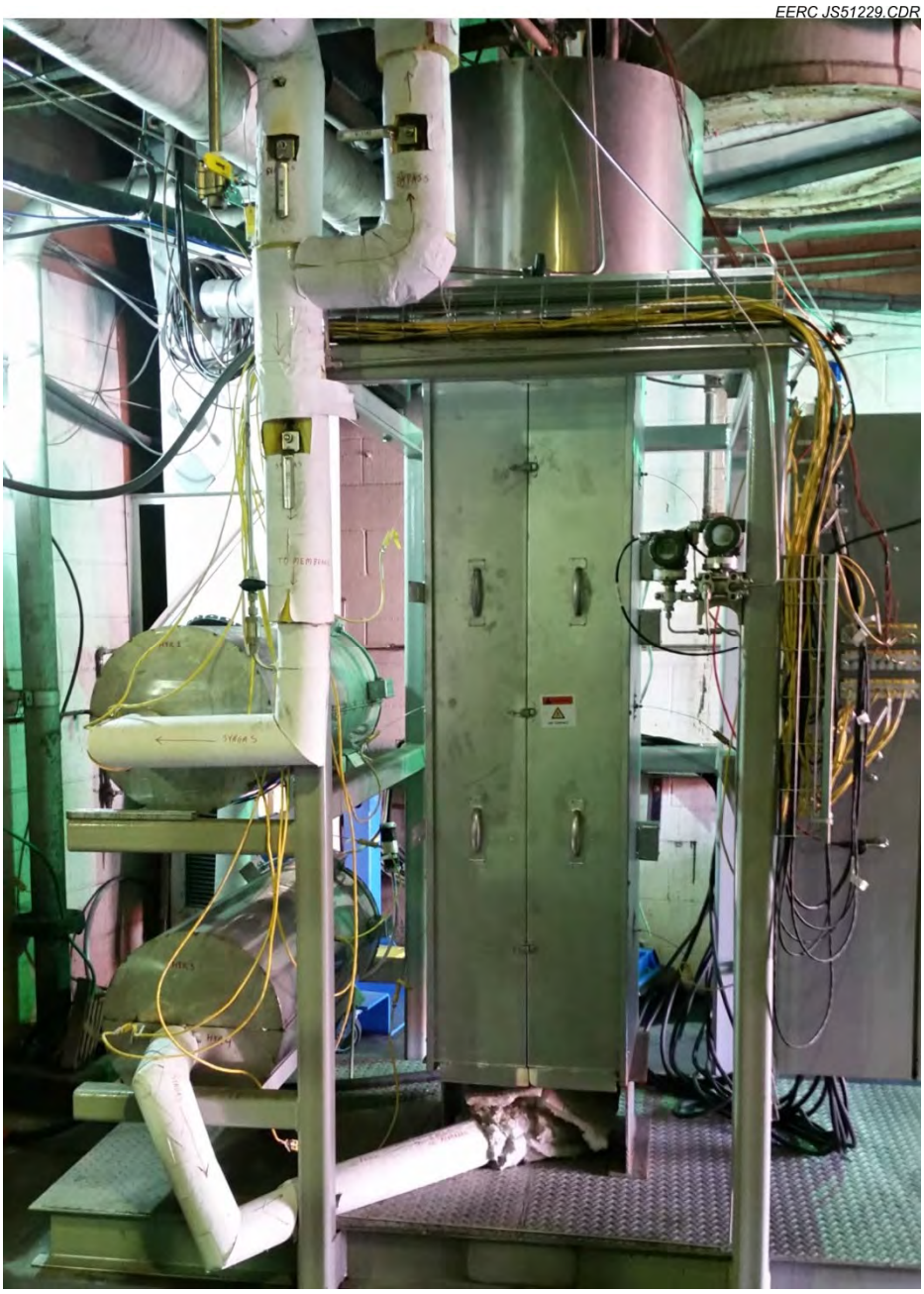

Figure 17. Praxair membrane module installed at the EERC.

The entire system was first mapped out with P&IDs. Figures 18–22 show the P&IDs that were developed for the system. Figure 18 provides an overview of the system and is more of a process flow diagram. Figure 19 provides the details of the layout for the WGS reactor, HGFV, and thermal oxidizer. Figure 20 shows the detailed P&ID for the compressor and fixed-bed desulfurization system. Figure 21 shows the preheater and membrane systems. Figure 22 shows the cooling loop for the syngas compressor.

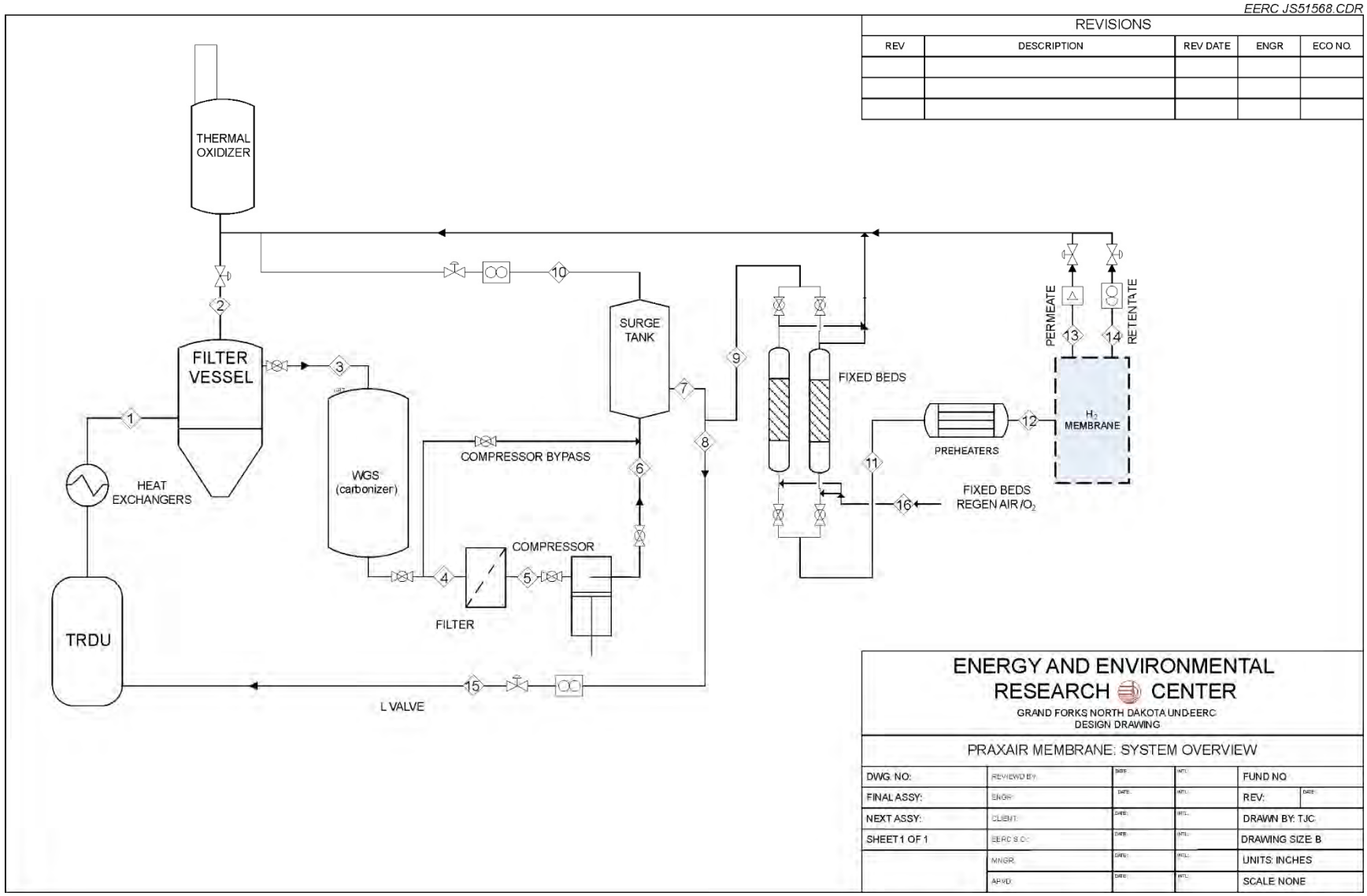

Figure 18. General layout of the gasifier, gas cleanup, and membrane separation system.

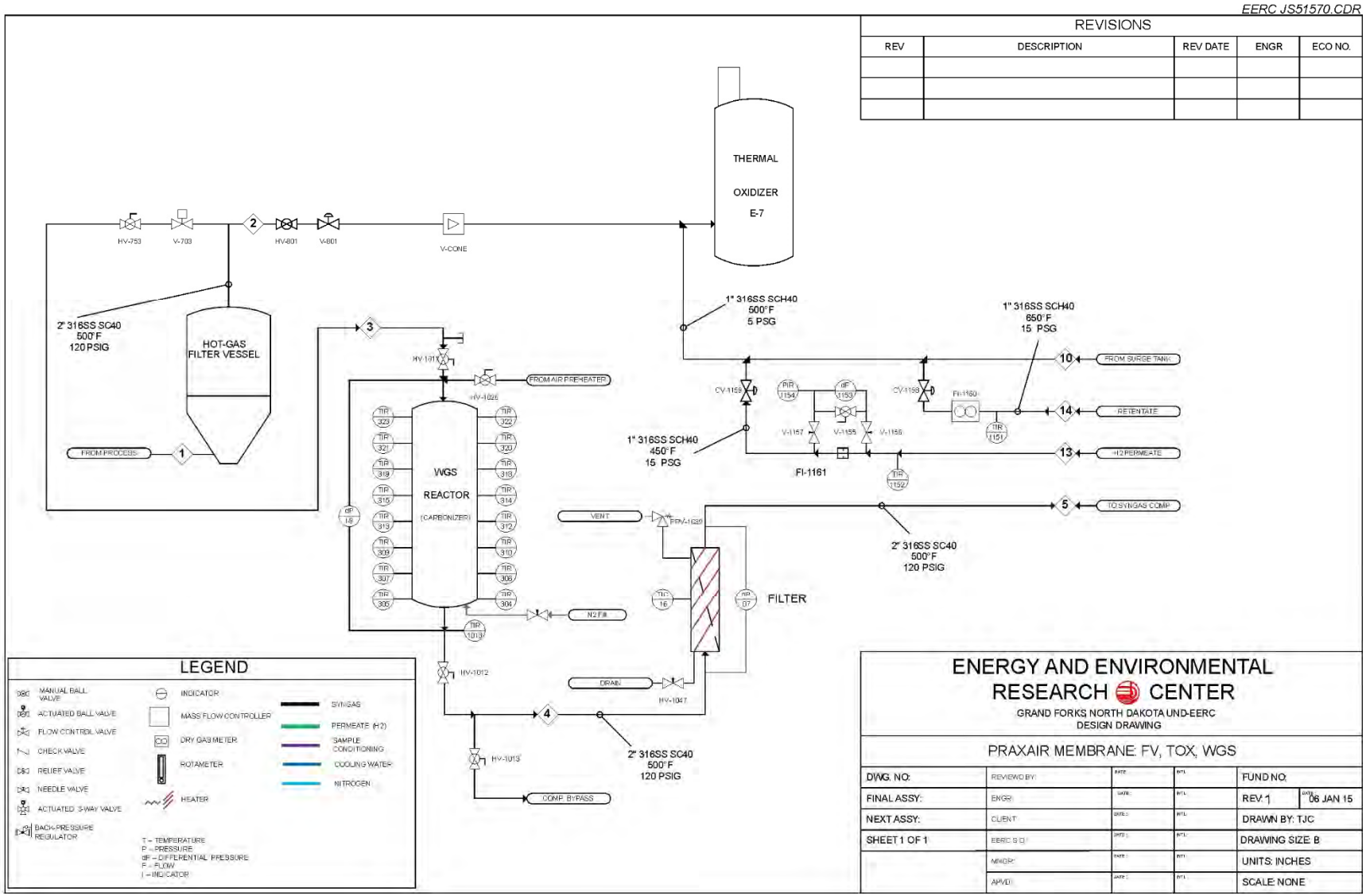

Figure 19. HGFV, WGS reactor, and thermal oxidizer P&ID.

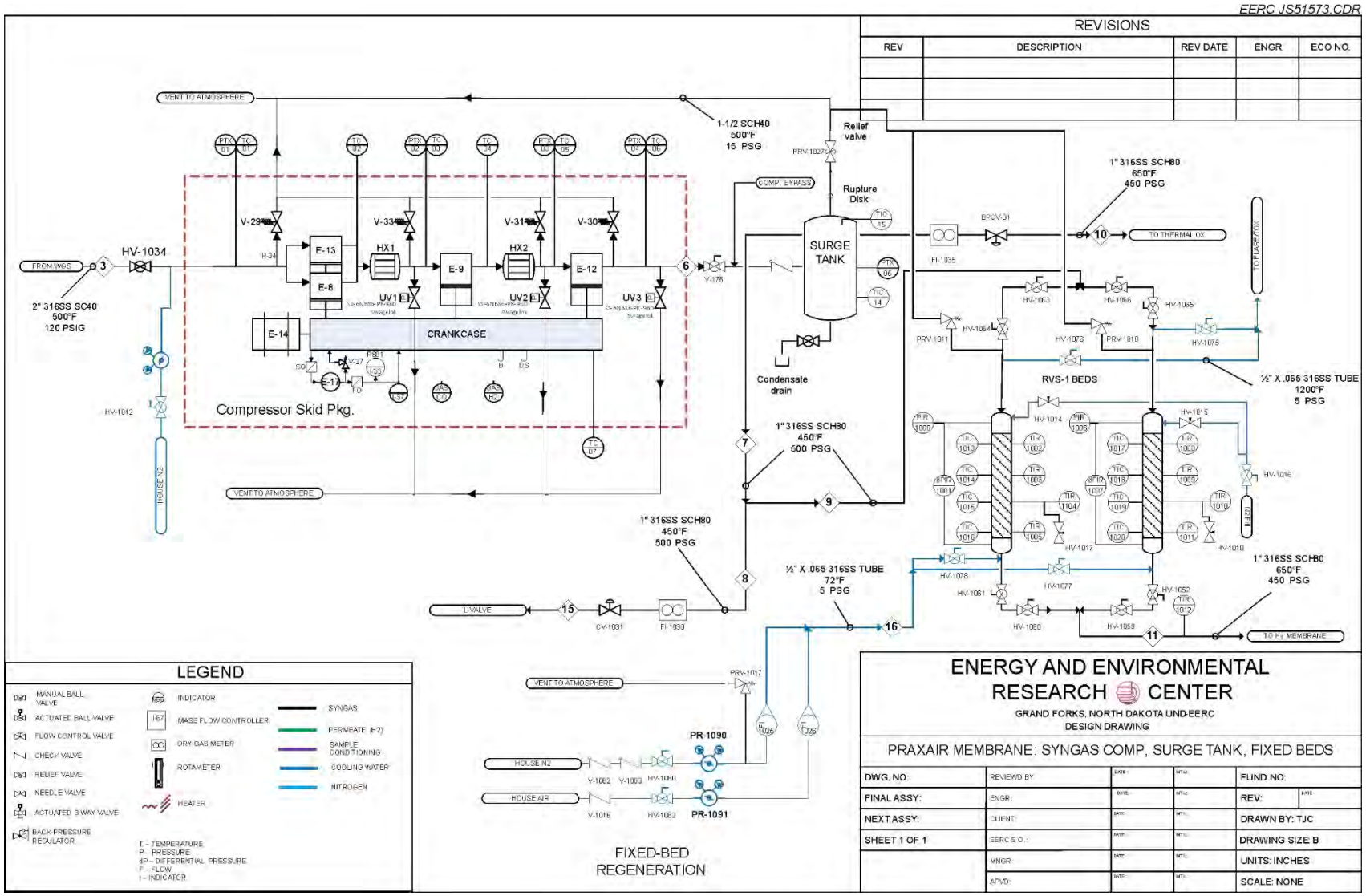

Figure 20. Compressor system and sulfur removal bed P&ID.

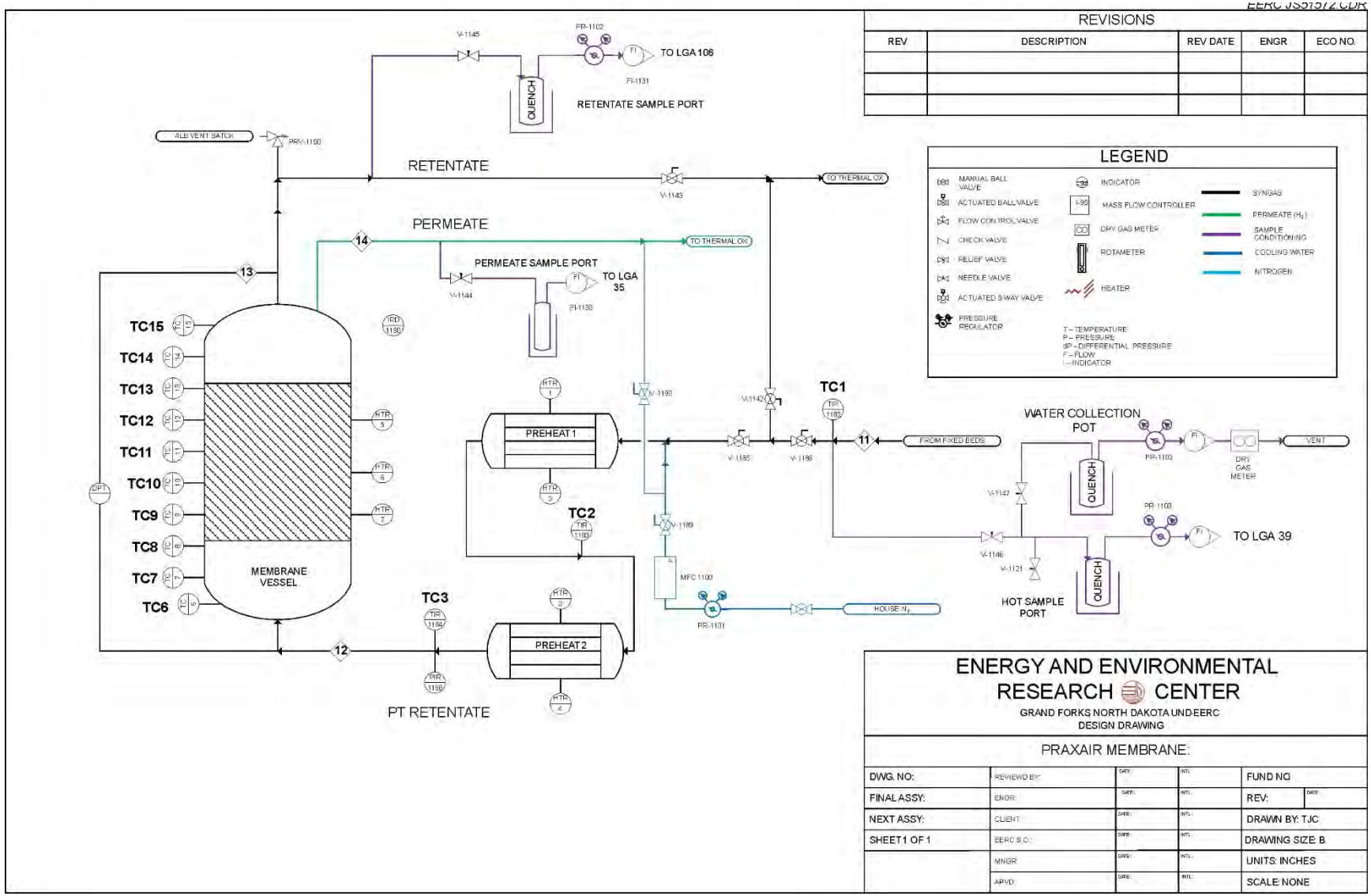

Figure 21. Membrane and preheat systems P&ID.

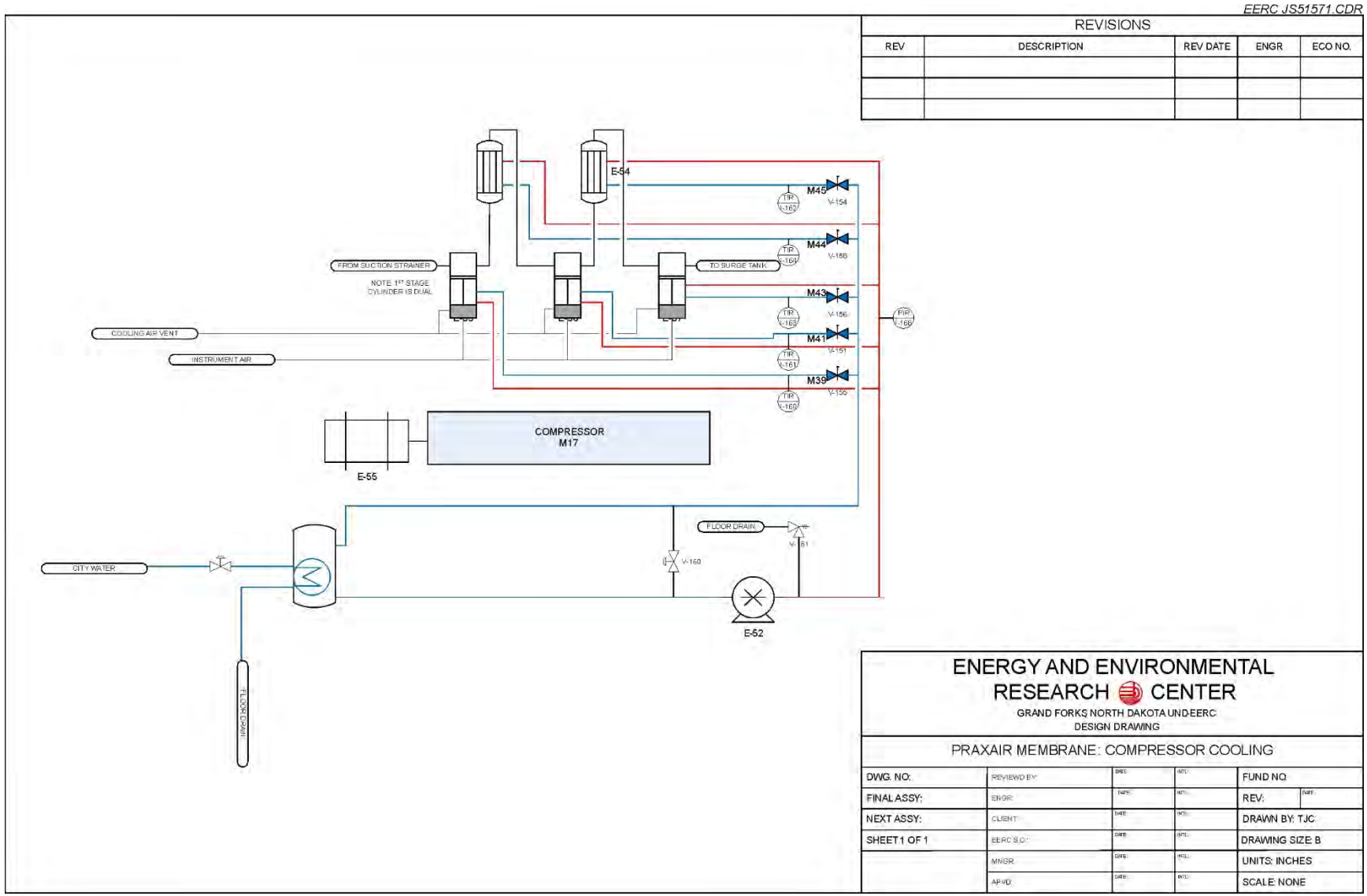

Figure 22. Compressor cooling loop.

WGS Reactor

The carbonizer was an existing mild gasification unit at the EERC that was colocated with the TRDU in the gasification tower. This vessel is refractory-lined and was heated prior to operation using preexisting TRDU air heaters. The air heaters are first used to preheat air to the TRDU for start-up of the system, then when the TRDU is transitioned to oxygen-blown mode, the air heaters are used to preheat the shift bed under nitrogen. The necessary piping modifications were made to accomplish the preheating of the reactor under an inert atmosphere. The vessel was modified for use as a WGS reactor by updating the inlet and outlet piping and adding a mesh screen at the bottom of the reactor to support the catalyst. Approximately 50% of the syngas generated by the TRDU was teed off and sent to the bed during operations. The syngas is sent to the WGS prior to desulfurization; therefore, a sour shift catalyst was needed to maximize hydrogen and minimize CO content of the syngas. The vessel was loaded with approximately 1200 lb of Katalco K8-11 sour shift catalyst, manufactured by Johnson Matthey.

Figures 23 and 24 show the top and bottom of the fixed-bed WGS reactor, respectively. Syngas compressor isolation valves were also installed as part of the outlet piping. The shift catalyst bed is highly instrumented with pressure transmitters, differential pressure transmitters, and thermocouples that enable continuous monitoring of the conditions in the system. The monitoring points were directly integrated with the TRDU control system.

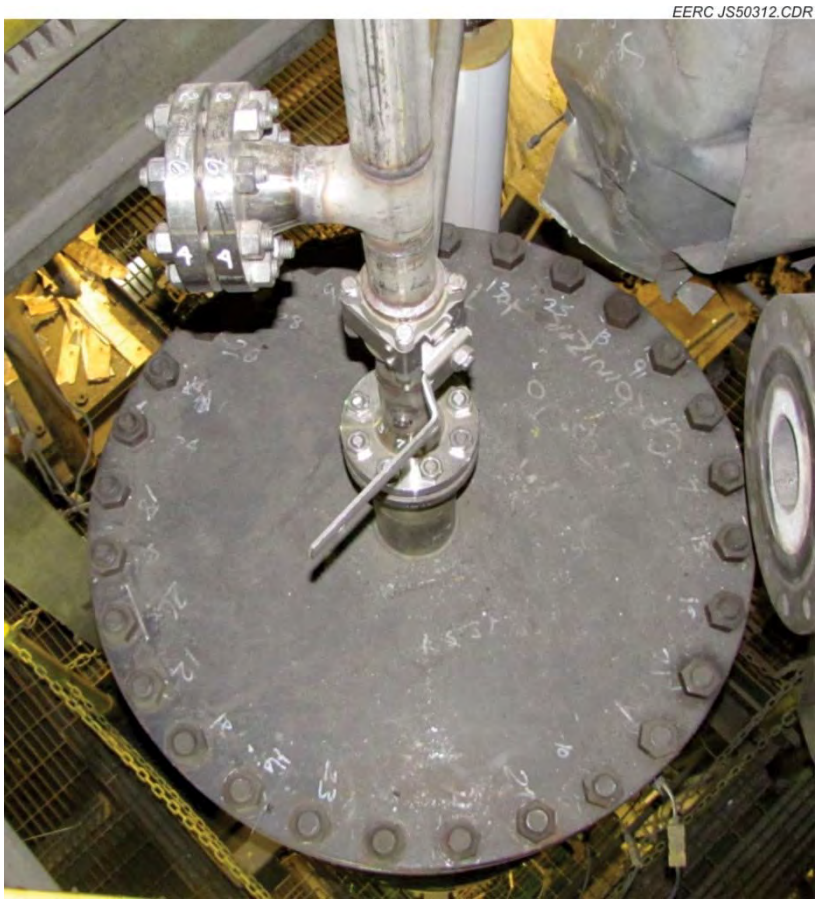

Figure 23. Shift catalyst inlet.

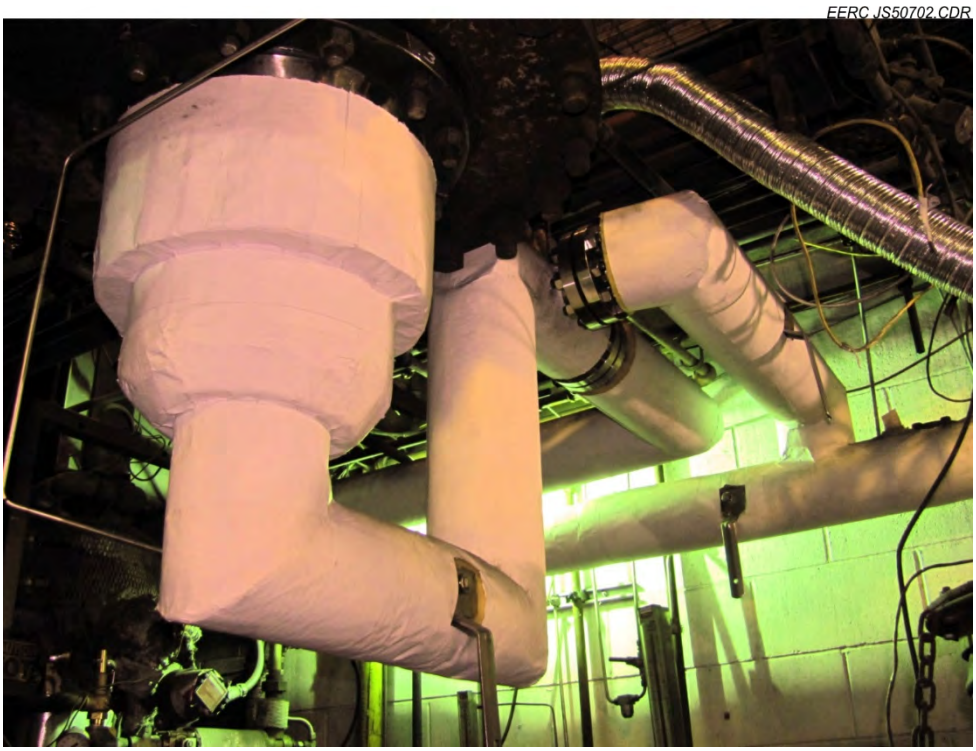

Figure 24. Shift catalyst outlet, also showing compressor bypass and isolation valves.

Compressor, Inlet Filter, and Surge Tank

An existing syngas compressor was used to compress the syngas from the TRDU operating pressure of 120 up to 500 psig for membrane operation. The compressor maintains the pressure of the system over 450°F; therefore, all of the moisture and tars in the system are not condensed prior to membrane separation. Thus the test system more closely represents gasifier syngas from a system operating at 500 psig and without cooling prior to membrane separation. This setup represents a high-efficiency gasification system, and the syngas provided is comparable to the composition of a commercial system.

The syngas compressor was built by RIX Industries as part of a separate project at the EERC. In addition an 18-µm particulate filter was installed at the inlet of the compressor after the sour shift bed to ensure that solids cannot enter the compressor. Plumbing from the newly installed guard filter and all associated plumbing to and from the unit were installed as part of the project. A surge tank is located directly after the compressor that helps to ensure consistent pressure delivery to the membranes and minimizes any potential pressure upsets. The surge tank had been installed at the EERC prior to the start of the project, but trim heaters were added to maintain temperature, and additional piping and flow control instrumentation were also added. A pressure control valve at the outlet of the surge tank sends any excess syngas to the thermal oxidizer, while the remainder is sent to the L-valve recycle and the desulfurization beds. Figure 25 shows the hot-syngas compressor, Figure 26 shows the particulate guard filter, and Figure 27 shows the compressor surge tank.

Figure 25. Hot-syngas compressor skid.

Figure 26. Compressor guard filter.

Figure 27. Compressor surge tank.

A modification was made to convert the compressor cooling system to use Dowtherm A heat-transfer fluid rather than pressurized water. Dowtherm A is a eutectic mixture of two organic compounds, biphenyl and diphenyl oxide, which can be used in temperature ranges from 60° to 750°F at low pressure. This change was made to mitigate hazards of working with pressurized hot water and steam in the cooling system. Additional thermocouples and a pressure transducer were installed to monitor the interstage temperatures on the compressor and in the Dowtherm reservoir, as shown in Figures 28–30. A control valve was also added to the cooling coil in the Dowtherm reservoir to automate temperature control. The coolant pump and coolant flow control valve were reconfigured for use with Dowtherm. The pump seal was also upgraded to prevent deterioration from the organic liquid.

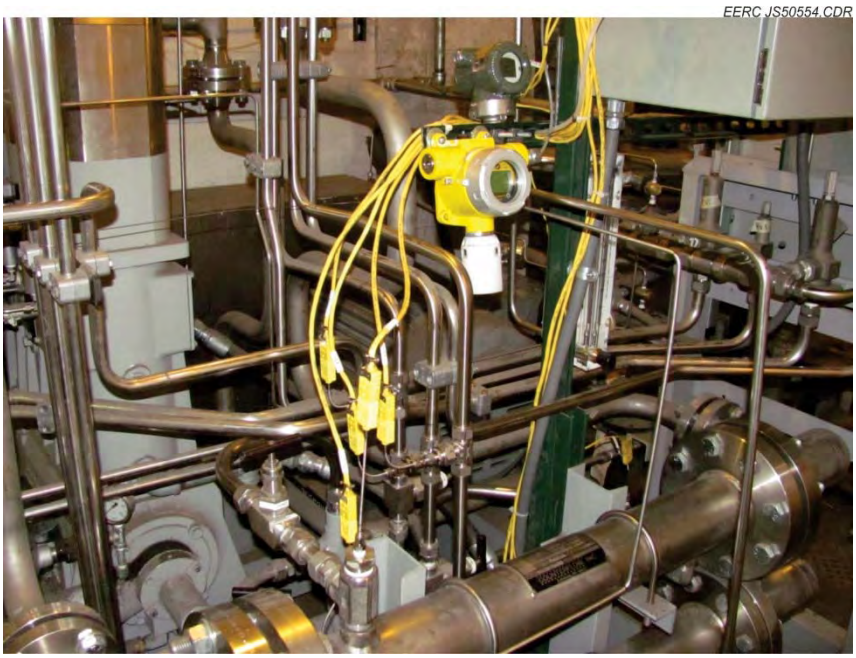

Figure 28. Instrumentation added to the syngas compressor.

Figure 29. Modified coolant pump and control valve.

Figure 30. Dowtherm reservoir and cooling control valve.

Recycle Syngas

Parts were procured and installed to upgrade the TRDU's L-valve to operate on recycled syngas. The L-valve is the horizontal leg located at the bottom of the gasifier, and transport gas is used to move solids across the L-valve and into the mixing zone. Nitrogen is typically used and results in a syngas diluent. The ability to use recycle syngas reduces the amount of nitrogen introduced into the system and, therefore, increases the partial pressure of hydrogen, which is desired for membrane testing. Addition of a syngas compressor to the overall system provides the opportunity to utilize recycle gas in strategic places to reduce nitrogen dilution. Piping was run from the surge tank to the L-valve location, and isolation valves were added so the system could be switched from nitrogen to recycle syngas and back at any time. A control valve and Coriolis meter were added to the line to control the flow of recycle syngas to the L-valve.

Fixed-Bed Desulfurization Reactors

Warm-gas removal of the sulfur from the syngas is a critical component to successful deployment of hydrogen separation membranes. Warm-gas cleanup technologies enable hydrogen membranes to take advantage of the thermal efficiency associated with high-temperature separation. Sulfur will typically poison the membrane material and can temporarily or permanently hinder the flux of hydrogen. To ensure the sulfur requirements were met for the Praxair membrane (<5 ppmv), a dual-bed desulfurization process was employed. Two pressure vessels were procured for fixed-bed desulfurization utilizing RVS-1 sulfur sorbent, manufactured by Clariant. The beds

were used in a dual-bed regeneration scheme, where one bed was online with syngas while the other was being regenerated. Upon saturation with sulfur, the regenerated bed was brought online, and the regeneration process was started on the other bed.

The fixed beds were specified by EERC personnel and procured through a certified pressure vessel manufacturer. The procurement process for the vessels was difficult because it required a material that could withstand both 500 psi and 1100°F, although these requirements were not needed simultaneously. Figure 31 shows the fixed beds as they were received at the EERC. The vessels arrived with thermocouple ports already installed and flanges at each end for loading and unloading of sorbent.

The vessels were each loaded with 460 lb of sorbent, which was enough to allow between 30 and 60 hours of operation between regeneration cycles. After loading, the fixed beds were purged with N_2 and sealed. The beds were then put in place in the gasification tower, and clamshell heaters were fabricated and added to the vessels. During regeneration, the catalyst beds needed to be heated to 1100°F and flooded with nitrogen and air to drive off the sulfur as SO_2. Piping was added to enable syngas feed and regeneration and to enable the utilization of one bed for each process simultaneously. Thermocouples were installed to monitor bed temperatures. The fixed-beds as installed at the EERC are shown in Figure 32. A power and control box was assembled and used to regulate the clamshell heaters during sulfidation and desorption. Automated flow

Figure 31. Sulfur capture fixed beds.

Figure 32. Sulfur capture fixed beds as installed on the second floor of the TRDU tower.

control valves were also installed to facilitate regeneration of the sorbent that were programmed to shut the air off if temperatures over 1200°F were observed. This provided a level of protection for the sorbent.

Control System, Data Acquisition, and Electrical Connections

Control and instrumentation wiring was run in the TRDU tower; electrical power circuits for the fixed-bed heaters and membrane were installed. Verification and calibration of pressure and differential pressure transducers were conducted. The National Instruments control software was modified for the TRDU and compressor control, and monitoring points for the WGS reactor and sulfur removal bed were added. Control points were added for the syngas recycle, surge tank pressure control, and sulfur bed regeneration. Monitoring interfaces were added for the gas analyzers throughout the system. The updated main control screen for the system is shown in Figure 33.

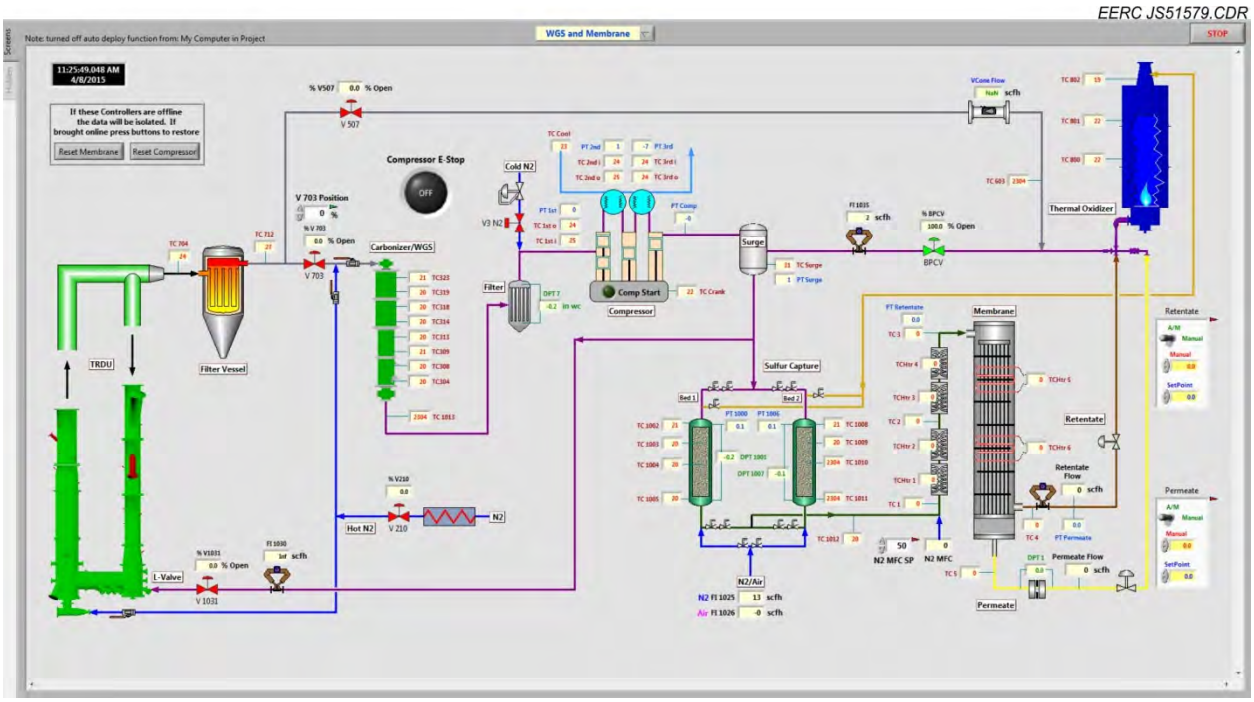

Figure 33. Data-monitoring and control system for integration of the membrane system with the TRDU.

An electrical load survey was compiled and completed to evaluate the available electrical overhead for the demonstration facility. Significant levels of power were needed to operate the electric heaters on the fixed beds, membrane preheaters, and membrane furnace. Electrical upgrades were made to the power system in the TRDU tower to account for the increased electrical load. Equipment costs for the electrical systems were covered by the EERC. A new switchgear was installed along with a new transformer to supply power to the system. Transmission line cutouts and fuses were replaced to appropriate sizes for the new equipment and heaters being installed.

Hazardous Operations Safety Review

All laboratory- and pilot-scale experimental systems at the EERC must undergo a HAZOP review, which involves reviewing the P&IDs, physical design layout, automated controls and software, and standard operating procedures (SOPs) for new equipment as well as reviewing a failure mode and effects analysis (FMEA) table. The review is conducted by the project's principal investigator, engineers, and technical staff who work directly on the project; the principal engineer at the EERC; the EERC safety manager; and other qualified individuals not directly involved in the project. The EERC safety manager must approve all new equipment for safe operation and compliance with University of North Dakota (UND) and EERC safety policies.

All piping and process vessels fabricated for this project operating in excess of 1 atm of gauge pressure are subject to all applicable American Society for Mechanical Engineers boiler and pressure vessel codes and applicable pressure piping codes. All pressurized systems must be

reviewed and approved by the EERC principal engineer prior to use. All field-welded piping is pressure-tested and each weld numbered and inspected. Detailed test sheets are available upon request.

All electrical modifications and installations are required to meet state electrical code. All work must be approved by the EERC on-site licensed electrician, and all work is subject to state inspection. The installation of the equipment for this project required an evaluation of the electrical capacity at the EERC.

The overall system design was reviewed, and preliminary HAZOP review was completed on September 5, 2014. Both an FMEA and a cause-and-effect diagram were used as the tools for the safety review. Several action items were developed as safety concerns were identified that were to be addressed in a follow-on meeting. SOPs were written for the fixed beds, compressor, and membrane system. The second HAZOP review for the system was completed on January 14, 2015, and the system approved for use by the EERC Safety Office. Six main action items identified in the safety reviews were addressed and approved by the EERC Safety Office prior to the start of shakedown testing.

Shakedown Testing

Shakedown testing occurred on the warm-gas cleanup systems and the compressor to ensure proper systems operation and identify any issues or leaks. Warm nitrogen was used to test the TRDU, shift bed, compressor, L-valve recycle, and desulfurization beds. The compressor was shown to perform adequately with the Dowtherm coolant, and pressures of up to 500 psi were achieved at the required temperatures. Proper flows and temperatures were achieved through each of the beds and subsystems, and the system was deemed ready for operation.

The fuel planned to be used for the testing was Antelope coal from Wyoming. This fuel is known to be low in sulfur, and there was some concern that it may take a significant amount of time to sulfide and activate the sour shift catalyst. Therefore, it was decided to bring in a cylinder of liquid H_2S to presulfide the catalyst prior to operation. Sulfidation of the sour shift catalyst occurred using the cylinder of liquid H_2S that was mixed with a high flow of preheated nitrogen. The sulfidation of the catalyst was completed in about 4 hours. The sulfidation process was expected to help the WGS catalyst perform with the high level of shift at the onset of the test.

Task 3 – Hydrogen Separation Testing on the EERC TRDU Gasifier

Two test campaigns were conducted on the TRDU, resulting in 263 hours of testing on the hydrogen separation membrane. Membrane tubes were removed for analysis by Praxair at the end of each campaign. The goal of each campaign was to provide a consistent flow of syngas to the membranes. To achieve that goal, the TRDU was operated at essentially the same conditions throughout, and those conditions were chosen to provide the best-quality syngas with the least risk of system upset in the TRDU. Unfortunately, a few issues over the course of each campaign required repair. Table 4 shows the operating hours that were achieved on the TRDU and the membrane.

Table 4. Hours of Operation

Campaign Number	TRDU Run Number	Dates of Operation	Coal	Hours on Coal	Hours on Membrane
1	P097A	07/05/15 to 07/10/15	Antelope PRB*	108	6
1	P097B	07/16/15 to 07/24/15	Antelope PRB	180	127
2	P098	08/09/15 to 08/15/15	Antelope PRB	122	90
2	P098	08/15/15 to 08/18/15	Freedom Lignite	60	40

* Powder River Basin.

Fuel Preparation and Analysis

PRB coal from the Antelope Mine was used for Campaign 1 and the first part of Campaign 2. North Dakota lignite from the Freedom Mine was used for the second part of Campaign 2. In May, approximately 75 tons total of low-sulfur PRB coal from the Antelope Mine was obtained for the project. This coal was received in three separate truckloads in which the fuel was crushed to less than 2 in. top size and then loaded to 25-ton-capacity fuel bunkers. In July, two 25-ton truckloads of North Dakota lignite from the Freedom Mine were received and nominally air-dried before storage in the 25-ton bunkers. Prior to utilization in the TRDU, the coals were then subjected to secondary crushing to produce a nominal −10-mesh fuel. Composite samples were prepared and were subjected to proximate, ultimate, HHV, and ash x-ray fluorescence analysis (XRFA).

North Dakota lignite has a relatively high sodium content, which can cause bed agglomeration in the TRDU. To reduce the risk of agglomeration, the bed temperature was reduced and kaolin added to the bed during the lignite testing. Previous experience with lignite in the TRDU determined both safe operating temperature and kaolin add rate. Table 5 shows the as-run fuel analyses for both coals tested. The sulfur content of the Antelope fuel was expected to be low in the 0.3%–0.4% range but turned out to be even lower than expected at 0.22%. This resulted in the addition of some elemental sulfur to the TRDU during the beginning of the first campaign in order to increase the activity of the catalyst. The ash chemistry of the two fuels was similar, with the exception of the North Dakota lignite having the higher sodium content.

TRDU Operations and Operational Data

The TRDU was operated over two separate test campaigns in July and August 2015. These tests generated over 470 hours with the TRDU firing either a PRB subbituminous coal or a North Dakota lignite and a total of 320 hours of syngas compression through the recycle compressor. Unscheduled interruptions in operation were the result of HGFV filter issues, including two separate candle filter failures, plus a separate dust leak associated with the filter gaskets during the initial start-up. Initial testing also suggested that the K8-11 sour WGS catalyst would perform better at higher operating temperatures, but filter operation was struggling at the higher filter face velocities. During the gasket replacement, previously tested ceramic SiC candles were added

Table 5. Proximate, Ultimate, HHV, and Ash XRFA Results from Coals Tested in TRDU Membrane Tests

	Antelope PRB	Freedom Lignite
Proximate, as run, wt%		
Moisture	27.6	31.8
Volatile Matter	29.7	27.1
Fixed Carbon	41.0	33.5
Ash	5.7	7.60
Ultimate, as run, wt%		
Hydrogen	6.44	6.43
Carbon	49.6	43.01
Nitrogen	0.75	0.67
Sulfur	0.22	0.91
Oxygen	37.25	41.41
Ash	5.74	7.59
Ash Chemistry, as oxides, wt%		
Silica, SiO_2	25.38	25.89
Aluminum, Al_2O_3	15.36	12.55
Ferric, Fe_2O_3	12.81	8.00
Titanium, TiO_2	1.42	0.54
Phosphorus, P_2O_5	1.37	0.22
Calcium, CaO	25.24	18.85
Magnesium, MgO	7.01	8.22
Sodium, Na_2O	1.01	9.69
Potassium, K_2O	0.33	1.23
Sulfur, SO_3	10.05	14.80
HHV, Btu/lb		
As Run	8470	7224
MF[1]	11693	10600
MAF[2]	12,698	11925

[1] Moisture-free.
[2] Moisture- and ash-free.

to the HGFV in order to increase surface area and lower the filter face velocity. This allowed the rest of the July test campaign to be completed successfully. The first candle failure, which was first detected at the start of the August test, was the result of the shutdown procedure of the July test campaign. This shutdown procedure consists of a controlled burnout of the carbon in the gasifier and HGFV. Normally, the burnout results in a small, short-duration temperature rise on the outlet of the HGFV as the residual carbon is oxidized. This time, the temperature rise was significantly higher and of longer duration than normal. It was later determined that the candle filter had experienced significant bridging between the filters at the top near the tube sheet. This resulted in a localized hot spot that burned a hole through one iron aluminide candle filter. The second candle failure occurred at the end of the test program as one of the SiC ceramic filters catastrophically failed, resulting in the complete loss of HGFV pressure drop.

Average operating conditions for the four main steady-state periods across both campaigns are shown in Table 6. Data include fuel and oxidant feed rates, fuel transport air/nitrogen feed rates, reaction steam feed rates, gasification temperature, and carbon conversion. The gasifier maximum temperature was kept near 950°C for the duration of the test in order to maximize carbon conversion while preventing agglomerates from forming. The fuel feed rate was maintained near 350 lb/hr for the Antelope coal and was run closer to 450 lb/hr for the Falkirk lignite. Carbon conversion for the Antelope PRB fuel ranged from ~90 wt% to as high as 98 wt% as the average mixing zone gasification temperature was increased from 876° to 917°C. During the second test campaign, a North Dakota lignite from the Freedom Mine was tested which is known to have higher levels of sodium in the ash. Steps were taken to avoid bed material agglomeration by adding some kaolinite to the gasifier as bed material and reducing gasifier operating temperature slightly, resulting in the lower carbon conversion of about 91% observed with the lignite fuel.

Table 6 also shows the gas composition at the exit of the TRDU before the WGS catalyst. The CO_2 concentration is typically higher than what is observed in a commercial-scale gasifier because of heat losses caused by the smaller surface area/volume ratio and the need to maintain process temperature. The high nitrogen content shown in the actual product gas composition (and commensurately low heating value) is an artifact of the nitrogen purges and nitrogen gas used for fuel transport. The use of the recycle syngas to the L-valve helped reduce the nitrogen content of the syngas appreciably. Hydrogen concentration was maximized during the start of Campaign 2 as optimum process conditions were determined. The hydrogen concentration dropped when the lignite was run because of less heat content of the fuel. The dry basis H_2S concentration was about 800 ppm during the Antelope tests and increased to 4000 ppm when the lignite was tested. Water sampling was also conducted throughout the testing to determine the moisture content of the syngas. The average moisture was maintained near 30% for the Antelope tests and increased to 35% for the lignite tests, likely due to the higher moisture content of the fuel.

WGS Performance

As was mentioned previously, the WGS catalyst was presulfided with a cylinder of liquid H_2S prior to testing to help with catalyst activity at the start of the test. In spite of this, the shift activity of the catalyst still appeared low at the start of the test. To aid with activity, elemental sulfur was added to the gasifier during P097. Table 7 shows the average operating conditions of the WGS bed and the corresponding syngas concentrations at the inlet and outlet. The catalyst was shown to perform the best at average temperatures above 340°C, indicating kinetic limitations at lower temperatures. The low sulfur content of the Antelope coal was also a factor in limiting the amount of CO shift that occurred. For the low sulfur fuel, the best shift was achieved when testing was run at an average temperature of 390°C, with CO levels dropping to 2.4%. When the Freedom lignite was fired, CO levels of 0.8% were achieved at an average temperature of 350°C, indicating that the higher levels of sulfur significantly increased the activity of the catalyst. The higher moisture levels may have also contributed to increased shift activity.

Table 6. TRDU Steady-State Gasifier Operating Conditions During Praxair Membrane Testing

Test No.:	P097	P097B	P098	P098B
Start:	07/09/2015 0530	07/17/2015 0530	08/11/2015 1200	08/15/2015 1700
End:	07/10/2015 1500	07/24/2015 1100	08/15/2015 1600	08/18/2015 0500
Fuel:	Antelope	Antelope	Antelope	Falkirk
Fuel Type:	PRB Sub.	PRB Sub.	PRB Sub.	ND Lignite
Peak Mix Zone Temperature, °C	933	962	962	902
Avg. Mix Zone Temperature, °C	876	917	905	836
Gasifier Exit Temperature, °C	804	853	833	770
Fuel Feed Rate, lb/hr	405	328	348	441
Airflow, lb/hr	57	53	57	56
O_2 Flow, lb/hr	244	226	226	216
N_2 Flow, lb/hr	349	267	262	263
Steam Flow, lb/hr (at average 300°C)	261	267	268	267
Steam/MAF Fuel Ratio, lb/lb	0.96	1.21	1.10	1.02
O_2/MAF Fuel Ratio, lb/lb	0.95	1.08	0.98	0.87
Recycle Syngas Flow, lb/hr	268	202	205	190
Recirculation Rate, lb/hr	4910	6450	6180	5980
Riser Velocity, ft/s	33.3	34.3	36.3	33.3
Carbon Conversion,[2] wt%	90.6	97.6	95.9	90.7
Product Gas Composition, dry basis, vol%				
H_2	16.3	17.0	18.9	18.1
CO	8.5	9.1	10.3	8.3
CH_4	2.9	2.7	3.1	2.5
C_2H_4/C_2H_6	0.45	0.26	0.59	0.41
CO_2	22.8	26.4	24.9	26.1
N_2	42.7	38.9	33.3	34.8
H_2S	0.086	0.076	0.085	0.400
Total	96.22	94.4	91.2	90.6
H_2/CO Ratio, dry basis	1.92	1.87	1.84	1.18
Product Gas Comp., vol% (wet)				
H_2	12.0	12.4	14.5	13.0
CO	6.2	6.6	7.9	6.0
CH_4	2.1	2.0	2.4	1.8
C_2H_4/C_2H_6	0.33	0.19	0.45	0.29
CO_2	16.7	19.2	19.1	18.7
N_2	31.3	28.3	25.6	25.0
H_2S	0.06	0.06	0.07	0.29
H_2O	31.3	31.3	30.0	35.0
Total	100.00	100.00	100.00	100.00
HHV, Btu/scf	117	116	135	118

Table 7. Average WGS Bed Operating Conditions

	P097	P097B	P098	P098B
Operating Temperature, °C	290	340	390	350
Operating Pressure Range, psig	110	110	110	110
Space Velocity, hr^{-1}	166	180	195	183
Inlet Product Gas Comp., vol% (wet) calc.				
H_2	12.0	12.4	14.5	13.0
CO	6.2	6.6	7.9	6.0
CH_4	2.1	2.0	2.4	1.8
$C_2H_4 + C_2H_6$	0.33	0.19	0.45	0.29
CO_2	16.7	19.2	19.1	18.7
N_2	31.3	28.3	25.6	25.0
H_2S	0.06	0.06	0.07	0.29
H_2O	31.3	31.3	30.0	35.0
Total	100.00	100.00	100.00	100.00
Outlet Product Gas Comp., vol% (wet) calc.				
H_2	14.1	16.6	20.9	19.0
CO	5.2	3.8	2.4	0.8
CH_4	1.5	1.3	1.6	1.3
$C_2H_4 + C_2H_6$	.19	.14	.69	.73
CO_2	19.9	24.2	25.8	25.5
N_2	36.1	30.9	26.6	27.4
H_2S	.06	0.5	0.6	.29
H_2O	23.0	23.0	22.0	25.0
Total	100.0	100.0	100.0	100.0

After the candle filter failure during Test P097B, the shift catalyst was removed from the bed and the fine filter ash screened out. Consultation with the product specifications indicated that the catalyst would not react with oxygen at ambient temperature (assuming it did not have any metal deposits). A test batch was first removed to ensure that catalyst was indeed nonpyrophoric. Upon verification of being able to safely remove the material, the entire catalyst batch was removed, screened, and blown clean with nitrogen. The results achieved for the P098 and P098B testing indicate that the screening was successful.

H_2S Sorbent and Sampling

Sulfur poisoning of palladium membranes is a critical issue in maintaining long-term performance. Adequate sulfur control is, therefore, important. With gasification, sulfur largely takes the form of H_2S and COS. For sulfur control, these tests utilized RVS-1 regenerable sorbent that was developed by DOE and currently manufactured by Clariant. The zinc-based sorbent is capable of capturing both H_2S and COS. The EERC has been successfully using RVS-1 for many years in fixed beds. The RVS-1 was loaded into two downflow fixed beds, referred to as Fixed-Bed 1 and Fixed-Bed 2. Each fixed bed had a sample port located 4 feet up from the exit. These sample locations were used to provide early detection of high H_2S concentrations moving down the fixed bed as it became saturated, thereby preventing high concentrations from breaking through.

A Dräger Accuro pump and Dräger tubes were used to sample the syngas and measure concentrations of H_2S, HCl, NH_3, and C_6H_6. The pump is used to draw a calibrated volume through the measuring tube. For H_2S measurements taken at the 4-foot elevations and exit of the fixed beds, Dräger sample tubes with a range of 0.2–6 ppm (Part Number 8101991) were used. The tubes require a single stroke (n = 1) of the pump to draw the calibrated volume and are direct-reading. No corrections were made for low temperature (32°–60°F) or atmospheric pressure. These tubes have a standard deviation of ±15%–20%. Since the syngas had a significant water concentration, the effects of water on the measurements were a concern. The Dräger documentation for these H_2S sample tubes indicated that gas with a relative humidity <100% has no effect on the measurement since the indicating reaction of this tube is an ion reaction. Also, because of the extraordinarily low solubility of metal sulfides, the upper limit of the humidity is not important with these tubes. To varying degrees, the H_2S sample tubes have a cross-sensitivity to mercaptans, AsH_3, PH_3, and NO_2. HCN changes the color of the entire indicating layer to bright orange but does not affect the H_2S reading.

To draw a syngas sample, a port was opened with a needle valve providing controlled flow of syngas prior to sampling. The sample port tubing was allowed to warm up, removing excess condensates. While warming up, the pump was tested, and then a tube was broken open and inserted into the pump. The tip of the sample tube was placed in the sample port gas stream, and a sample was drawn. At no time was the pressure of the gasifier allowed to drive flow through the sample tube. The indicated concentration was immediately read and recorded following sampling. Tubes were not retained for archival purposes since reactions in the tubes continue over time.

Table 8 shows the average operating conditions for the sulfur sorbent beds. Temperatures were maintained near 300°F for the duration of the testing. The pressure varied with the membrane pressure from 260 to 460 psi. The pressure itself does not impact sorbent performance, but lower pressures result in increased space velocity and lower residence time. Inlet sulfur concentration was near 800 ppm during the Antelope tests and near 4000 ppm during the Freedom lignite tests. Sulfur removal efficiency was approximately 99.75% during the Antelope tests and 99.9% during the lignite tests.

The H_2S concentration in the raw syngas during P097 was observed to be approximately 800 to 900 ppm, as shown in Figure 34. The concentration is similar to what was expected based on syngas calculations. Figure 35 shows the H_2S concentration during P098. The H_2S concentration increased during P098 because of the change in fuel from the Antelope Mine PRB to the Freedom Mine North Dakota lignite. The increase is commensurate with the higher sulfur levels observed in the fuel analysis.

Table 8. Average Sulfur Sorbent Bed Operating Conditions

	P097	P097B	P098	P098B
Operating Temperature, °C	290	305	305	320
Operating Pressure Range, psig	260	260–460	260–460	260–460
Inlet H_2S Concentration, ppmv	850	760	850	3970
Outlet H_2S Conc., ppmv	<2	<2	<2	<4
H_2S Removal Efficiency, %	99.76	99.74	99.76	99.90

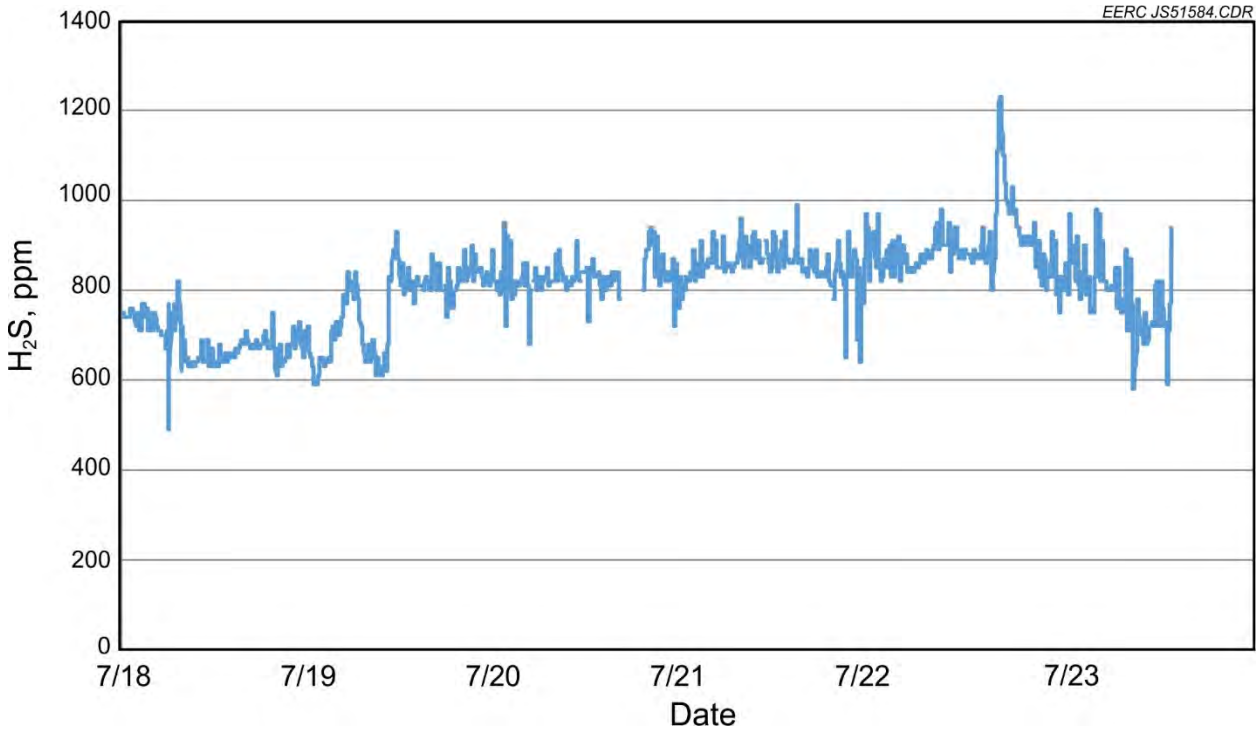

Figure 34. P097B GC H_2S sampling of raw syngas.

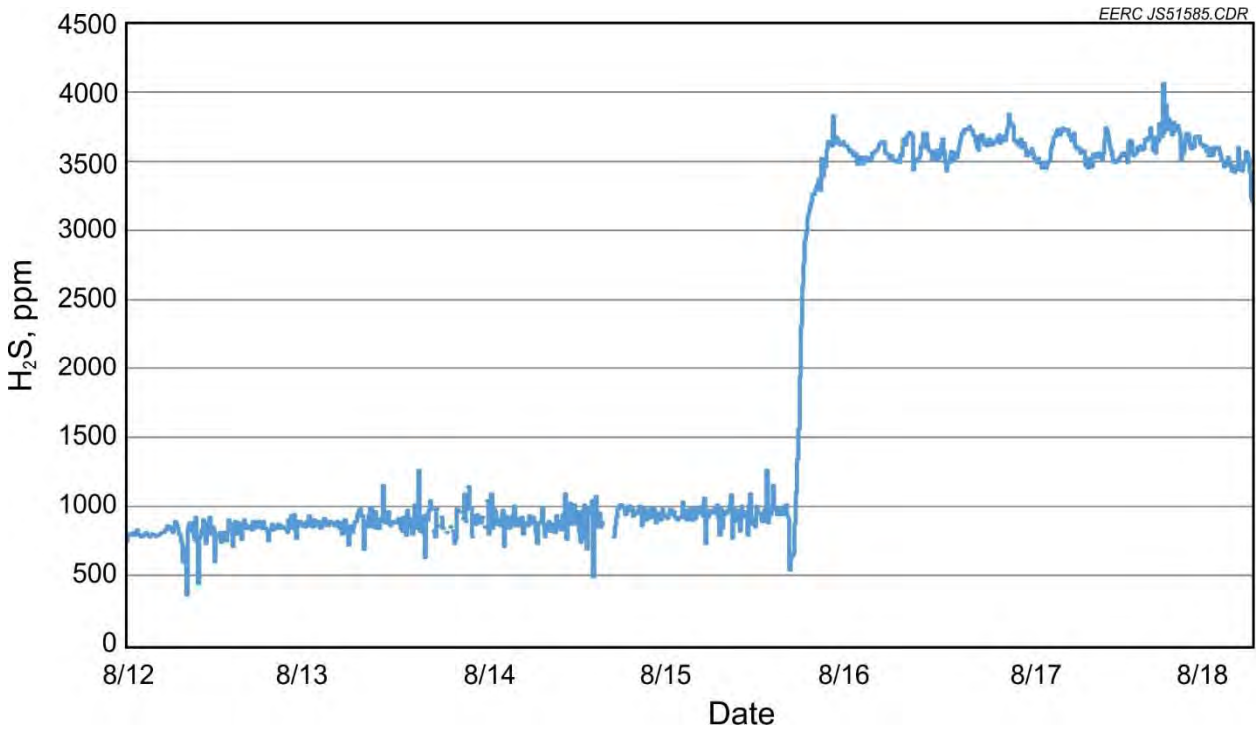

Figure 35. P098 GC H_2S sampling of raw syngas.

The H_2S concentration of the syngas supplied to the membrane was required to be below 5 ppm during the test campaigns. Dräger tube measurements of H_2S concentrations after the fixed-bed desulfurization process for P097A and P097B are shown in Figures 36 and 37, respectively. The majority of the measurements occurred at the 4-foot level in order to provide advanced warning of potential breakthrough. The level of sulfur sent to the membrane is represented by the measurements that were taken at the bed exit. All of these measurements were at 0.5-ppm H_2S or less, indicating that the beds were performing adequately. Fixed-Bed 2 was used for the majority of the P097B testing. The data indicated it could be operated for several days on syngas derived from Antelope coal without experiencing sulfur breakthrough.

Figure 38 represents H_2S sampling data for P098. Fixed-Bed 1 was used until H_2S levels reached about 5.0 ppm at the 4-foot level after about 3 days of operation. Fixed-Bed 2 was then brought online, and Fixed-Bed 1 was regenerated. After the brief system shutdown on August 16 and at the start of the lignite tests, Fixed-Bed 1 was again brought online. Although the H_2S level reached 5 ppm, as sampled at the 4-foot elevation, at no time was the H_2S concentration observed to exceed the 5-ppm limit at the fixed-bed exit. Sulfur levels at the exit remained below 2 ppm when the Antelope coal was fired and reached as high as 4 ppm during the lignite tests.

A few spot checks for other minor and trace species were conducted using Dräger tubes. Sampling for HCl, NH_3, and BTX (total benzene, toluene, and xylene) was performed in a similar manner to H_2S sampling during P097B, and the concentrations can be seen in Table 9. HCl in the syngas is derived from chlorine in the fuel, and ammonia is typically produced from fuel-bound nitrogen. The organic BTX species are derived from the devolatilization of the organic and aromatic species in the coal. The measured concentrations were within expected ranges for each species.

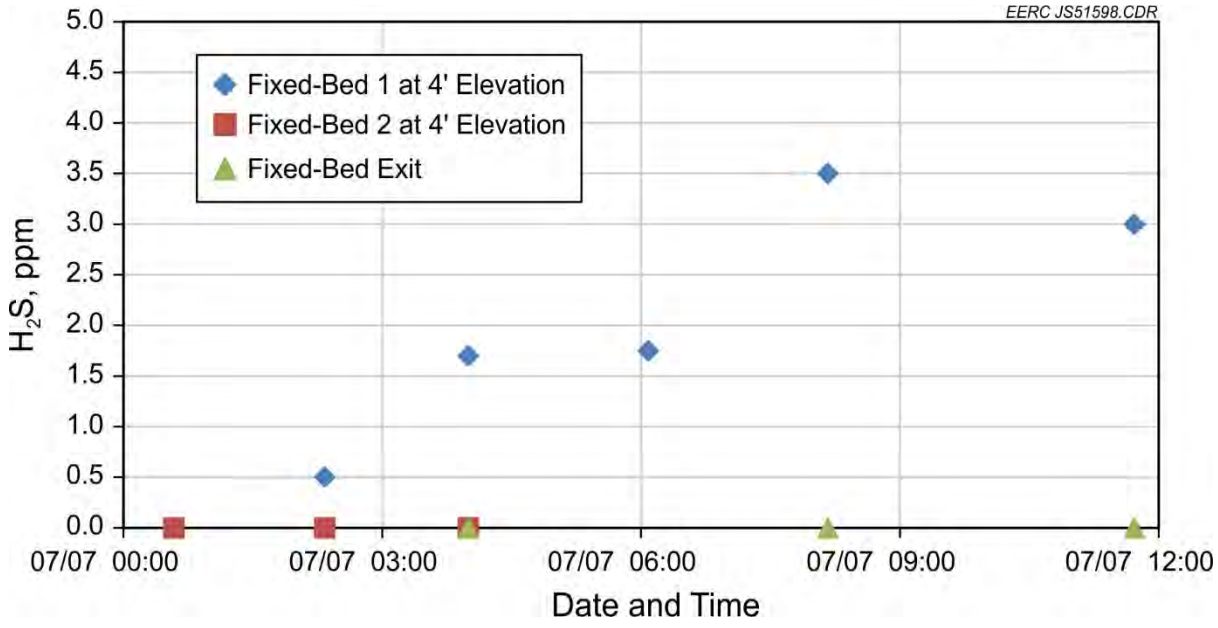

Figure 36. P097A syngas H_2S concentration after sulfur removal.

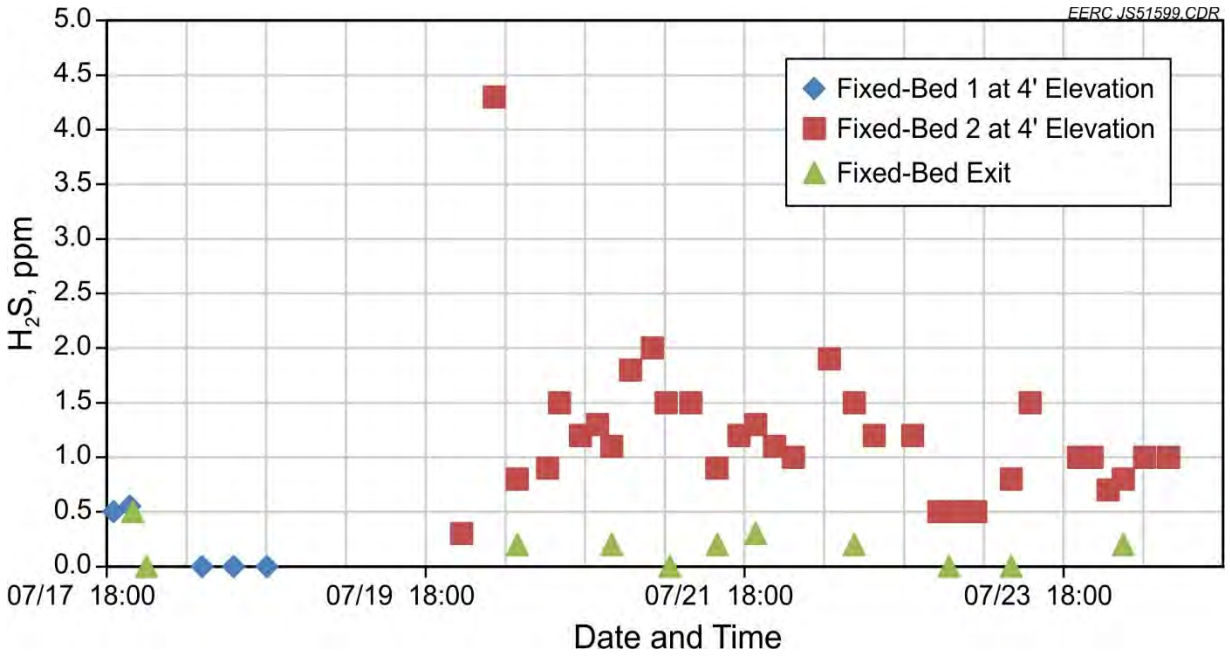

Figure 37. P097B syngas H_2S concentration after sulfur removal.

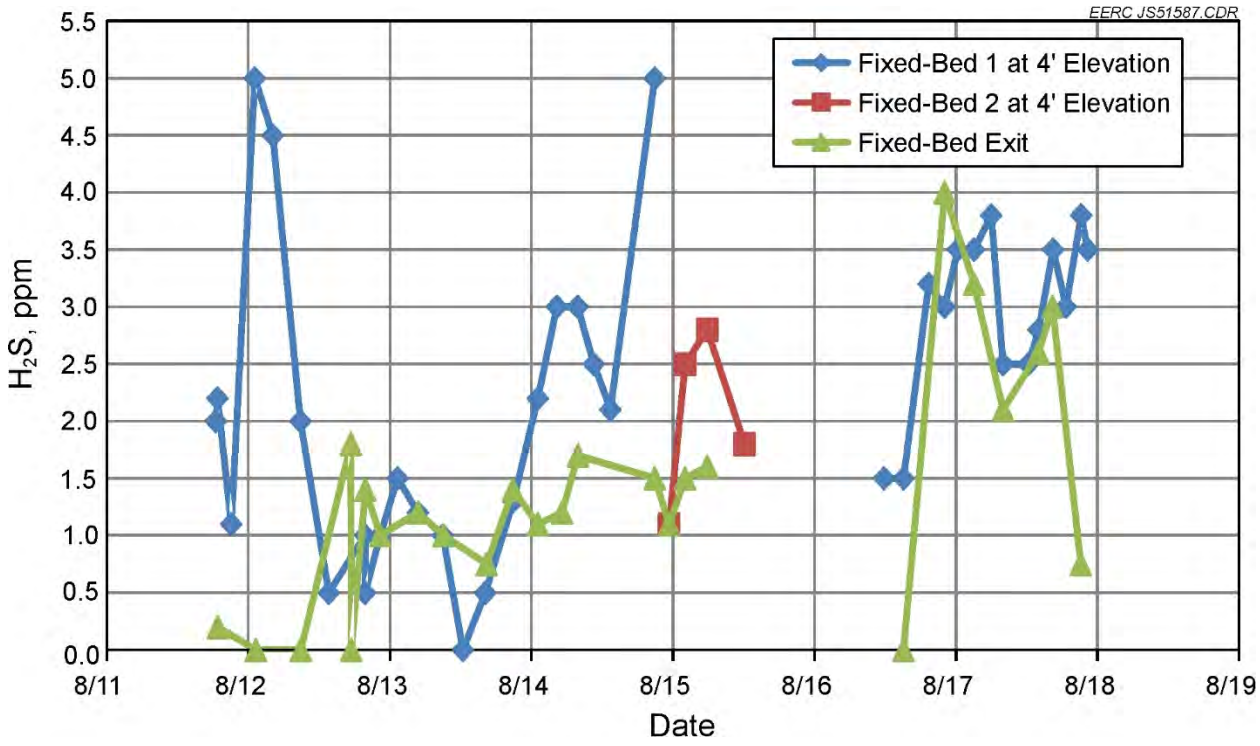

Figure 38. P098 syngas H_2S concentration after sulfur removal.

Table 9. Concentration of Minor and Trace Species in the Syngas

Date/Time	Component	Concentration
07/23/15 0214	HCl	17 ppm
07/23/15 0220	NH_3	0.34%
07/23/15 0225	BTX	210 ppm
07/24/15 0300	HCl	20 ppm
07/24/15 0310	NH_3	0.17%

Membrane Feed Gas Composition

Typically, the TRDU has been operated to evaluate fuel properties and adaptations of the core gasifier design. Diverging from that, these tests required the gasifier to produce syngas for hydrogen membrane testing. The hydrogen membrane testing, in turn, required the addition of a WGS reactor to increase the hydrogen concentration with the trade-off of also increasing CO_2 and reducing CO and water. The analyzers used in the operation of the TRDU are dedicated to sampling the raw syngas as it leaves the system and, therefore, do not sample the higher hydrogen concentration of the shifted gas being fed to the hydrogen membrane. The analyzers employed on the membrane system all require dried gas to prevent condensation problems. As a result, there were no analyzers measuring the gas composition on a wet basis, which would account for the steam diluent. To compensate for this, condenser pots with a dry gas meter were employed to measure the dry gas composition of the feed gas to the membrane. The water collected in the condenser pots was periodically drained and weighed. Combined with the dry gas meter's volumetric data and the dry gas analysis data, periodic wet gas compositions were determined. Figure 39 represents the periodic feed gas concentrations for P097A and P097B on a wet basis. Gaps in the trend lines represent interruptions in feed gas and membrane operation. Hydrogen concentration on a wet basis was near 15% during the P097 tests.

Wet gas compositions for P098 are shown in Figure 40. A leak in one of the quench pot seals was found, and there was an interruption in power, causing a gap in the data. A switch from the Antelope Mine PRB coal to North Dakota lignite from the Freedom Mine was made on August 15, 2015, at 1641. Since changes were being made to the gasifier's operating parameters during the transition, it was decided to take the membrane offline. This also presented an opportunity to flush the membrane with N_2 and then H_2 in an attempt to remove any potential sulfur buildup, possibly improving performance. The higher water concentration seen from 2141 on August 16, 2015, through the end of the testing was caused by the higher moisture content of the lignite. Steam injection flow into the TRDU was reduced toward the end of August 17, 2015. Hydrogen concentration near 20% on a wet basis was achieved during the Antelope coal testing. This level could not be sustained during the lignite testing because of the lower heating value of the fuel; therefore, hydrogen concentration was closer to 17% on a wet basis.

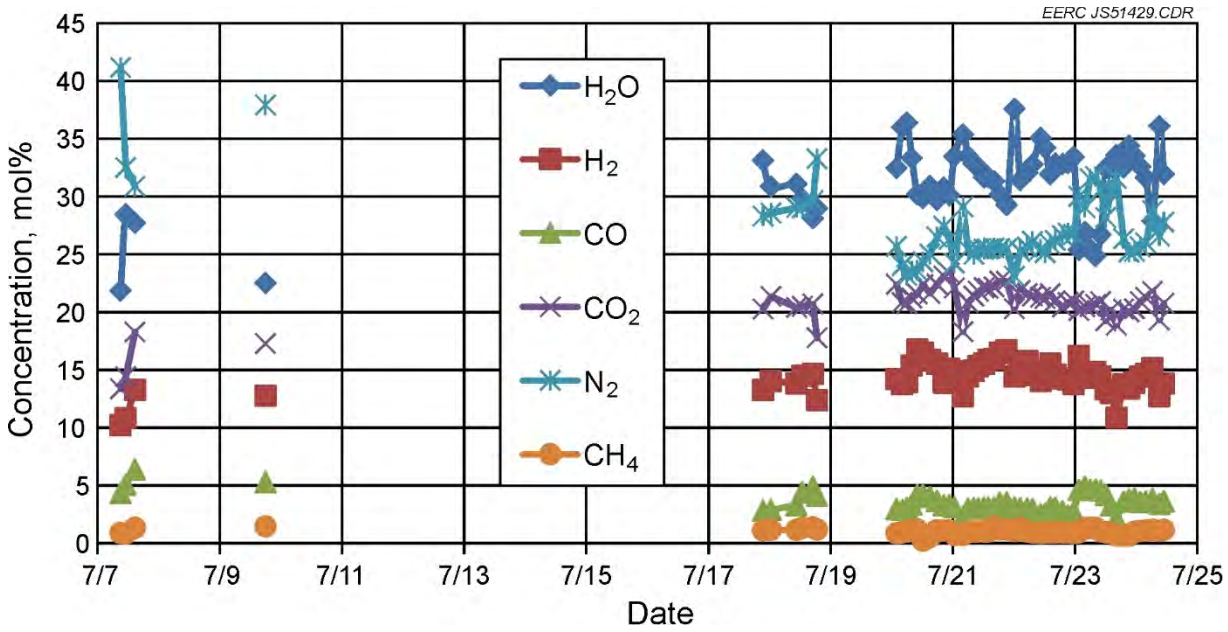

Figure 39. P097A and P097B feed gas concentrations on a wet basis.

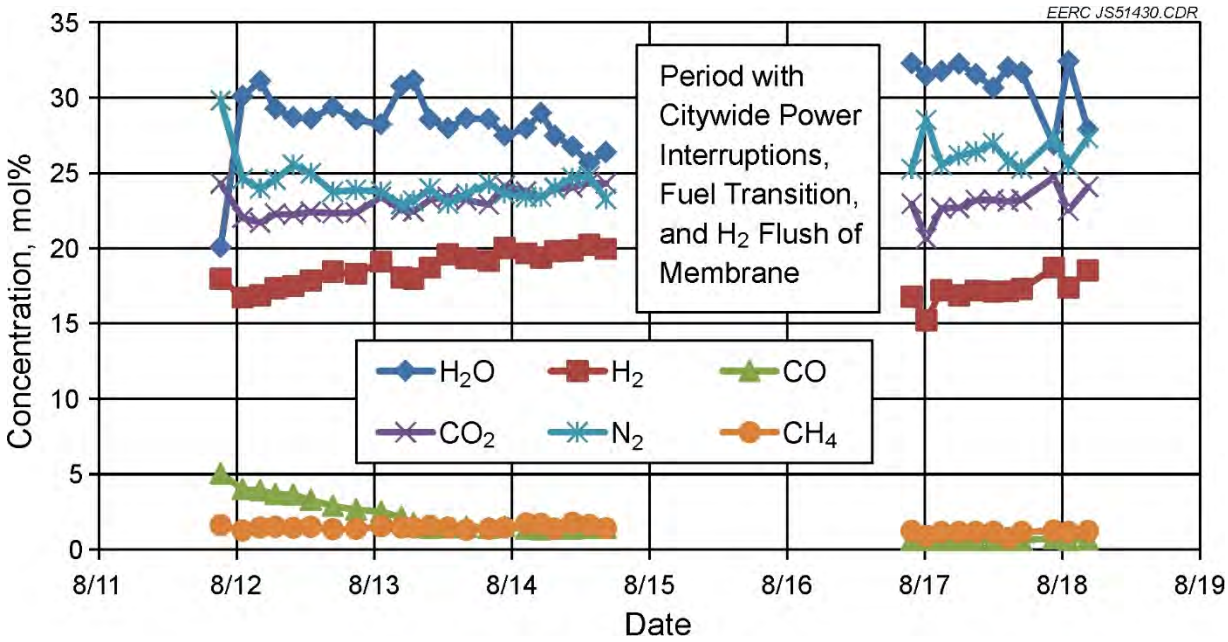

Figure 40. P098 feed gas composition on a wet basis.

Membrane Performance – P097

The gasifier was started on July 6, 2015, and the membrane was brought online the morning of July 7. The system was only online for a few hours before a system leak forced a shutdown. The observed flux was lower than expected; therefore, it was decided to keep the membrane offline until higher hydrogen concentrations could be established in the gasifier. The poor initial performance of the shift catalysts also contributed to this. The membrane was to be brought online on July 10; however, a candle filter failure forced a systemwide shutdown. The system was restarted on July 16, and the gasifier ran until it was shut down in a controlled manner on July 24. The second test period was referred to as P097B. In total, 180 hours of gasifier operation and 127 hours of membrane operation were completed during P097B. On the morning of July 24, a hydrogen enrichment test was performed for approximately 2.5 hours in order to increase the partial pressure of hydrogen to the membrane.

Table 10 shows the average operating conditions observed in the membrane during testing. The membrane temperature was maintained at 400°C for the entire P097 campaign. The supply pressure was started lower at 200 psi and was worked up to about 450 psi by the end of P097. The feed flow ranged from about 4000 to just over 5000 scfh over the course of the testing. The variations were typically caused by operational adjustments to the TRDU that were required to maintain a consistent flow of syngas. The table also shows the resulting retentate and permeate flows and the concentration of hydrogen at all three locations. It should be noted that the retentate and permeate flow are both measured on a wet basis, but the hydrogen measurement on the retentate and permeate was on a dry basis. The feed hydrogen is presented on a wet basis as the analyzer was corrected for moisture based on data obtained from the moisture-sampling pots. The permeate pressure was originally set at 10 psig but was reduced to 5 psig midway through the testing to try to increase flux through the membrane. Additional hydrogen was added to the feed side of the membrane for the last test, at a flow rate of 380 scfh.

Table 11 shows various calculations that were performed to provide estimates of common membrane metrics. The first calculation estimates the flow rate of the leak in the membrane and compares it to the estimated hydrogen flux through the membrane material. The leak rate was estimated based on the hydrogen concentration in the permeate and the permeate flow rate. It was assumed that the gas that leaks through the membrane has the same composition as the feed gas. The wet basis composition of the permeate was taken into account when this calculation was performed since the permeate flow is measured on a wet basis. It can be seen that for all of the P097 tests, except for the last one, the leak rate was greater than the hydrogen flux rate.

Hydrogen partial pressures for the feed stream and permeate stream are calculated, again noting that the wet basis hydrogen concentration was calculated and used to determine the permeate hydrogen partial pressure. The difference in partial pressures is shown as the H_2 dP in the next column. Flux is calculated assuming 18 ft^2 of membrane area and is calculated for two cases. The first case uses only the estimated hydrogen transport flow through the membrane material and is referred to as “without leak.” The second case takes into account the hydrogen that leaked through the membrane with the syngas and is referred to as “with leak.” This is a measure of the total hydrogen in the permeate stream. The permeance is then calculated by dividing by the

Table 10. Average Membrane Operating Characteristics for P097

Test No.	Start Date	Start Time	End Date	End Time	Temp., °C	Supply Pressure, psig	Feed Flow, scfh	Retentate Flow, scfh	Permeate Flow, scfh	Feed H_2 Conc., wet%	Retentate H_2 Conc., dry%	Permeate H_2 Conc., dry%	Permeate Pressure, psig	Addl. H_2 Flow, scfh
P097A-1	7/7/15	0809	7/7/15	1438	407	212	4829	4724	105.2	12.2	16.0	42.6	10.0	0
P097B-1	7/17/15	0053	7/18/15	2052	400	218	4910	4836	74.2	13.8	19.6	46.2	10.0	0
P097B-2	7/18/15	0254	7/18/15	0337	405	303	5147	5026	120.5	13.8	20.4	53.5	10.0	0
P097B-3	7/18/15	0342	7/18/15	0415	406	309	5064	4942	121.7	13.8	20.3	54.2	10.0	0
P097B-4	7/18/15	0420	7/18/15	0549	407	314	5162	5041	120.7	13.8	20.2	49.9	10.0	0
P097B-5	7/18/15	0634	7/18/15	0729	408	331	5093	4963	130.3	13.8	19.4	53.1	10.1	0
P097B-6	7/18/15	0804	7/18/15	1830	403	353	5206	5068	138.6	14.0	19.7	52.9	10.0	0
P097B-7	7/20/15	0037	7/20/15	0240	402	358	3891	3769	122.1	14.4	18.8	56.9	10.0	0
P097B-8	7/20/15	0241	7/20/15	0404	405	361	3929	3803	125.6	14.0	19.5	57.6	10.1	0
P097B-9	7/20/15	0428	7/20/15	0651	407	367	4033	3901	131.8	14.2	20.7	60.2	10.0	0
P097B-10	7/20/15	0743	7/20/15	1242	406	366	4380	4230	150.7	16.6	21.9	63.3	5.0	0
P097B-11	7/20/15	1619	7/20/15	1931	405	359	4074	3954	119.6	15.0	18.5	52.0	5.0	0
P097B-12	7/20/15	2019	7/20/15	2218	406	355	3953	3839	114.5	15.0	18.7	58.4	5.0	0
P097B-13	7/20/15	2234	7/20/15	2304	406	353	4415	4308	107.1	15.1	20.0	62.6	5.0	0
P097B-14	7/20/15	2305	7/21/15	0003	406	351	4612	4494	117.7	15.1	20.3	60.1	5.0	0
P097B-15	7/21/15	0336	7/21/15	0528	403	351	4678	4559	119.0	12.9	17.1	57.5	5.0	0
P097B-16	7/21/15	0821	7/21/15	1426	405	364	4637	4499	138.0	15.4	20.7	62.0	5.0	0
P097B-17	7/21/15	1515	7/21/15	1910	406	358	4546	4408	137.3	16.3	20.9	63.6	5.0	0
P097B-18	7/21/15	1959	7/22/15	0805	405	356	4708	4582	126.0	15.6	20.6	59.8	5.0	0
P097B-19	7/22/15	0837	7/22/15	1752	405	453	5190	5008	182.5	14.1	19.4	62.3	5.0	0
P097B-20	7/23/15	0118	7/23/15	0603	407	440	4429	4259	169.8	15.0	18.0	58.6	5.0	0
P097B-21	7/23/15	1705	7/24/15	0800	403	446	4424	4262	161.6	15.0	18.3	63.1	5.0	0
P097B-22	7/24/15	0847	7/24/15	1100	399	439	4764	4513	250.3	21.1	29.2	79.7	5.0	380

Table 11. Calculated Membrane Performance Parameters for P097

Test No.	Estimated Permeate Leak Flow, scfh	Estimated Hydrogen Flux Flow, scfh	Feed H_2 Partial Pressure, psia	Permeate H_2 Partial Pressure, psia	H_2, dP	H_2 Flux, without leak, scfh/ft^2	H_2 Flux, with leak, scfh/ft^2	H_2 Permeance, without leak, ft^3/(ft^2·hr·dP)	H_2 Permeance, with leak, ft^3/(ft^2·hr·dP)	Flux at 100 psi dP, without leak, ft^3/(ft^2·hr)	Flux at 100 psi dP, with leak, ft^3/(ft^2·hr)	Flux at 100 psi dP Sievert's Law, without leak	Flux at 100 psi dP Sievert's Law, with leak	H_2 Recovery, without leak, %	H_2 Recovery, with leak, %
P097A-1	79.4	25.8	27.6	8.3	19.3	1.43	2.0	0.074	0.102	7.4	10.2	4.14	5.69	4.4	6.1
P097B-1	56.0	18.2	32.1	8.6	23.5	1.01	1.4	0.043	0.061	4.3	6.1	2.53	3.61	2.7	3.9
P097B-2	81.3	39.2	43.8	10.3	33.5	2.18	2.8	0.065	0.084	6.5	8.4	4.38	5.63	5.3	6.8
P097B-3	81.2	40.5	44.7	10.5	34.2	2.25	2.9	0.066	0.084	6.6	8.4	4.48	5.72	5.6	7.1
P097B-4	86.3	34.4	45.3	9.5	35.8	1.91	2.6	0.053	0.072	5.3	7.2	3.58	4.83	4.7	6.3
P097B-5	88.5	41.8	47.6	10.3	37.4	2.32	3.0	0.062	0.080	6.2	8.0	4.30	5.55	6.0	7.7
P097B-6	92.9	45.6	51.5	10.5	41.1	2.53	3.3	0.062	0.079	6.2	7.9	4.40	5.66	6.0	7.8
P097B-7	78.7	43.4	53.7	11.1	42.6	2.41	3.0	0.057	0.071	5.7	7.1	4.12	5.20	8.2	10.4
P097B-8	82.0	43.6	52.5	10.9	41.7	2.42	3.1	0.058	0.073	5.8	7.3	4.20	5.30	8.3	10.5
P097B-9	82.5	49.2	54.1	11.4	42.6	2.73	3.4	0.064	0.079	6.4	7.9	4.71	5.84	8.7	10.8
P097B-10	87.5	63.2	63.1	10.2	52.9	3.51	4.3	0.066	0.082	6.6	8.2	5.06	6.22	9.0	11.1
P097B-11	83.0	36.7	55.9	8.1	47.8	2.04	2.7	0.043	0.057	4.3	5.7	3.01	4.03	6.6	8.8
P097B-12	70.8	43.7	55.4	9.3	46.0	2.43	3.0	0.053	0.066	5.3	6.6	3.79	4.71	7.9	9.9
P097B-13	62.9	44.2	55.3	9.9	45.5	2.45	3.0	0.054	0.066	5.4	6.6	3.91	4.75	7.1	8.6
P097B-14	72.8	44.9	55.2	9.4	45.8	2.49	3.1	0.054	0.068	5.4	6.8	3.91	4.87	6.9	8.5
P097B-15	76.2	42.9	47.3	8.7	38.5	2.38	2.9	0.062	0.076	6.2	7.6	4.16	5.11	7.8	9.6
P097B-16	81.7	56.3	58.4	9.8	48.6	3.13	3.8	0.064	0.079	6.4	7.9	4.76	5.82	8.2	10.0
P097B-17	78.0	59.3	60.8	10.3	50.5	3.30	4.0	0.065	0.079	6.5	7.9	4.93	5.98	8.4	10.2
P097B-18	78.3	47.7	57.7	9.4	48.3	2.65	3.3	0.055	0.069	5.5	6.9	4.01	5.03	6.9	8.7
P097B-19	107.8	74.8	66.0	9.7	56.3	4.16	5.0	0.074	0.089	7.4	8.9	5.68	6.84	10.5	12.6
P097B-20	107.5	62.3	68.3	9.1	59.2	3.46	4.4	0.058	0.074	5.8	7.4	4.52	5.69	10.6	13.4
P097B-21	87.1	74.5	69.0	10.7	58.3	4.14	4.9	0.071	0.083	7.1	8.3	5.63	6.61	11.3	13.3
P097B-22	85.8	164.4	95.7	13.9	81.8	9.14	9.8	0.112	0.120	11.2	12.0	10.33	11.10	15.8	17.0

partial pressure differential, and the theoretical flux at 100 psi dP is calculated by multiplying by 100. This theoretical flux is derived from Fick's law. A second theoretical flux measurement was also calculated using Sievert's law by evaluating difference of the square root of the partial pressures. For the Sievert's law transport mechanism, the driving force at 100-psi differential pressure changes based on the absolute pressure of the feed and permeate; therefore, it was assumed that the permeate stream was pure hydrogen at atmospheric pressure. Finally, the hydrogen recovery is calculated without and with the leak in the system.

The measurements indicated that the observed and theoretical hydrogen flux values were lower than expected for all cases. Hydrogen recovery was also lower than expected. During testing, the reason for the low flux numbers was not immediately known. Sulfur levels at the fixed-bed exit remained below 0.5 ppm for the entire test. Increased flux and permeance were observed during Test P097B-22, indicating that increased partial pressure differential may have a positive impact on membrane performance. This also indicates that increased hydrogen concentration in the feed may help to alleviate the impact of a potential contaminant that is inhibiting flux.

System Turnaround and Replacement of Membrane Tubes

Standard TRDU maintenance was performed between the test campaigns, which consists of removing the bed material from the reactor and performing standard cleaning and maintenance checks. All tubular membrane elements used in P097 were removed and replaced with new ones for Test Campaign P098. One tube as observed to be broken upon disassembly. It is not known whether the tube failed in service or was broken during disassembly. Based on this, the effective surface area of the membrane elements was assumed to be 18 ft^2 while in service. There were no apparent cracks or holes in any of the elements. No visible coking or dust loading was noticed on the elements or inside the pressure vessel. The tubular membrane elements were sent to Praxair for further postrun analysis.

Membrane Performance – P098

Testing for campaign P098 commenced on August 12, 2015, and was shut down on August 18, 2015, because of a candle filter failure in the HGFV. Parametric testing was conducted on the membrane system during the operation that evaluated the impact of temperature, pressure, and flow rate on the membrane performance. Table 12 shows the operating conditions of the membrane for P098. Tests P098-1 through P098-10 utilized a target temperature of 400°C. Pressure changes from 260 to 450 psig were also performed in a conservative, incremental manner through Tests P098-1 through P098-10. Flows were also increased as the pressure increased in an effort to determine the operational limits of the combined gasifier and membrane systems. It was found that the gasifier's syngas production peaked at about 5800 scfh on the Antelope Mine PRB coal. As testing progressed, the syngas production capacity was reduced to approximately 5200 scfh when the fuel was changed to Freedom Mine lignite.

Tests P098-26 and P098-27 (not shown on the table) consisted of a nitrogen purge of the membrane for a period of approximately 4 hours, followed by a bottle gas hydrogen purge. It was decided to use H_2 in attempt to observe the potential recovery effects of adding hydrogen to the membrane without impurities. The hydrogen flow rate was set to approximately 50 scfh with a supply pressure of 50 psig for a little over 12 hours.

Table 12. Average Membrane Operating Characteristics for P098

Test No.	Start Date	Start Time	End Date	End Time	Temp., °C	Supply Pressure, psig	Feed Flow, scfh	Retentate Flow, scfh	Permeate Flow, scfh	Feed H_2 Conc., wet %	Retentate H_2 Conc., dry %	Permeate H_2 Conc., dry %	Permeate Pressure, psig	Addl. H_2 Flow, scfh
P098-1	8/11/15	2330	8/12/15	0130	402.7	259.6	2806	2601	205	25.3	26.3	80.9	4.01	330
P098-2	8/12/15	0300	8/12/15	0500	401.6	275.0	2998	2786	213	26.5	27.8	80.7	4.01	380
P098-3	8/12/15	0830	8/12/15	1030	403.1	306.3	4150	3991	160	17.8	21.9	68.4	4.00	0
P098-4	8/12/15	1130	8/12/15	1330	401.2	334.5	4280	4101	179	18.2	21.6	68.9	4.00	0
P098-5	8/12/15	1400	8/12/15	1723	401.3	352.9	4280	4100	179	18.6	22.0	73.2	4.00	0
P098-6	8/12/15	1730	8/12/15	2300	400.8	398.9	4769	4541	228	19.1	21.9	73.2	4.00	0
P098-7	8/13/15	0000	8/13/15	0300	400.8	394.1	4270	4044	226	18.8	21.9	74.2	4.00	0
P098-8	8/13/15	0540	8/13/15	0743	400.8	443.7	4213	3963	250	18.8	21.4	73.8	4.00	0
P098-9	8/13/15	0830	8/13/15	1030	400.3	450.8	4759	4494	265	19.9	22.1	74.9	4.00	0
P098-10	8/13/15	1130	8/13/15	1330	398.4	450.3	5807	5526	280	20.5	21.2	76.8	4.00	0
P098-11	8/13/15	1500	8/13/15	1640	425.8	448.3	5779	5437	342	20.2	21.2	80.9	4.00	0
P098-12	8/13/15	1805	8/13/15	2205	426.0	426.6	5787	5458	328	20.1	21.7	81.4	4.00	0
P098-13	8/13/15	2040	8/13/15	2314	425.5	398.6	5817	5514	303	20.4	22.2	82.0	4.00	0
P098-14	8/14/15	0110	8/14/15	0310	425.8	374.3	5727	5457	270	20.3	22.5	81.6	4.00	0
P098-15	8/14/15	0345	8/14/15	0615	425.8	350.7	5689	5442	247	20.1	23.5	82.0	4.00	0
P098-16	8/14/15	0730	8/14/15	0930	424.8	325.0	5742	5532	210	20.3	24.2	81.9	4.00	0
P098-17	8/14/15	1000	8/14/15	1200	425.2	302.3	5723	5533	191	20.9	24.2	82.2	4.00	0
P098-18	8/14/15	1230	8/14/15	1430	426.0	277.0	5653	5484	169	21.0	24.2	82.4	4.00	0
P098-19	8/14/15	1500	8/14/15	1800	426.0	250.6	5680	5538	142	20.8	21.6	81.2	4.00	0
P098-20	8/14/15	2121	8/15/15	0220	425.4	449.8	5688	5371	317	20.5	20.5	81.2	4.00	0
P098-21	8/15/15	0300	8/15/15	0530	427.7	449.5	5048	4745	303	20.4	21.5	80.4	4.00	0
P098-22	8/15/15	0600	8/15/15	0800	426.9	451.6	4372	4078	294	20.4	21.5	79.8	4.00	0
P098-23	8/15/15	0830	8/15/15	1030	422.2	459.7	3349	3080	268	20.1	19.8	77.3	4.00	0
P098-24	8/15/15	1150	8/15/15	1350	423.4	448.6	2274	2028	246	20.3	17.7	75.9	4.00	0
P098-25	8/15/15	1415	8/15/15	1530	424.5	448.9	1712	1485	227	20.1	16.8	73.7	4.00	0
P098-28	8/16/15	1530	8/16/15	1739	425.1	251.2	5117	5009	108	17.9	23.5	81.2	4.00	0
P098-29	8/16/15	1930	8/16/15	2130	425.2	275.8	5057	4934	123	18.5	25.0	81.2	3.99	0
P098-30	8/16/15	2200	8/17/15	0000	424.6	300.3	5179	5041	138	18.0	22.2	80.8	4.00	0
P098-31	8/17/15	0030	8/17/15	0230	424.5	323.5	5191	5038	153	17.5	25.2	81.0	4.00	0
P098-32	8/17/15	0245	8/17/15	0545	424.5	352.4	5206	5038	168	17.2	24.9	80.2	4.00	0
P098-33	8/17/15	0625	8/17/15	0825	424.8	374.6	5135	4958	177	17.0	24.4	79.8	4.00	0
P098-34	8/17/15	0915	8/17/15	1115	425.1	403.8	5243	5041	202	17.3	21.9	79.7	4.00	0
P098-35	8/17/15	1200	8/17/15	1400	425.7	425.2	5157	4938	218	17.2	21.9	79.5	4.00	0
P098-36	8/17/15	1430	8/17/15	1702	425.9	452.2	5257	5017	241	17.4	21.4	79.6	4.00	0
P098-37	8/17/15	2000	8/17/15	2237	425.1	451.1	5768	5519	248	18.7	21.4	79.4	4.00	0
P098-38	8/17/15	2300	8/18/15	0100	427.0	452.5	4999	4747	252	17.3	20.9	79.9	4.00	0
P098-39	8/18/15	0130	8/18/15	0400	427.0	448.6	4021	3780	241	18.5	20.9	79.2	4.00	0

Table 13 shows various calculations that were performed to provide estimates of common membrane metrics. The calculations were performed in the same manner that was described for Test P097 and include estimations of the leak through the membrane. The hydrogen partial pressure delivered to the membrane for this set of tests was generally increased as compared to P097. As a result, the observed flux and permeance were also higher. The increased partial pressure was due to the increased hydrogen content of the syngas that was achieved through optimization of the gasifier operation and improved WGS performance. As expected, the hydrogen flux was greatest at high flow conditions with a high driving force of hydrogen. A surface area of 18 ft^2 was assumed for the membrane area when the flux calculations were performed. Hydrogen recovery was maximized at the lowest flow condition, which is a typical trait for hydrogen separation membranes. The average flux observed for the testing was still significantly lower than expected for these tests. Upon completion of the test, the membrane tubes were again removed and sent to Praxair for analysis to determine the root cause of the low flux numbers.

A graphical representation of the parametric pressure, temperature, and flow parameters tested on the membrane is shown in Figure 41. The pressure was varied throughout the test period. The temperature was increased after Test 10 from 400° to 425°C and held there for the remainder of the test conditions. The flow was intentionally varied periodically in order to test conditions of highest flux and highest recovery. Figure 42 shows the flux and permeance that were achieved by test number. The pressure and, in turn, the H_2 partial pressure difference played a strong role in the flux of the membrane. Also, the increase in flows had a large impact on the permeation. Temperature had a lesser impact on the permeance, but it was still a good predictor of increased permeance and flux.

Figure 43 shows the increasing hydrogen flux as flow across the membrane assembly is increased while the pressure is held at 450 psig and the temperature is held at 425°C. The partial pressure differential shows good uniformity for these data. These data were acquired roughly midway through the campaign. In contrast, the data represented in Figure 44 were from the final four tests conducted on syngas. The flux of the tests at the end of the campaign was lower than from the middle of the campaign. Figure 45 compares the permeance of the midrun tests with the final four syngas-based tests. The permeance at the end of the campaign showed slightly lower values at similar conditions, indicating the potential for sulfur degradation.

Figure 46 shows the increasing hydrogen flux as the pressure to the membrane assembly is increased while the temperature is held at 425°C and approximately 5000 scfh of syngas flows through the membrane assembly. The trend of increasing flux with increasing pressure is relatively uniform for these data.

Figure 47 shows the increasing hydrogen flux as the syngas delivery to the membrane assembly is increased while the temperature is held at 425°C and approximately 5500 scfh of syngas flows through the membrane assembly. The test runs represent P098-11 through P098-19. The partial pressure differential and flux trend uniformly for these data.

Table 13. Calculated Membrane Performance Parameters for P098

Test No.	Estimated Permeate Leak Flow, scfh	Estimated Hydrogen Flux Flow, scfh	Feed H_2 Partial Pressure, psia	Permeate H_2 Partial Pressure, psia	H_2, dP	H_2 Flux, without leak, scfh/ft^2	H_2 Flux, with leak, scfh/ft^2	H_2 Permeance, without leak, ft^3/(ft^2·hr·dP)	H_2 Permeance, with leak, ft^3/(ft^2·hr·dP)	Flux at 100 psi dP, without leak, ft^3/(ft^2·hr)	Flux at 100 psi dP, with leak, ft^3/(ft^2·hr)	Flux at 100 psi dP Sievert's Law, without leak	Flux at 100 psi dP Sievert's Law, with leak	H_2 Recovery, without leak, %	H_2 Recovery, with leak, %
P098-1	74.1	131.2	69.4	13.7	55.7	7.29	8.3	0.131	0.150	13.1	15.0	10.78	12.32	7.9	9.0
P098-2	80.2	132.7	76.8	13.5	63.3	7.37	8.6	0.116	0.135	11.6	13.5	9.93	11.52	7.6	8.8
P098-3	80.7	79.0	57.1	10.9	46.2	4.39	5.2	0.095	0.112	9.5	11.2	7.07	8.36	3.9	4.6
P098-4	89.5	89.2	63.6	11.0	52.5	4.95	5.9	0.094	0.112	9.4	11.2	7.30	8.63	4.2	5.0
P098-5	80.2	98.9	68.4	11.9	56.5	5.50	6.3	0.097	0.112	9.7	11.2	7.81	8.99	4.5	5.1
P098-6	101.4	126.5	79.1	12.0	67.1	7.03	8.1	0.105	0.121	10.5	12.1	8.87	10.22	5.0	5.8
P098-7	100.1	126.3	76.9	12.0	64.9	7.01	8.1	0.108	0.124	10.8	12.4	9.06	10.41	5.8	6.6
P098-8	112.4	137.5	86.2	11.9	74.4	7.64	8.8	0.103	0.118	10.3	11.8	8.96	10.33	6.4	7.4
P098-9	112.7	152.3	92.5	12.3	80.1	8.46	9.7	0.106	0.121	10.6	12.1	9.49	10.89	5.9	6.8
P098-10	112.2	168.2	95.4	12.8	82.7	9.34	10.6	0.113	0.128	11.3	12.8	10.33	11.74	5.2	6.0
P098-11	115.3	227.1	93.3	13.7	79.7	12.62	13.9	0.158	0.175	15.8	17.5	14.49	15.98	6.8	7.5
P098-12	107.8	220.5	88.6	13.8	74.8	12.25	13.5	0.164	0.180	16.4	18.0	14.73	16.17	6.6	7.2
P098-13	95.5	207.2	84.3	14.0	70.3	11.51	12.6	0.164	0.179	16.4	17.9	14.49	15.86	6.0	6.6
P098-14	87.3	182.5	78.9	13.9	65.1	10.14	11.1	0.156	0.171	15.6	17.1	13.46	14.77	5.4	5.9
P098-15	78.4	169.0	73.3	14.0	59.4	9.39	10.3	0.158	0.173	15.8	17.3	13.33	14.57	5.0	5.5
P098-16	65.9	144.3	69.1	14.0	55.0	8.02	8.8	0.146	0.159	14.6	15.9	12.03	13.15	4.2	4.6
P098-17	58.6	132.2	66.4	14.2	52.2	7.34	8.0	0.141	0.154	14.1	15.4	11.47	12.53	3.8	4.1
P098-18	51.8	117.3	61.3	14.2	47.1	6.51	7.1	0.138	0.151	13.8	15.1	10.98	12.00	3.4	3.7
P098-19	46.2	95.8	55.1	13.9	41.3	5.32	5.9	0.129	0.142	12.9	14.2	9.85	10.84	2.8	3.1
P098-20	103.4	213.4	95.1	13.8	81.2	11.86	13.0	0.146	0.160	14.6	16.0	13.47	14.81	6.3	7.0
P098-21	102.5	200.4	94.6	13.7	81.0	11.13	12.3	0.137	0.152	13.7	15.2	12.64	13.96	6.8	7.5
P098-22	102.1	191.5	95.0	13.5	81.5	10.64	11.8	0.131	0.145	13.1	14.5	12.00	13.31	7.5	8.3
P098-23	103.2	165.2	95.3	13.0	82.4	9.18	10.3	0.111	0.125	11.1	12.5	10.20	11.48	8.7	9.8
P098-24	100.1	146.0	93.9	12.6	81.3	8.11	9.2	0.100	0.114	10.0	11.4	9.05	10.31	11.6	13.2
P098-25	99.7	127.8	93.1	12.2	80.9	7.10	8.2	0.088	0.101	8.8	10.1	7.89	9.13	13.9	16.1
P098-28	33.9	74.4	47.7	13.9	33.8	4.13	4.5	0.122	0.132	12.2	13.2	8.91	9.63	2.5	2.7
P098-29	38.9	84.3	53.8	13.9	39.9	4.68	5.1	0.117	0.127	11.7	12.7	8.89	9.65	2.8	3.1
P098-30	45.6	92.7	56.8	13.6	43.1	5.15	5.6	0.119	0.130	11.9	13.0	9.18	10.00	3.1	3.4
P098-31	51.2	101.7	59.3	13.5	45.8	5.65	6.1	0.123	0.134	12.3	13.4	9.62	10.47	3.5	3.9
P098-32	58.3	109.5	63.2	13.3	49.8	6.09	6.6	0.122	0.133	12.2	13.3	9.70	10.59	3.9	4.2
P098-33	62.0	115.3	66.2	13.3	52.9	6.40	7.0	0.121	0.132	12.1	13.2	9.76	10.65	4.1	4.5
P098-34	70.4	131.6	72.4	13.3	59.1	7.31	8.0	0.124	0.135	12.4	13.5	10.30	11.25	4.5	5.0
P098-35	77.9	140.2	75.5	13.2	62.3	7.79	8.5	0.125	0.137	12.5	13.7	10.55	11.55	5.0	5.5
P098-36	85.5	155.2	81.1	13.2	67.9	8.62	9.4	0.127	0.139	12.7	13.9	10.99	12.05	5.4	6.0
P098-37	85.4	163.1	87.1	13.5	73.7	9.06	9.9	0.123	0.135	12.3	13.5	10.96	12.03	4.9	5.3
P098-38	89.2	163.0	80.8	13.2	67.6	9.05	9.9	0.134	0.147	13.4	14.7	11.59	12.69	6.0	6.6
P098-39	84.3	156.5	85.6	13.4	72.3	8.70	9.6	0.120	0.132	12.0	13.2	10.64	11.70	6.8	7.5

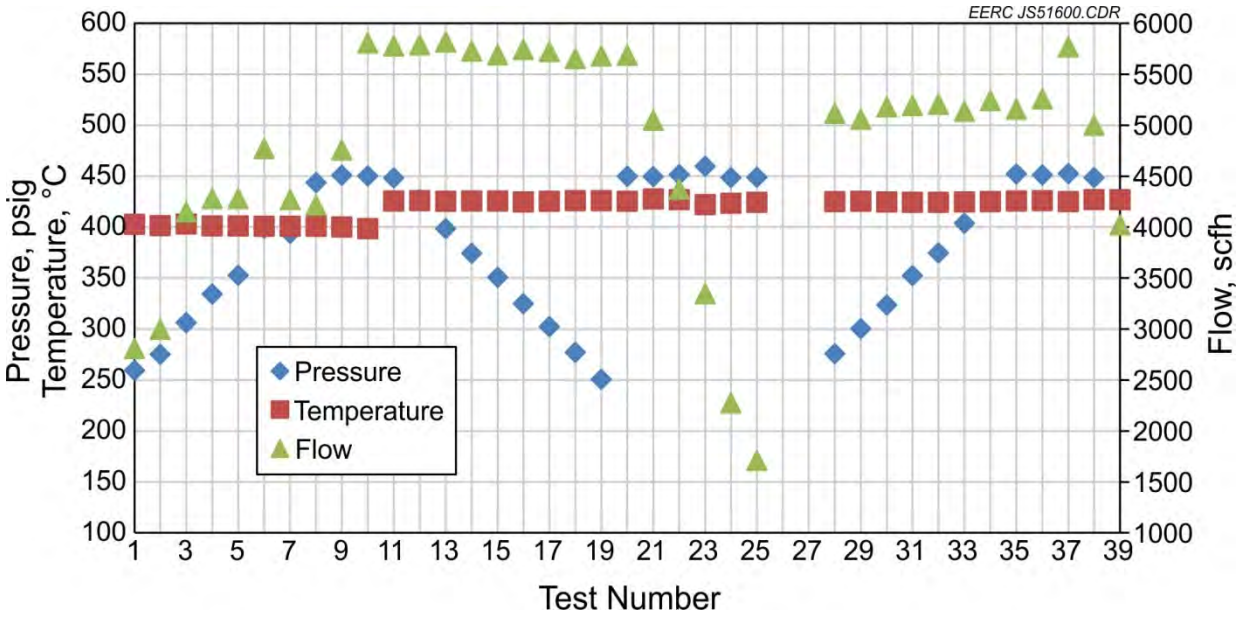

Figure 41. P098 pressure, temperature, and flow by test number.

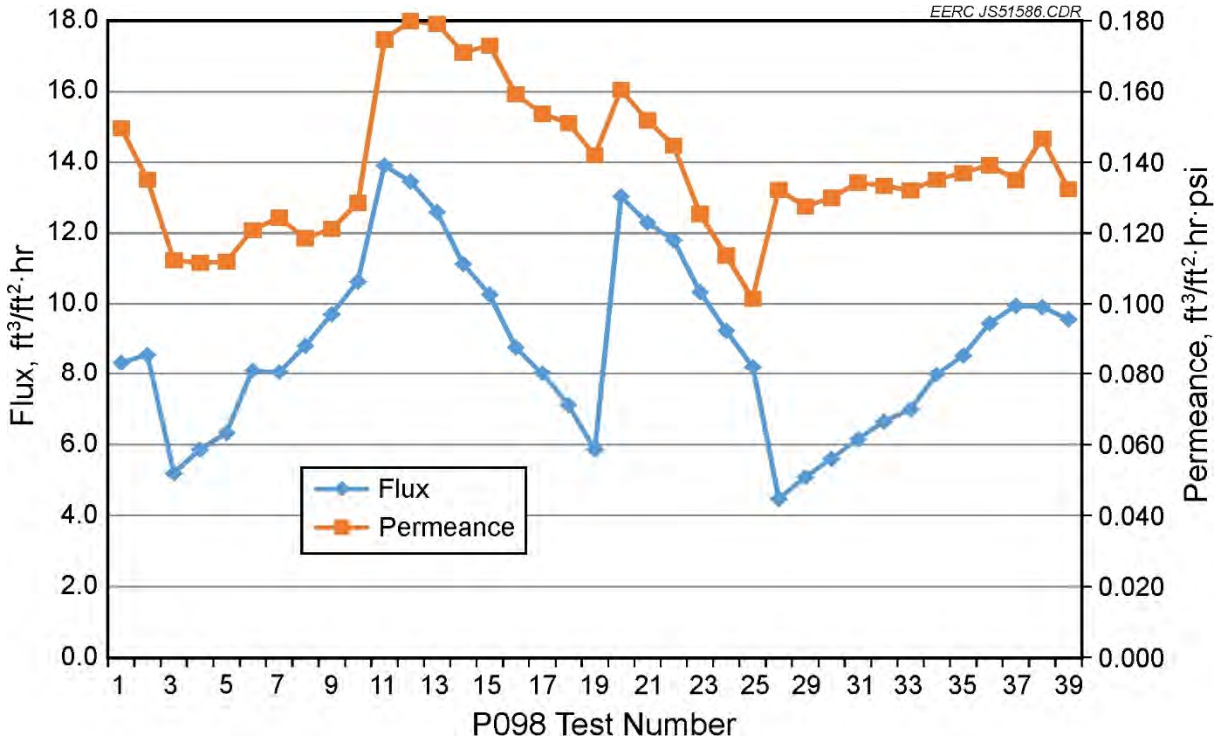

Figure 42. P098 flux and permeance by test number.

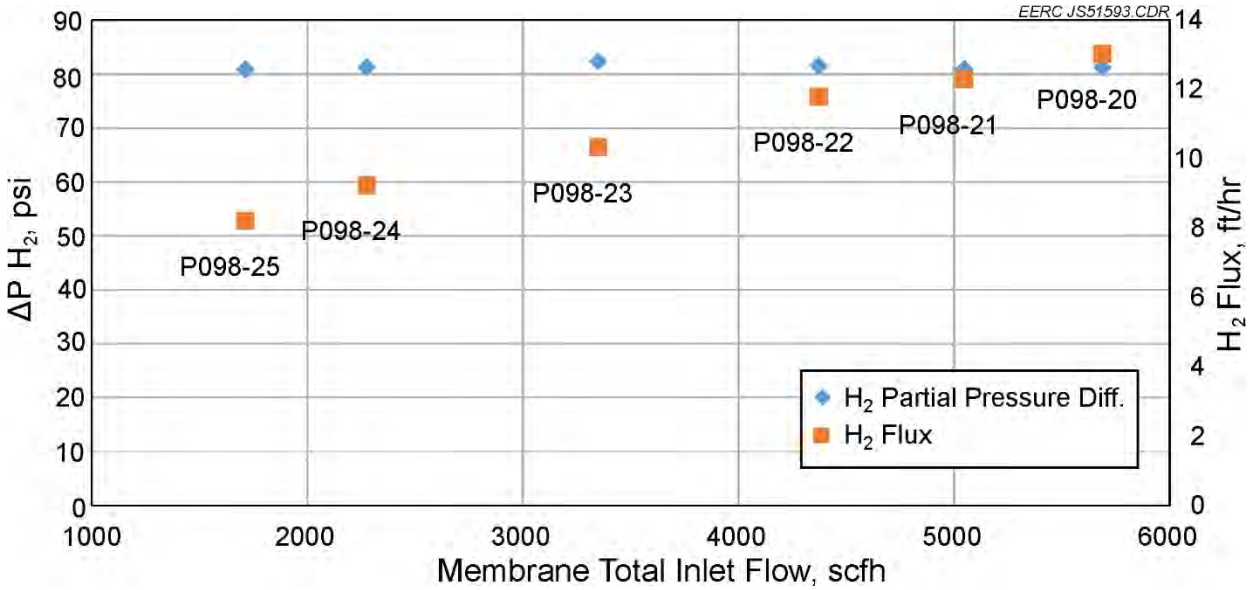

Figure 43. Membrane performance trend at 450 psig and 425°C.

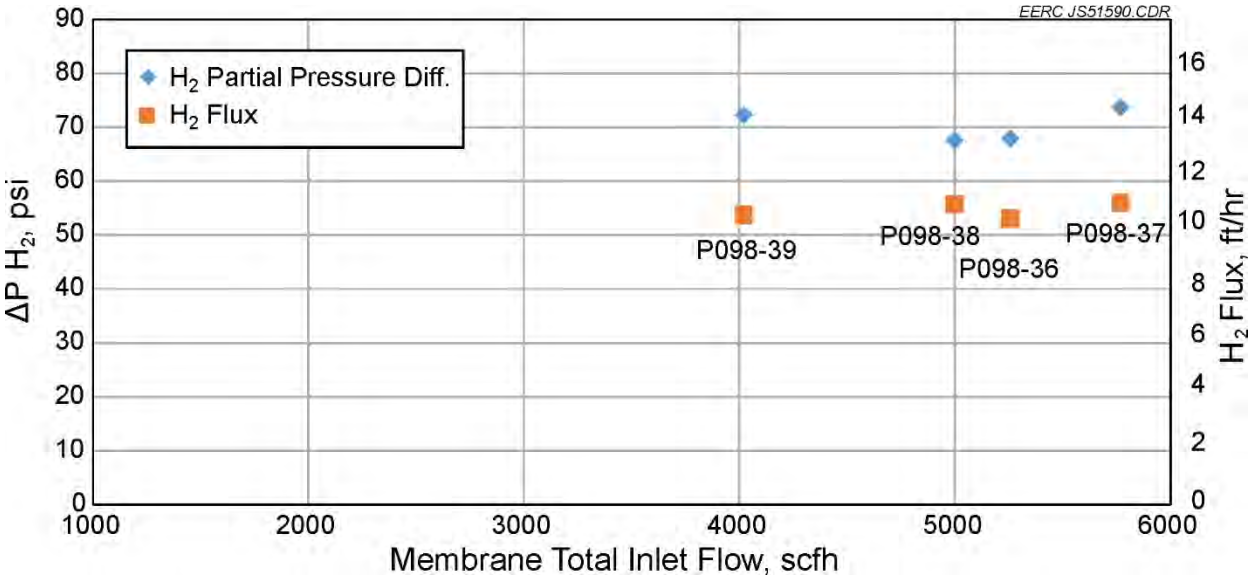

Figure 44. Membrane performance trend at 450 psig and 400°C.

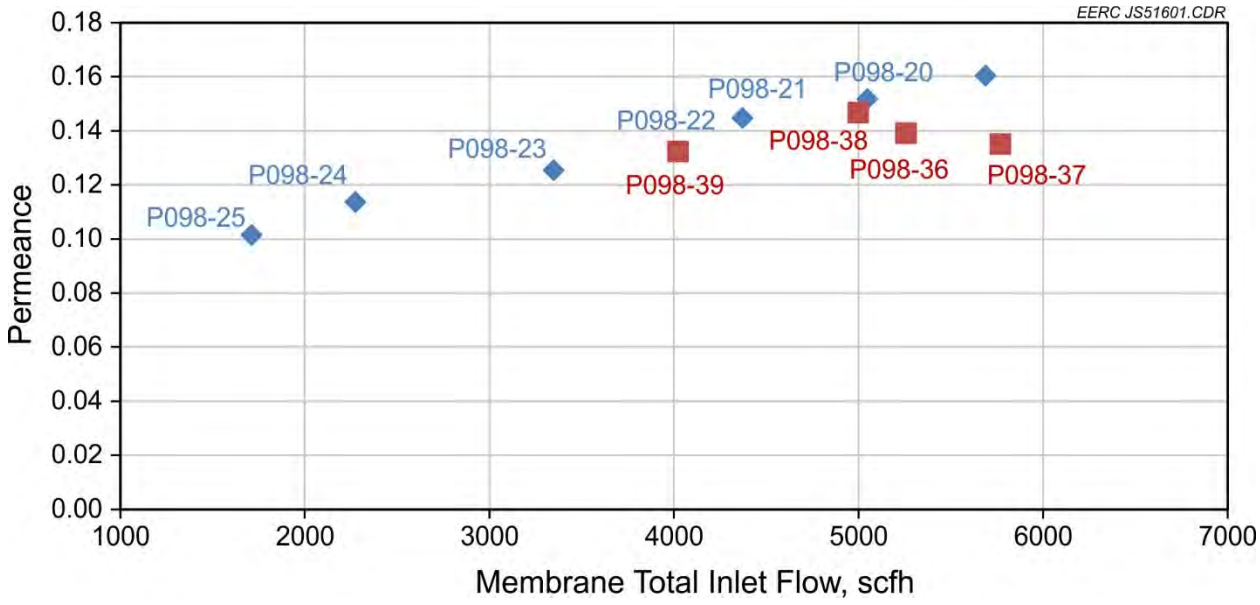

Figure 45. Membrane permeance trend at 450 psig and 425°C.

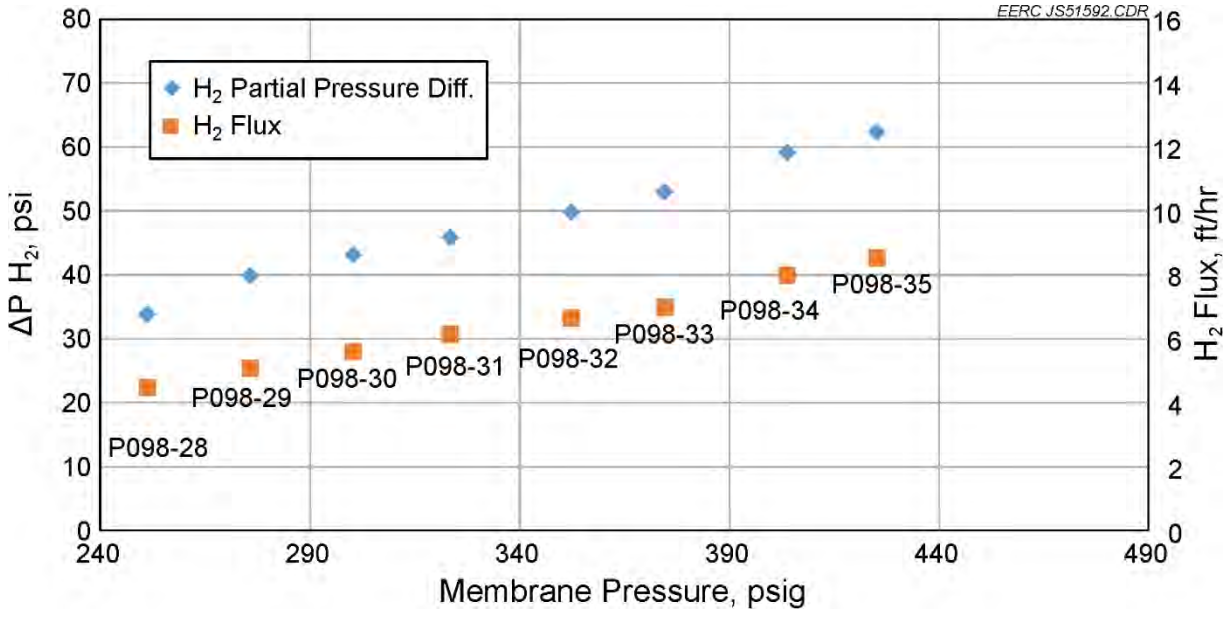

Figure 46. Membrane performance trend at 5000 scfh and 425°C.

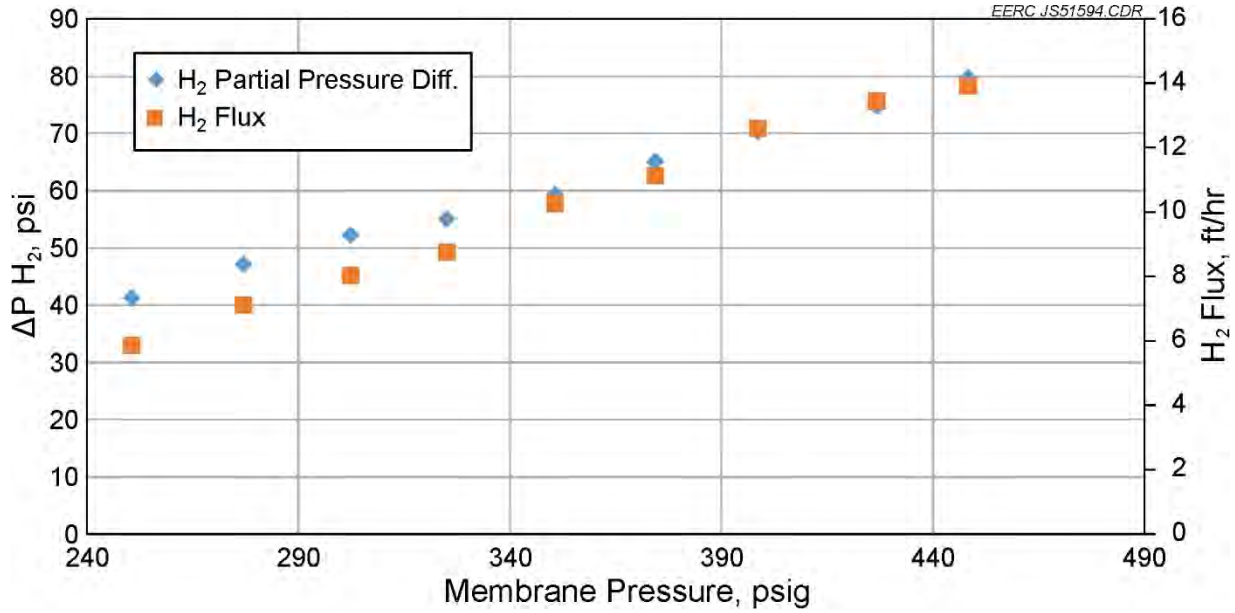

Figure 47. Membrane performance trend at 5500 scfh and 425°C.

Figure 48 shows the increasing hydrogen flux as the syngas delivery to the membrane assembly is increased, while the temperature is held at 400°C and 4200–4700 scfh of syngas flows through the membrane assembly. The test data represent Runs P098-3 through P098-9. The partial pressure differential and flux show good uniformity for these data. Figure 49 indicates that the permeance across the range of pressures had a slightly increasing trend with the increase in pressure over the 300–450-psi range.

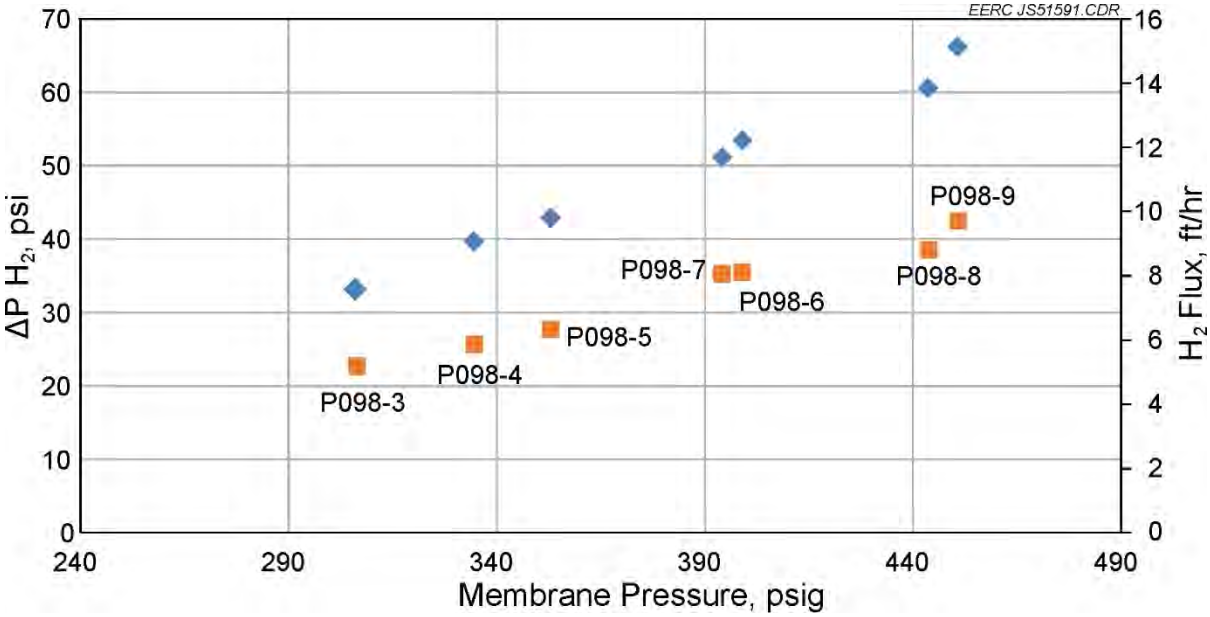

Figure 48. Membrane performance trend at 4200–4700 scfh and 400°C.

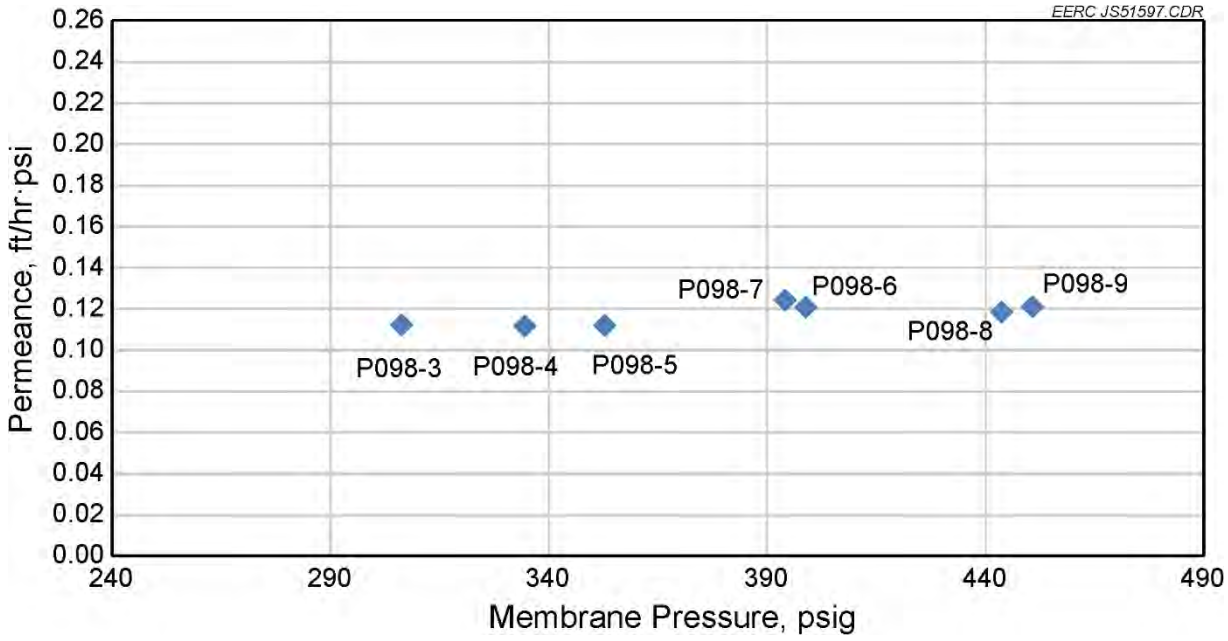

Figure 49. Membrane permeance at 4200–4700 scfh and 400°C.

The membrane permeance for all of the test runs plotted as a function of temperature and flow is shown in Figures 50 and 51. The higher-temperature tests show an increase in the average permeance, although other variables besides temperature are also influencing the data. The increase in flow also results in an increase in permeance, as expected. Variation in the data can be attributed to other variables influencing the membrane performance, including temperature.

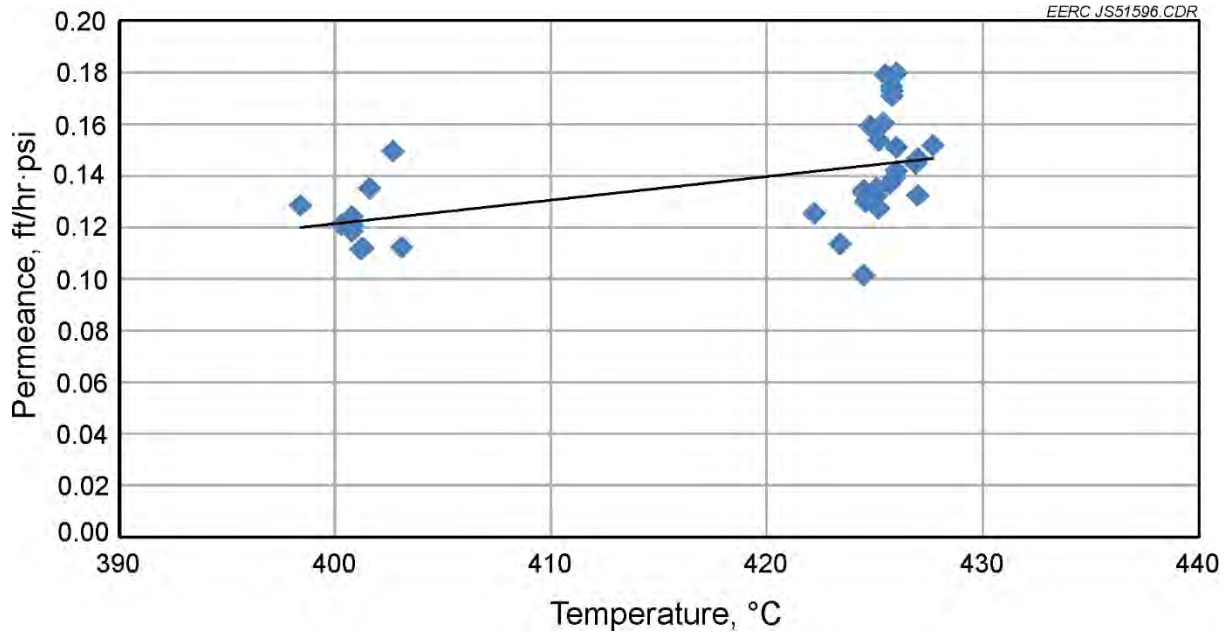

Figure 50. P098 permeance vs. temperature.

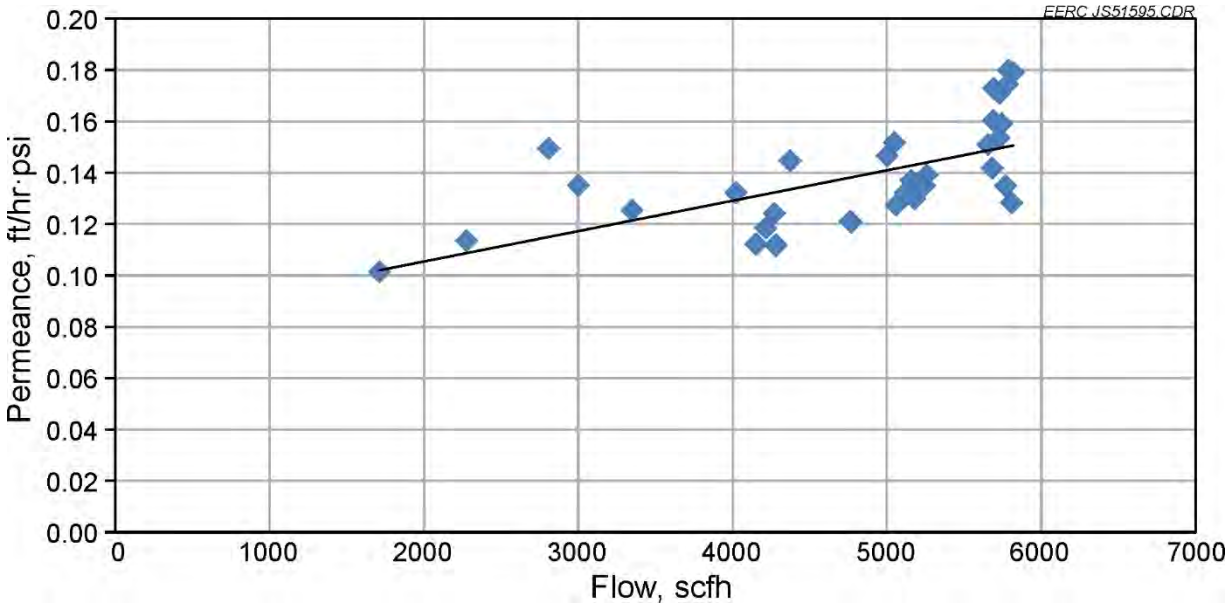

Figure 51. P098 permeance vs. flow.

Bottle Gas Testing

After the system was shut down, bottle gas testing with mixtures of hydrogen and nitrogen was performed on the membrane to develop comparable data to testing that had occurred at Praxair prior to exposing the membranes to coal-derived syngas. The bottle testing was initiated on the morning of August 19, 2015, and concluded later that evening for a total of 10.5 hours of testing. Three separate test periods were conducted. The membrane was first exposed to 30% hydrogen–70% nitrogen flowing at about 5000 scfh for 1 hour. Next a 25% hydrogen–75% nitrogen mixture was flowed through the membrane for a period of approximately 8 hours. This was done in an attempt to purge any impurities such as sulfur from the system. Finally, another 1-hour test at 30% H_2–70% N_2 and 5000 scfh was conducted to determine if there was any increase in flux after soaking in hydrogen for a period of time. The membrane was operated at 200 psi and 400°C for the tests. The operational data for the test are shown in Table 14.

Calculated membrane performance parameters for the bottle gas tests are shown in Table 15. The calculations were performed in the same manner as before and include estimations with and without leaks. The data indicate that a slight performance improvement was observed for the bottle gas tests versus the syngas tests. The permeance for all tests, including the bottle gas testing, is shown in Figure 52. The permeance for Test C1 improved significantly over Test 39, although it was not significantly higher than the permeance observed in Test 12. After the 8-hour hydrogen soak, the permeance was shown to improve further to nearly 0.2 ft/hr·psi. Although this improvement is encouraging, the flux and permeance attained in these tests were significantly lower than the flux obtained during the testing at Praxair, prior to exposing the tubes to syngas. The tubes were removed from the membrane vessel after testing and shipped to Praxair for analysis to determine if there were contaminants present on the surface of the membrane.

Table 14. Average Membrane Operating Characteristics for the P098 Bottle Gas Tests

Test No.	Start Date	Start Time	End Date	End Time	Temp., °C	Supply Pressure, psig	Feed Flow, scfh	Retentate Flow, scfh	Permeate Flow, scfh	Feed H_2 Conc., wet %	Retentate H_2 Conc., dry %	Permeate H_2 Conc., dry %	Permeate Pressure, psig	Addl. H_2 Flow, scfh
P098-C1	8/19/15	1035	8/19/15	1135	400.2	203.0	5102.1	4929	173.1	30	27.3	91.6	4	1500
P098-C2	8/19/15	1145	8/19/15	1925	406.1	201.0	304.6	245	59.6	25	9.32	66.1	4	80
P098-C3	8/19/15	2005	8/19/15	2105	408.1	200.0	5024.2	4842	182.2	30	29	92.1	4	1500

Table 15. Calculated Membrane Performance Parameters for the P098 Bottle Gas Tests

Test No.	Estimated Permeate Leak Flow, scfh	Estimated Hydrogen Flux Flow, scfh	Feed H_2 Partial Pressure, psia	Permeate H_2 Partial Pressure, psia	H_2, dP	H_2 Flux, without leak, scfh/ft^2	H_2 Flux, with leak, scfh/ft^2	H_2 Permeance, without leak, ft^3/(ft^2·hr·dP)	H_2 Permeance, with leak, ft^3/(ft^2·hr·dP)	Flux at 100 psi dP, without leak, ft^3/(ft^2·hr)	Flux at 100 psi dP, with leak, ft^3/(ft^2·hr)	Flux at 100 psi dP Sievert's Law, without leak	Flux at 100 psi dP Sievert's Law, with leak	H_2 Recovery, without leak, %	H_2 Recovery, with leak, %
P098-C1	20.8	152.3	65.3	17.1	48.2	8.46	8.8	0.176	0.183	17.6	18.3	14.70	15.30	3.3	3.4
P098-C2	26.9	32.7	53.9	12.4	41.6	1.81	2.2	0.044	0.053	4.4	5.3	3.25	3.92	16.2	19.6
P098-C3	20.6	161.6	64.4	17.2	47.2	8.98	9.3	0.190	0.198	19.0	19.8	15.87	16.48	3.5	3.6

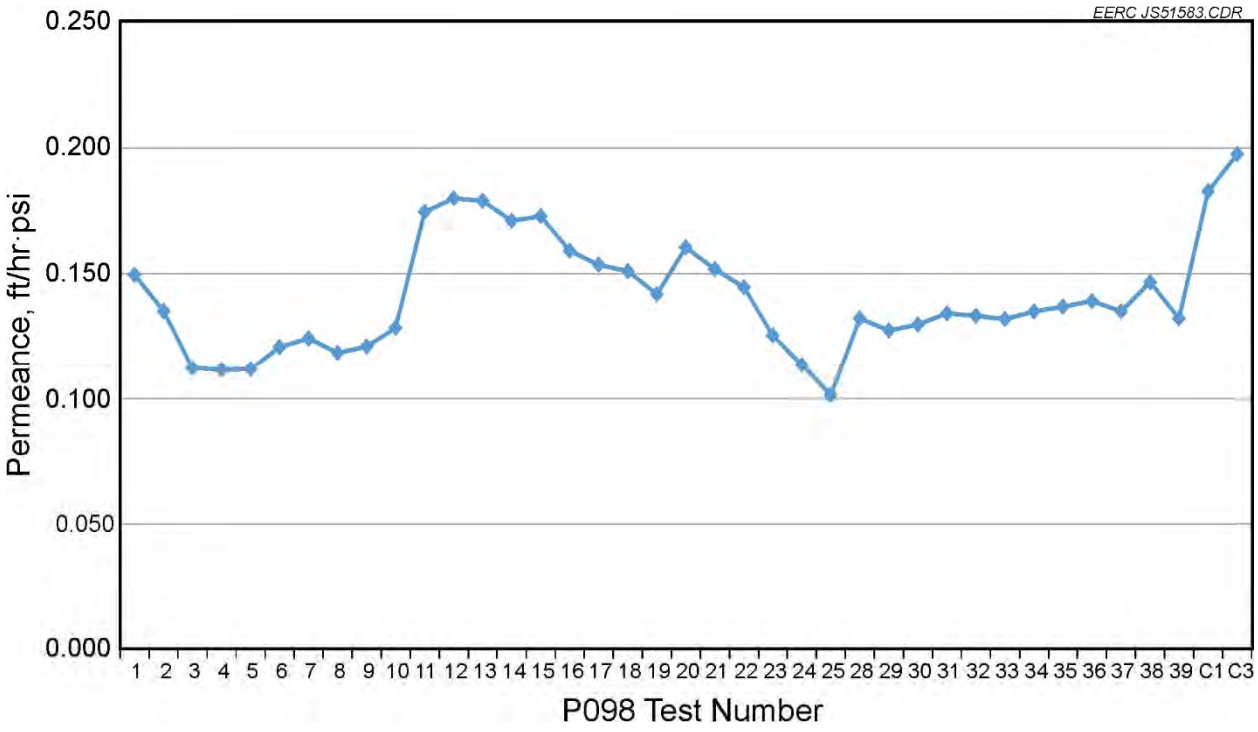

Figure 52. Permeance observed for the P098 test campaign, including the bottle gas tests C1 and C3.

Considerations for Operation of the System with Brown Coals from Australia

The transport reactor technology can be used for various low-rank fuel types, including subbituminous coal, lignite from North Dakota, and Australian brown coal. Specific challenges for running the system on Australian brown coal can include high moisture content, high sodium content, and friability of the fuel. Brown coals must be dried before running in almost any gasifier; however, the moisture levels can be as high as 30% coming into the TRDU, which can limit the amount of drying required. Sodium content can be a challenge because it lowers the fusion temperature of the ash and can lead to particle agglomeration. The EERC has successfully used kaolin as a sodium gettering agent in past tests. The friability of the fuel is a challenge because the operating principle of the TRDU depends on the recirculation of the unconverted carbon to the mixing zone. If the fuel has a high tendency to break apart into small particles, it may only be exposed to one pass of the riser section of the gasifier and this may lead to significantly reduced carbon conversion. In spite of these challenges, the high reactivity of the fuel allows for fast conversion at lower temperatures, making brown coals good candidates for transport reactor technology.

A modeling effort was undertaken to understand the impact of utilizing brown coal in the TRDU on syngas and hydrogen production. The basic properties of two fuels from Australia were used in Aspen Plus to evaluate the high-level mass and energy balance of the system. The fuels chosen were from the Loy Yang mine and Lochiel mine. The process model used proximiate, ultimate, and heating value analysis of the fuel to evaluate the performance in the TRDU. The

model uses a Gibbs free energy minimization calculation in both the mixing zone and riser, and the equilibrium and carbon conversion of each zone is restricted to account for kinetic limitations. Cyclones are used to recirculate solids and unburned carbon from the riser section back to the mixing zone. For the effort herein, a PRB coal with known operational characteristics was also modeled for comparison. Then the syngas production characteristics were compared for the two Australian fuels.

The fuel compositions used in the model were based on fuels received at the EERC for a test run in 2003. The as-run fuel compositions, along with the Antelope coal used in this project, are shown in Table 16. The antelope coal did not require further drying from what was achieved during the fuel preparation process. The Loy Yang and Lochiel brown coals were both dried in a rotary dryer before sizing to –10 mesh for operation in the TRDU. As the table shows, a high level of drying was achieved, and the fuels were possibly dried down further than required. Both fuels exhibited high sodium concentrations in the ash, however, the Loy Yang fuel was very low in ash content; therefore, the overall sodium content delivered to the gasifier was low enough that mitigation measures were not required. Overall, after drying, the properties of the Loy Yang fuel were very similar to the properties of the Antelope PRB. The Loy Yang does contain higher levels of oxygen and volatile matter, whereas the Antelope coal has higher concentration of fixed carbon. The Lochiel fuel was much higher in ash, and therefore the overall sodium content must be taken into account when operating the pilot plant. No considerations for sodium content were made in the process model.

The Aspen Plus process model used for the evaluations is shown in Figure 53. It should be noted that the model is not intended to provide a rigorous kinetic simulation of the gasifier but rather is used to evaluate high-level mass and energy balances around the system. The decomposition block uses the proximate, ultimate and heating value analysis of the coal to break down the feedstock into basic elements that can be modeled in the simulation. The syngas equilibrium compositions are limited by temperature, and carbon conversion in the mixing zone and riser are set based on past experience with the system. The model uses a compression system to recycle syngas back to the mixing zone (via the loop seal in the pilot system), and split flows are set based on operational data. The hydrogen split at the end of the model shows how much hydrogen is being delivered to the membrane.

Each of the three fuels was modeled in Aspen Plus to evaluate the potential for hydrogen production. Table 17 shows the results of the modeling effort. The fuel feed rate was adjusted for each case to maintain similar carbon and heating value inputs. In the case of the Loy Yang fuel, the dried coal was similar in properties to the Antelope coal, so no adjustments were made. For the Lochiel coal, the feed rate was increased to account for the reduced carbon content as compared to the other fuels. Oxygen to carbon ratio was about 0.9 on a weight basis for each of the cases. The calculation does not account for oxygen input from coal. The steam to carbon ratio was also about 0.9 for each case, and the calculation does not consider moisture in the fuel. The dry basis syngas composition leaving the TRDU is shown in the table. The hydrogen and CO contents are similar for each of the cases, and the H_2S concentration is significantly higher for the Lochiel fuel because of high sulfur concentrations in the ash. The postshift wet syngas composition indicates that it is possible to achieve greater than 30% hydrogen concentration in the syngas for each of these fuels, although in the Lochiel case, an additional 62 lb/hr of fuel was required to meet this target. The final hydrogen delivery to the membranes was just over 6 lb/hr for each of the cases.

Table 16. Properties of PRB and Australian Brown Coal

	Antelope PRB Coal	Dried Loy Yang Brown Coal	Dried Lochiel Brown Coal
Proximate Analysis, as run, wt%			
Moisture	27.6	15.0	18.0
Volatile Matter	29.7	48.7	43.8
Fixed Carbon	41.0	35.3	25.9
Ash	5.7	0.9	12.3
Ultimate Analysis, Moisture-Free, 1 wt%			
Carbon	68.5	65.4	56.1
Hydrogen	4.6	4.6	4.3
Nitrogen	1.0	0.8	0.7
Sulfur	0.3	0.4	3.6
Oxygen	17.6	27.7	20.4
Ash	7.9	1.1	15
Ash Composition, % as oxides			
Calcium, CaO	25.2	6.9	11.8
Magnesium, MgO	7.0	13.2	10.4
Sodium, Na_2O	1.0	10.3	9.1
Silica, SiO_2	25.4	26	27.9
Aluminum, Al_2O_3	15.4	8.4	6.5
Ferric, Fe_2O_3	12.8	10.4	4.7
Titanium, TiO_2	1.4	0.7	0.8
Phosphorus, P_2O_5	1.4	0.1	0
Potassium, K_2O	0.3	1.4	0.4
Sulfur, SO_3	10.1	22.7	28.4
HHV			
Moisture-Free, Btu/lb	11,693	11,112	9,011
As-Received, Btu/lb	8,470	9,445	7,389

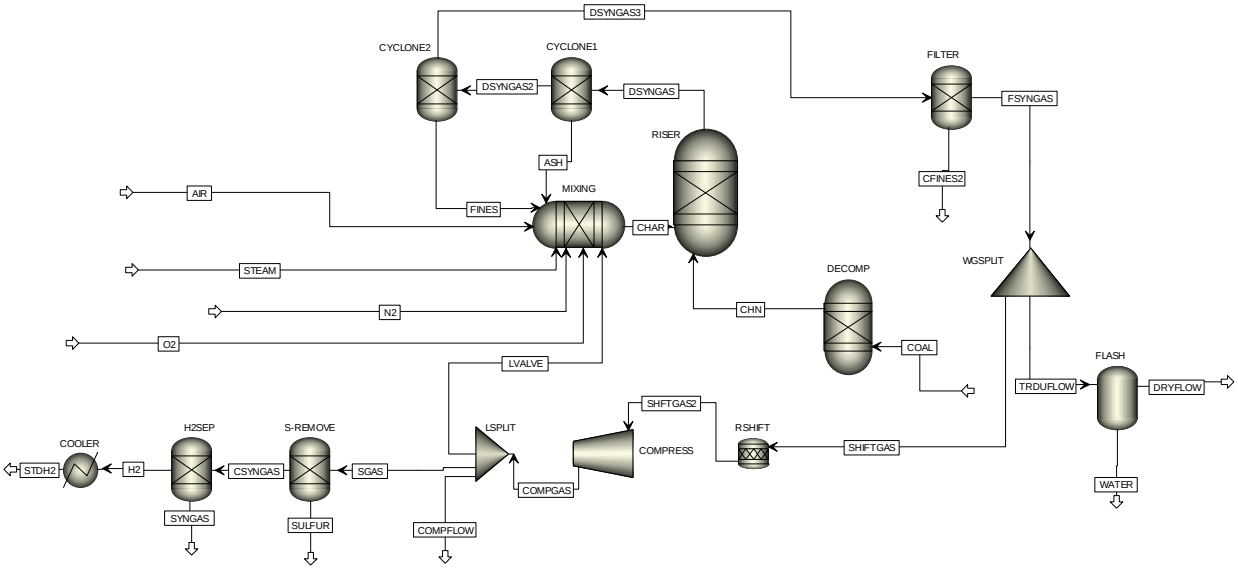

Figure 53. Aspen Plus model for coal gasification in the TRDU.

Table 17. Model Inputs and Results for PRB and Australian Brown Coals

	Antelope	Loy Yang	Lochiel
Input flows, lb/hr			
Oxygen	190	190	190
Steam	185	185	185
Coal	375	375	437
Carbon Input Flow	208	213	208
Ratios, wt basis			
O_2/C	0.91	0.89	0.92
Steam/C	0.89	0.87	0.89
Preshift Syngas Composition, mol%, dry			
N_2	36.1%	35.6%	35.3%
H_2	24.5%	23.1%	24.2%
CO	14.4%	15.4%	14.3%
CO_2	20.8%	21.6%	21.1%
CH_4	3.9%	4.0%	3.7%
H_2S	0.07%	0.10%	0.96%
Postshift Syngas Composition, mol%, wet			
H_2O	7.3%	4.8%	7.3%
N_2	29.5%	29.7%	28.9%
H_2	31.1%	31.3%	30.8%
CO	0.8%	0.8%	0.8%
CO_2	28.0%	30.1%	28.3%
CH_4	3.2%	3.3%	3.1%
H_2S	0.05%	0.08%	0.79%
Output Flows, lb/hr			
Syngas Flow, Gasifier Exit	1356	1379	1393
Hydrogen Flow to Membrane	6.07	6.08	6.13

The high-level mass balance on the system indicates that it is possible to achieve similar hydrogen production rates with an Australian brown coal as with a subbituminous coal. However, the model does not take into consideration the potential operational difficulties associated with gasifying brown coal in the TRDU. Operational problems can result in reduced carbon conversion and reduced levels of syngas production. The EERC tested these two brown coals in the TRDU system in 2003, and a summary of the results is presented herein.

Overall, it has been shown that when dried, the brown coals have the potential to produce as much hydrogen as an Antelope coal from the PRB. Because of the high shipping cost, only a limited amount of the Australian brown coals were shipped to North Dakota. After drying the original 60 wt% fuel to than 20 wt% moisture for testing, even less fuel was available for testing. The lack of fuel resulted in limited testing at the EERC that was further hampered by several operational challenges that limited the amount of steady-state operational data achieved. These operational challenges included one interruption for a broken fuel feed auger and several interruptions for bed material agglomeration (especially during oxygen-blown testing) that would limit solids circulation rates in the transport reactor. After the first interruption, the operating temperature was reduced to around 800°C. Operation at these lower temperatures then resulted in lower carbon conversions and lower syngas heating values as compared to North Dakota lignites

tested at similar temperatures. A contributing factor in the lower carbon conversion was the particle-size distribution for the brown had significantly more fines (22 and 32 wt%, respectively, less than 100 μm) than the other fuels previously tested in TRDU which were typically 10 wt% less than 100 μm.

The tests on the TRDU utilized thermally dried Australian brown coals from the Loy Yang and Lochiel Mines over 5 days of testing in December 2003. This test generated 59 hours of coal feed and 57 hours of gasification, including 44 hours of air-blown gasification and 13 hours of oxygen-blown gasification. Toward the end of the testing, some of the Lochiel brown coal had the fines less than 60 mesh screened from coal in an effort to understand the effects of the initial feed particle size on the carbon conversion. Operating results achieved with these brown coals are shown in Tables 18 and 19 and summarize some results from the brown coal tests. Removal of the fines did not appear to improve carbon conversion, possibly because the high friability of brown coals would result in significant fines production as it was handled through the feed system and as it was exposed to a very high heatup rate upon injection into the gasifier itself.

Analysis of the collected ash samples indicates that while most of the sodium was leaving with the filter ash, the bed material ash was building up sodium (especially for the high-ash Lochiel brown coal), which would be consistent with the bed material agglomeration and deposition that was experienced with these brown coals. Previous tests with high-sodium North Dakota lignite at these lower operating temperatures did not have the bed agglomeration issues experienced with the Australian brown coals possibly because the sodium is mostly organically associated, which could form a either vapor phase or fine aerosol fume that is not recycled by the cyclones as much as the brown coals, which predominately have the sodium present as NaCl salt crystals.

Several developments with the TRDU technology have been made since these tests were conducted in 2003 that would improve the performance of the brown coals in the TRIG™ (transport reactor integrated gasification) technology. These developments include decreasing the size on the primary cyclone on the TRDU to improve the cyclone efficiency and recycle more of the char back to the mixing zone. Another development is the utilization of kaolin as an additive to capture the sodium as a higher-melting-temperature sodium aluminosilicate instead of the lower-melting-temperature sodium silicate. Increases in operating temperature to over 950°C have been demonstrated on high-sodium North Dakota lignites at both the EERC pilot scale and the Wilsonville, Alabama, Power Systems Development Facility demonstration-scale systems without bed agglomeration issues while achieving high carbon conversion. These developments would likely overcome most of the operational challenges experienced with the previous brown coal testing. Additional testing of the brown coals on the TRDU to determine the optimum conditions to achieve high carbon conversion while minimizing bed agglomeration issues would be recommended. Implementation of these changes could lead to syngas production levels similar to the PRB coal, resulting in similar membrane performance as was observed in this project.

Table 18. Corrected TRDU Product Gas Compositions for TRDU Tests Utilizing Australian Brown Coal

Coal	Loy Yang	Loy Yang	Lochiel	Lochiel	Lochiel Without Fines
Product Gas Composition, vol%	Air	Oxygen	Air	Oxygen	Air
H_2	7.4	12.5	6.3	13.8	4.5
CO	5	8.3	4.6	4.9	4.2
CH_4	1.7	3.5	1.5	3.5	1.5
CO_2	12.7	17.7	13.9	24.7	15.2
N_2	73.5	58.4	74.9	56.0	76.2
Total	100.3	98.0	101.2	102.9	101.4
Heating Value, Btu/scf	57	103	50	96	43
% N_2 in Dry Feed	32.0	70.0	32.8	74.8	38.0
N_2-Free Heating Value, Btu/scf	84	207	70	192	63
Product Gas, vol%	Adjusted for 450,000 Btu/hr Heat Loss and N_2 Purge Free				
H_2	17.9	29.6	13.1	33.2	10.9
CO	12.1	19.7	9.6	11.8	10.1
CH_4	4.1	8.3	3.1	8.4	3.6
CO_2	18.5	24.1	19.5	39.1	24.4
N_2	47.5	18.3	54.8	7.4	51.0
Total	100	100	100	100	100
Heating Value, Btu/scf	138	243	105	231	104

Table 19. TRDU Operating Conditions and Gasification Efficiency Results for Tests Utilizing Australian Brown Coal

Coal	Loy Yang	Loy Yang	Lochiel	Lochiel	Lochiel without fines
Oxidant	Air	Oxygen	Air	Oxygen	Air
Gasifier Temp., °C	882	877	785	741	784
Coal/Sorbent Feed Rate, lb/hr	267	342	479	482	479
Air Flow, lb/hr	766	0	1004	0	763
O_2 Flow, lb/hr	0	180	0	168	0
Steam Flow, lb/hr	125	311	124	293	118
Steam:Coal Ratio, lb/lb	0.46	0.91	0.31	0.61	0.31
O_2:maf Coal Ratio, lb/lb	0.78	0.52	0.86	0.50	0.74
Recirculation Rate, lb/hr	11,880	12200	8305	11,225	9800
TRDU Riser Velocity, ft/s	35.8	34.0	41.8	30.3	38.3
Carbon Conversion Solid Accountability	77.3	71	72.0	74.4	74.0

Task 4 – Process Modeling

Overview

A process modeling effort was undertaken to help understand the potential benefit of hydrogen separation membranes when utilized in a full-scale IGCC process. The basis for the process model was developed from the DOE report entitled "Cost and Performance Baseline for Fossil Energy Plants; Volume 3a: Low Rank Coal to Electricity: IGCC Cases" (32). In the report, a base case is developed for the cost of electricity using Rosebud subbituminous coal from the PRB in Montana with a full-scale TRIG system. The first base case is referred to as Case S2A and includes IGCC with the aforementioned coal and reactor but does not include CO_2 capture. A second base case entitled Case S2B includes the same elements but also includes CO_2 capture using Selexol as part of the process. The present membrane modeling effort is identical to Case S2B but uses membrane technology for CO_2 separation in place of Selexol. The membrane modeling case is referred to herein as "Case S2B Membrane."

Aspen Plus process modeling software was used to first develop an accurate representation of Case S2B. The Cost and Performance Baseline report contains much of the necessary information to develop the full mass and energy balance around the IGCC system. However, upon commencement of the modeling effort, it was determined that there was not enough information in the report to completely close the mass and energy balance. Therefore, a conference call was held with DOE modeling personnel to fill in the missing information and complete the process model.

The model did not replicate the entire IGCC system but rather focused on the areas that would change as a result of the addition of hydrogen separation membrane technology. This included the membrane separation itself, as well as the gas turbine, heat recovery steam generator (HRSG), and steam turbines. The remaining process areas including the air separation unit (ASU), gasification system, and WGS reactors did not change, and data from Case S2B were used directly for these areas.

One small change from the base case was implemented for this modeling effort. It was found that a small amount of methane contained in the syngas stream has a significant impact on the overall performance of the IGCC system when hydrogen separation membranes are used. The methane concentrations do not impact the Selexol case because the methane and hydrogen are not absorbed by the solvent and are sent directly to the gas turbine. In the membrane case, the hydrogen is separated from the syngas, and the methane remains with the CO_2-rich stream. Flash recovery is used to gather a portion of the methane during compression, but a significant portion of the methane remains with the CO_2. Therefore, it was assumed in this analysis that the transport reactor was operated such that the exit methane concentration was lowered to 1% on a wet basis. This estimate was based on the EERC experience with operation of the TRIG gasifier. The data indicate that an entrained-flow gasification system is likely a better fit for a membrane application simply because of the conversion of all methane to hydrogen and CO. A sensitivity analysis was also performed and is presented here to illustrate this impact.

The membrane module tested in the current project has not been optimized for IGCC performance; therefore, it is difficult to assess the potential performance of the Praxair membrane directly in the IGCC base case. As a result, an optimized hydrogen separation membrane was used to identify the potential overall performance benefits of a hydrogen separation membrane technology when applied to a gasification system. The membrane performance in the model sets the benchmark for required commercial system goals.

Model Description

A block flow diagram for the overall process is shown in Figure 54. In DOE Case S2B, an oxygen-fired TRIG system is used to convert Rosebud PRB coal to syngas and, ultimately, electricity in an IGCC system. Coal is dried to approximately 20% moisture before being sent to the gasification system. Air is separated into oxygen and nitrogen components. The oxygen is fed to the gasifier, and the nitrogen is used as a working fluid in the gas turbine. The gasifier also uses steam for reaction with the coal and is operated at a pressure of 605 psia. The syngas exits the system at 1800°F and enters a syngas cooler for heat recovery. The syngas is cooled to 650°F while high-pressure boiler feed water is converted to saturated steam for the combined-cycle system. A HGFV is used for filtration of particulate, and a portion of the syngas is then recycled back to the gasifier. The syngas is shifted to H_2 and CO_2 in a three-stage sour shift reactor system, and steam is generated after each stage.

At this point, the model for the membranes diverges from Case S2B. Instead of a syngas cooler and a low-temperature mercury removal step followed by the Selexol process, a warm mercury and sulfur control step is used followed by the hydrogen separation membrane. For the purposes of this analysis, it is assumed that the mercury removal is accomplished at the same cost as the base case and that the sulfur removal uses the same amount of energy as the Sulfinol process in Case S2A. Studies indicate that warm-gas cleanup technologies for sulfur removal may have an advantage over cold-gas technologies in terms of auxiliary power requirements, but no performance benefit was credited for this effort (33).

The membrane performance was assumed to be 95% recovery, with the hydrogen recovered at 405 psia in a stream of sweep nitrogen. This high level of performance is made possible by using a countercurrent nitrogen sweep. All of the nitrogen recovered in the ASU is used for the sweep, which drops the partial pressure of hydrogen to that below the partial pressure on the syngas side through the entire length of the membrane module. This concept is illustrated in Figure 55. Even at the membrane exit, there is still driving force available for hydrogen separation. For illustrative purposes, the membrane was broken up into five stages, with the first stage representing the first 25% of the membrane and the last stage representing the membrane exit. As shown in Figure 55, positive driving force is available for membrane separation across the length of the membrane. If a higher-pressure gasification system were used, more driving force would be available for separation.

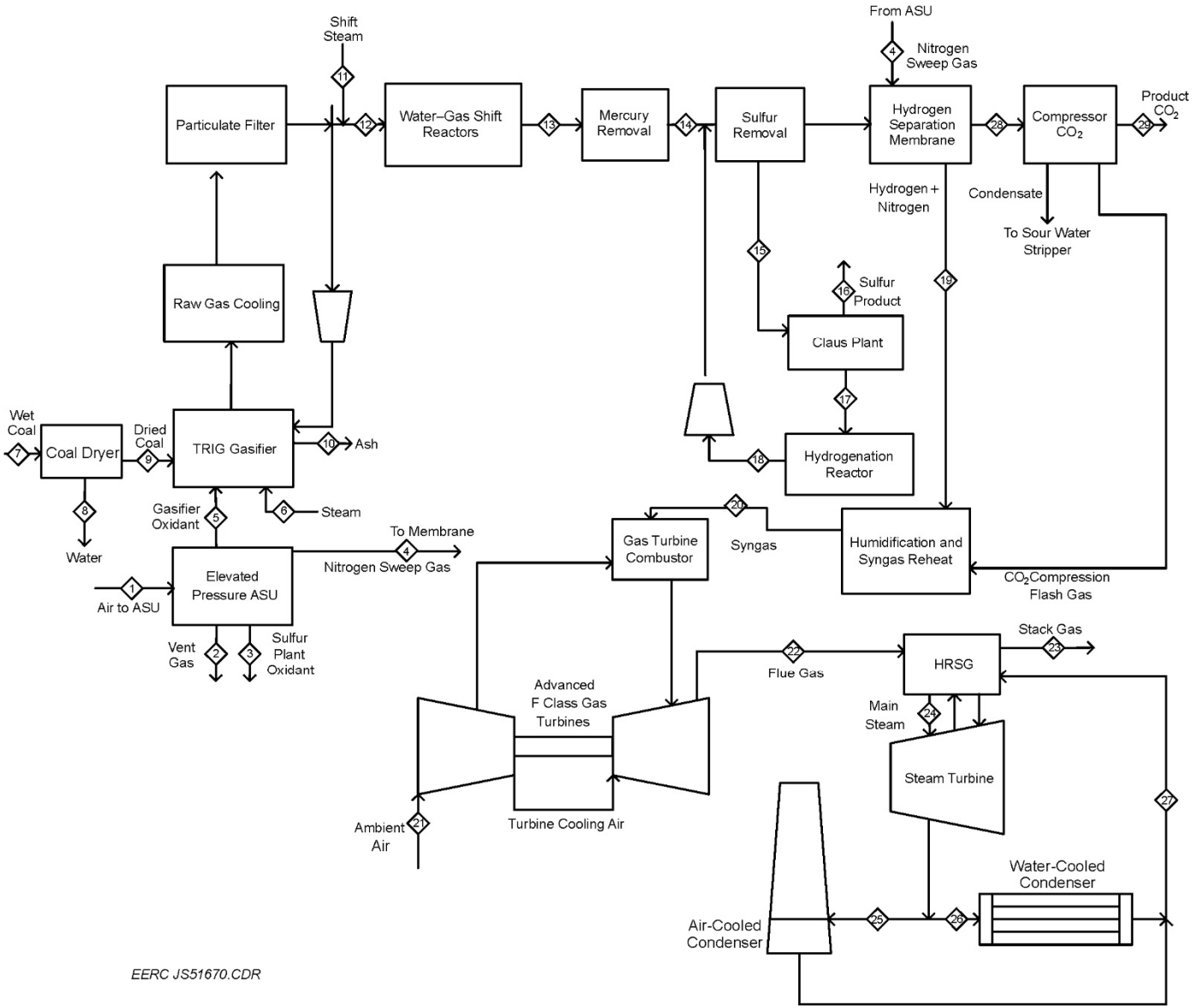

Figure 54. Block flow diagram for Case S2B membrane.

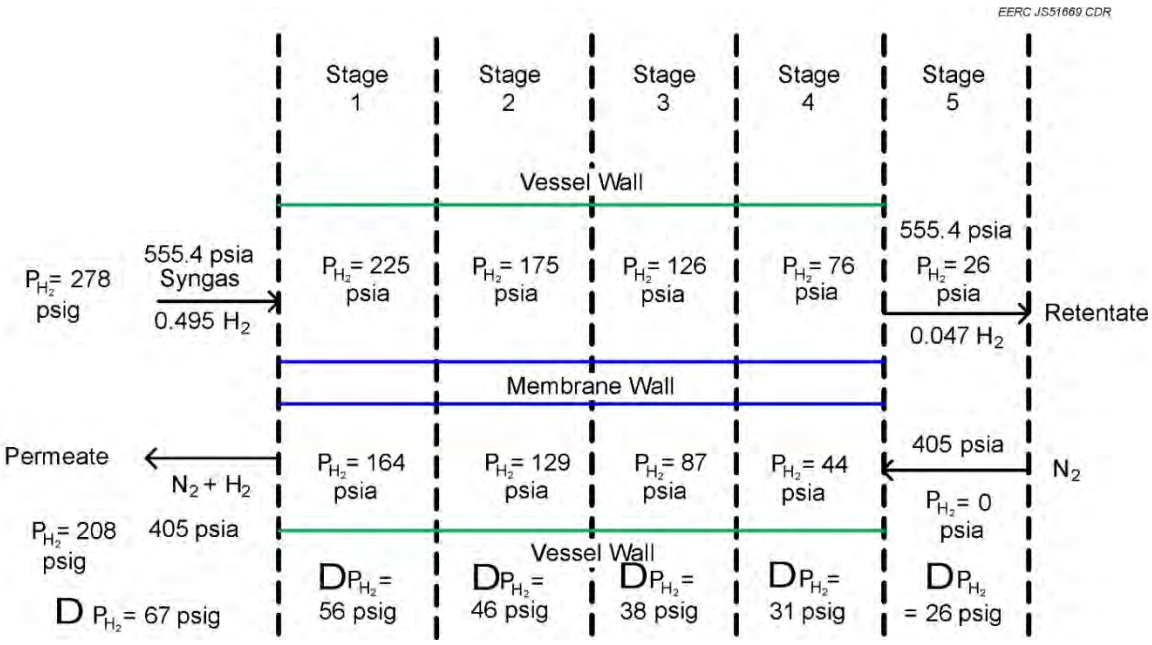

Figure 55. Membrane flow concept with a countercurrent nitrogen sweep.

After the membranes, the hydrogen-rich syngas is sent to the gas turbine combustor and expander for power generation. The retentate stream remains at elevated pressure and is sent to the compression train. An intermediate flash is used to recover as much of the hydrogen and methane as possible. The compressed CO_2 stream exits with a purity greater than 95% but also contains traces of hydrogen, methane, and argon. The applicability of this type of stream for enhanced oil recovery would need to be determined based on the end user. An oxidation system could be used to convert the methane and hydrogen to CO_2 and water followed by a water separation if determined necessary. Because the CO_2 is maintained at elevated pressure through the membrane system, the compression costs are significantly reduced.

The hot flue gas exiting the gas turbine is used in a HRSG to generate steam for additional power production. The steam cycle is highly integrated with both the HRSG and overall gasification system to extract as much energy as possible from the system. In the case of the membrane, the flue gas exits at a slightly higher temperature from the turbine; therefore, a small amount of additional steam is generated for power production.

Model Results

Table 20 shows the detailed stream compositions for the process streams labeled in Figure 53. Additionally, Figures 56–58 represent the detailed mass and energy balance developed for the membrane case. Figure 56 is nearly identical to Case S2B, but significant changes are shown in Figures 57 and 58 because of the inclusion of the membrane technology.

Table 20. Composition, Flow, and Enthalpy of the Main Process Streams for Case S2B Membrane

	1	2	3	4	5	6	7	8	9	10	11	12	13	14
V-L Mole Fraction														
Ar	0.0092	0.0237	0.0318	0.0023	0.0360	0.0000	0.0000	0.0000	0.0000	0.0000	0.0000	0.0049	0.0049	0.0049
CH_4	0.0000	0.0000	0.0000	0.0000	0.0000	0.0000	0.0000	0.0000	0.0000	0.0000	0.0000	0.0100	0.0100	0.0100
CO	0.0000	0.0000	0.0000	0.0000	0.0000	0.0000	0.0000	0.0000	0.0000	0.0000	0.0000	0.2761	0.0012	0.0012
CO_2	0.0003	0.0081	0.0000	0.0000	0.0000	0.0000	0.0000	0.0000	0.0000	0.0000	0.0000	0.0607	0.3355	0.3355
COS	0.0000	0.0000	0.0000	0.0000	0.0000	0.0000	0.0000	0.0000	0.0000	0.0000	0.0000	0.0000	0.0000	0.0000
H_2	0.0000	0.0000	0.0000	0.0000	0.0000	0.0000	0.0000	0.0000	0.0000	0.0000	0.0000	0.1952	0.4700	0.4700
H_2O	0.0064	0.1540	0.0000	0.0002	0.0000	1.0000	0.0000	1.0000	0.0000	0.0000	1.0000	0.4484	0.1736	0.1736
H_2S	0.0000	0.0000	0.0000	0.0000	0.0000	0.0000	0.0000	0.0000	0.0000	0.0000	0.0000	0.0019	0.0019	0.0019
N_2	0.7759	0.6137	0.0178	0.9920	0.0140	0.0000	0.0000	0.0000	0.0000	0.0000	0.0000	0.0029	0.0029	0.0029
NH_3	0.0000	0.0000	0.0000	0.0000	0.0000	0.0000	0.0000	0.0000	0.0000	0.0000	0.0000	0.0000	0.0000	0.0000
O_2	0.2081	0.2005	0.9504	0.0054	0.9500	0.0000	0.0000	0.0000	0.0000	0.0000	0.0000	0.0000	0.0000	0.0000
SO_2	0.0000	0.0000	0.0000	0.0000	0.0000	0.0000	0.0000	0.0000	0.0000	0.0000	0.0000	0.0000	0.0000	0.0000
Total	1.0	1.0	1.0	1.0	1.0	1.0	1.0	0.0	0.0	1.0	0.0	1.0	1.0	1.0
V-L Flow Rate, kgmol/hr	20,872	842	66	14,035	4231	3557	0	1455	0	0	10,253	30,881	30,881	30,881
V-L Flow Rate, kg/hr	603,087	23,325	2117	393,817	136,368	64,074	0	26,217	0	0	184,714	598,379	598,379	598,379
Solids Flow Rate, kg/hr	0	0	0	0	0	0	262,152	0	237,311	24,089	0	0	0	0
Temperature, °C	6	20	32	196	32	343	6	16	71	982	288	311	311	311
Pressure, MPa, abs	0.09	0.11	0.86	2.62	0.86	5.10	0.09	0.10	0.10	4.24	4.14	4.02	3.83	3.83
Enthalpy, kJ/kg*	–77.5	–1698.4	4.2	174.7	4.2	–12907.4	–	-16014.5	–	–	–13061.4	–7979.8	–520.4	–8520.4
Density, kg/m^3	1.1	1.5	11.0	18.7	11.0	20.1	–	1002.6	–	–	18.2	15.5	0.8	0.8
V-L Molecular Weight	28.895	27.685	32.181	28.061	32.229	18.015	–	18.015	–	–	18.015	19.377	19.377	19.377
V-L Flow Rate, lb/mol/hr	46,014	1857	145	30941	9328	7841	0	3208	0	0	22,604	68,081	68,081	68,081
V-L Flow Rate, lb/hr	1,329,580	51423	4668	868,218	300,640	141,259	0	57798	0	0	407,225	1,319,200	1,319,200	1,319,200
Solids Flow Rate lb/hr	0	0	0	0	0	0	577,946	0	523,182	53,107	0	0	0	0
Temperature, °F	42	68	90	385	90	650	42	60	160	1800	550	592.5	592.5	592.5
Pressure, psia	13.0	16.4	125.0	380.0	125.0	740.0	13.0	14.5	14.6	615.0	600.0	582.5	555.4	555.4
Enthalpy, Btu/lb*	–33.3	-–730.2	1.8	75.1	1.8	–5549.2	–	-6885.0	–	–	–5615.4	–3430.7	–3663.1	–3663.1
Density, lb/ft^3	0.07	0.093	0.687	1.167	0.688	1.257	–	62.589	–	–	1.135	0.967	0.049	0.049

* Reference conditions are 77°F and 14.696 psia.

Continued. . .

Table 20. Composition, Flow, and Enthalpy of the Main Process Streams for Case S2B Membrane (continued)

	15	16	17	18	19	20	21	22	23	24	25	26	27	28	29
V-L Mole Fraction															
Ar	0.0076	0.0000	0.0063	0.0074	0.0012	0.0028	0.0093	0.0081	0.0081	0.0000	0.0000	0.0000	0.0000	0.0090	0.0098
CH_4	0.0000	0.0000	0.0055	0.0000	0.0000	0.0082	0.0000	0.0000	0.0000	0.0000	0.0000	0.0000	0.0000	0.0181	0.0026
CO	0.0000	0.0000	0.1128	0.0076	0.0000	0.0006	0.0000	0.0000	0.0000	0.0000	0.0000	0.0000	0.0000	0.0023	0.0021
CO_2	0.0002	0.0000	0.3578	0.5528	0.0000	0.0502	0.0003	0.0161	0.0161	0.0000	0.0000	0.0000	0.0000	0.6082	0.9516
COS	0.0000	0.0000	0.0002	0.0000	0.0000	0.0502	0.0000	0.0000	0.0000	0.0000	0.0000	0.0000	0.0000	0.0000	0.0000
H_2	0.0002	0.0000	0.0590	0.2189	0.4956	0.4126	0.0000	0.0000	0.0000	0.0000	0.0000	0.0000	0.0000	0.0426	0.0278
H_2O	0.1187	0.0000	0.3947	0.1381	0.0001	0.1193	0.0064	0.1528	0.1528	1.0000	1.0000	1.0000	1.0000	0.3147	0.0011
H_2S	0.1238	0.0000	0.0008	0.0018	0.0000	0.0000	0.0000	0.0000	0.0000	0.0000	0.0000	0.0000	0.0000	0.0000	0.0000
N_2	0.6356	0.0000	0.0625	0.0735	0.5004	0.4041	0.7759	0.7189	0.7189	0.0000	0.0000	0.0000	0.0000	0.0052	0.0050
NH_3	0.0000	0.0000	0.0000	0.0000	0.0000	0.0000	0.0000	0.0000	0.0000	0.0000	0.0000	0.0000	0.0000	0.0000	0.0000
O_2	0.0000	0.0000	0.0000	0.0000	0.0027	0.0022	0.2081	0.1041	0.1041	0.0000	0.0000	0.0000	0.0000	0.0000	0.0000
SO_2	0.1137	0.0000	0.0004	0.0000	0.0000	0.0000	0.0000	0.0000	0.0000	0.0000	0.0000	0.0000	0.0000	0.0000	0.0000
Total	1.0	1.0	1.0	1.0	1.0	1.0	1.0	1.0	1.0	1.0	1.0	1.0	1.0	1.0	1.0
V-L Flow Rate, kgmol/hr	249	0	492	418	27823	34565	12588	128261	128261	33222	13219	13219	41292	17033	9062
V-L Flow Rate, kg/hr	7916	0	13917	12493	421613	582063	552664	3495687	3495687	598502	238139	238139	743891	568564	385930
Solids Flow Rate, kg/hr	0	1903	0	0	0	0	0	0	0	0	0	0	0	0	0
Temperature, °C	593	177	232	49	252	246	6	568	134	534	32	32	39	311	20
Pressure, MPa, abs	0.101	0.119	0.085	0.073	2.792	2.792	0.090	0.093	0.090	12.512	0.005	0.005	0.827	3.829	15.272
Enthalpy, kJ/kg*	–1443.3	–	–8550.6	–8398.3	437.8	–2529.1	–77.5	–963.7	–1468.4	–12546.4	–13631.3	–13631.3	–15815.9	–9177.9	–9065.8
Density, kg/m^3	0.4	–	0.6	0.8	9.6	10.8	1.1	0.4	0.7	36.7	0.0	0.0	992.9	27.0	598.8
V-L Molecular Weight	31.766	–	28.000	29.884	15.153	16.840	28.895	27.254	27.254	18.015	18.015	18.015	18.015	33.380	42.587
V-L Flow Rate, lbmol/hr	549	0	1084	922	61,340	76,203	222,306	282,766	282,766	73,242	29,142	29,142	91,034	37,552	19,979
V-L Flow Rate, lb/hr	17,451	0	30,682	27,543	929,498	1,283,230	6,423,439	7,706,670	7,706,670	1,319,470	525,007	525,007	1,640,000	1,253,470	850,831
Solids Flow Rate, lb/hr	0	4196	0	0	0	0	0	0	0	0	0	0	0	0	0
Temperature, °F	1100	350	450	120	485.7	475	42	1055	274	994	90	90	102	593	68
Pressure, psia	14.7	17.3	12.3	10.6	405	405	13.0	13.5	13.0	1,814.7	0.7	0.7	120.0	555.4	2215.0
Enthalpy, Btu/lb*	–620.5	–	–3676.1	–3610.6	188.2	–1087.3	–33.3	–414.3	–631.3	–5394.0	–5860.4	–5860.4	–6799.6	–3945.8	–3897.6
Density, lb/ft^3	0.028	–	0.036	0.051	0.599	0.676	0.070	0.023	0.045	2.292	0.002	0.002	61.983	1.683	37.383

* Reference conditions are 77°F and 14.696 psia.

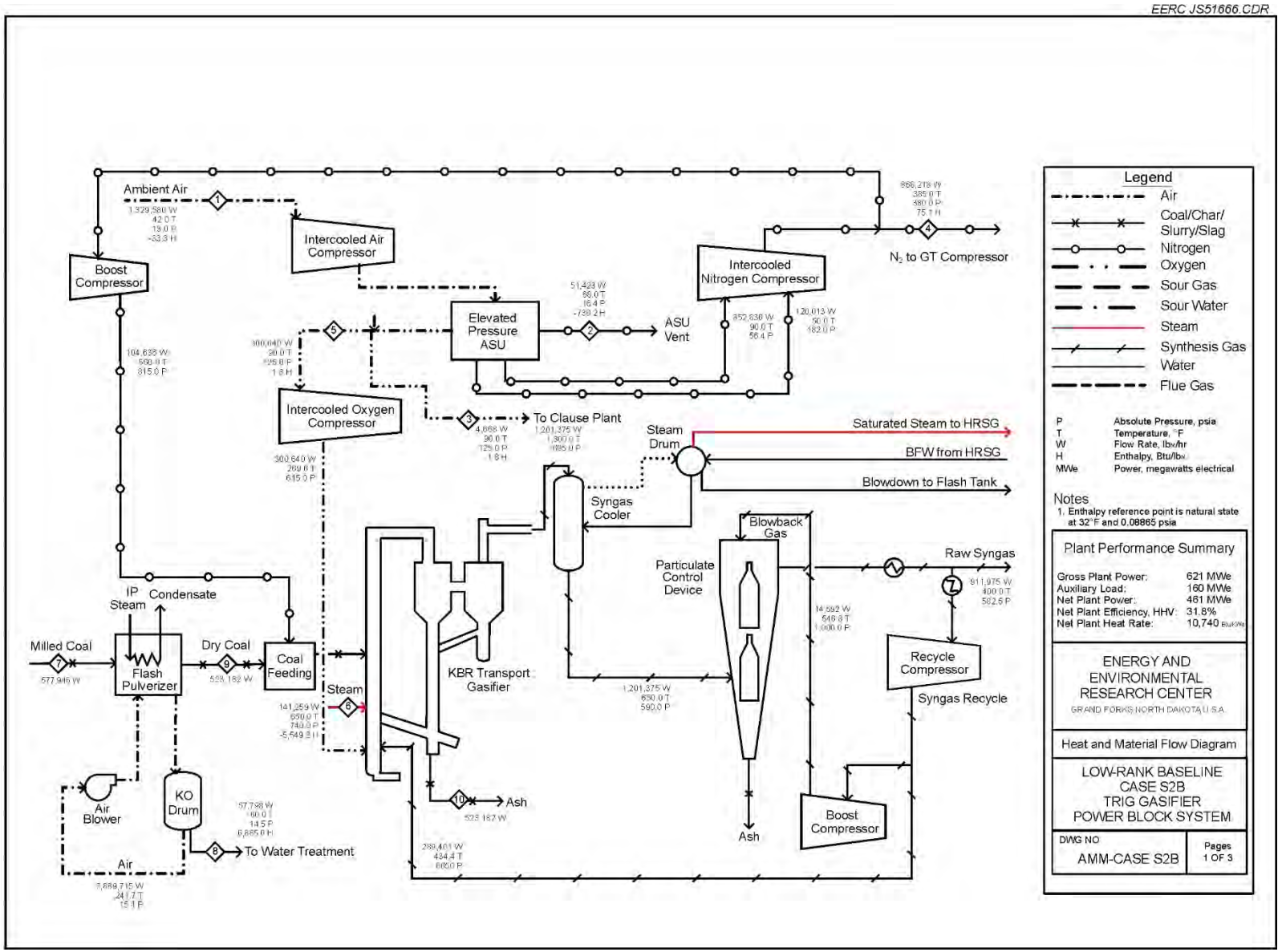

Figure 56. Mass and energy balance, ASU, and gasification.

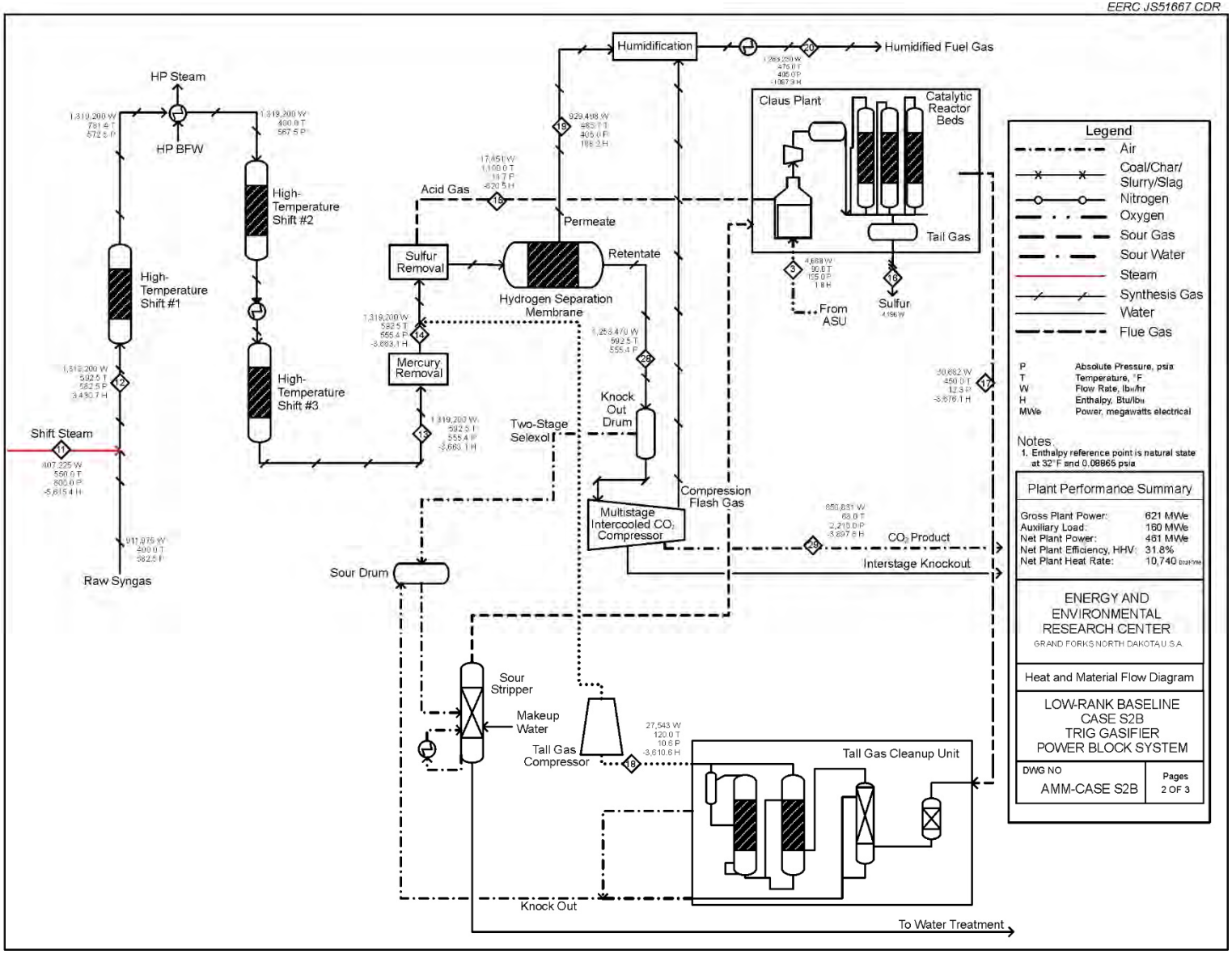

Figure 57. Mass and energy balance, gas cleanup, and membrane separation.

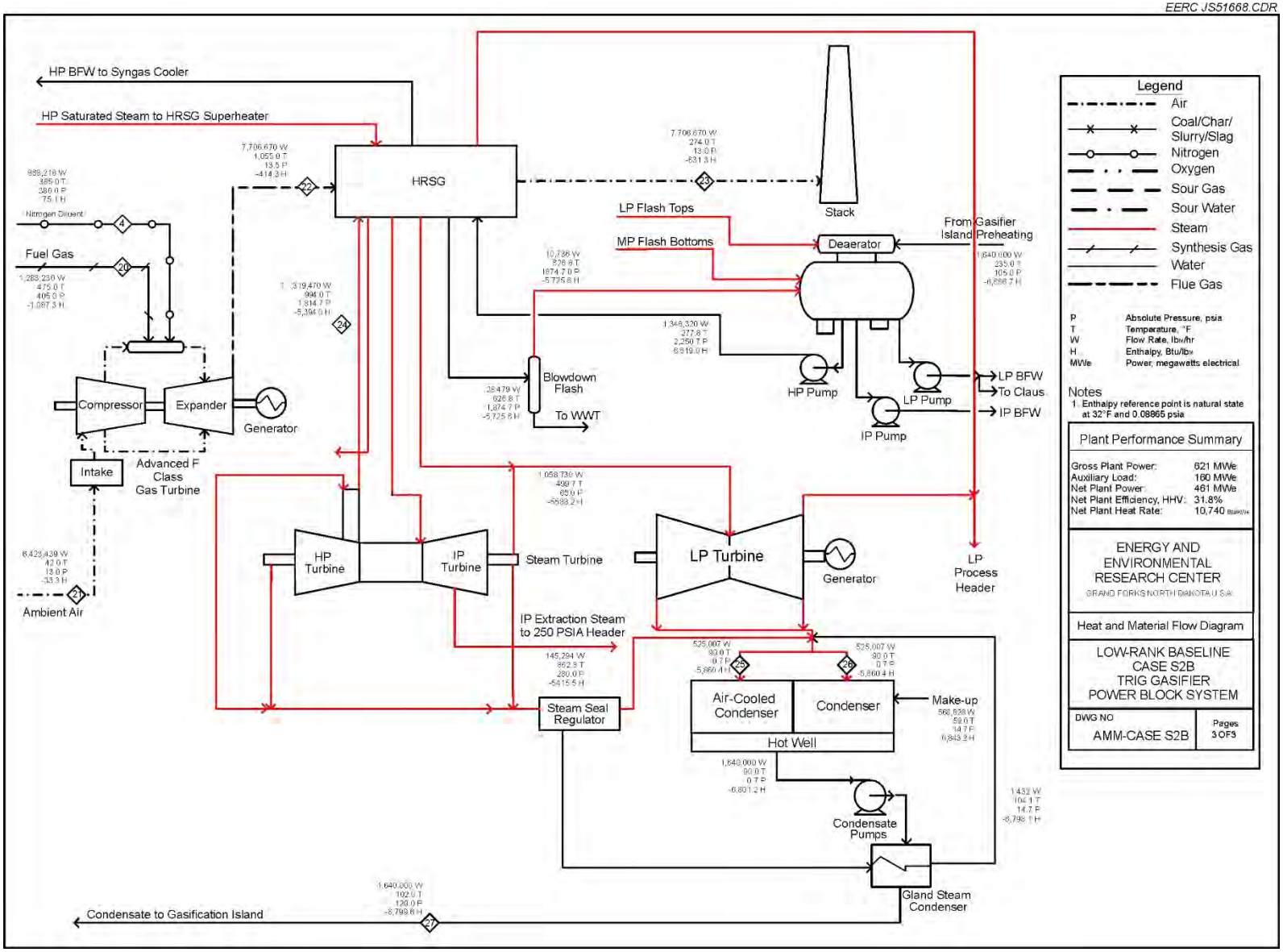

Figure 58. Mass and energy balance, power block.

Overall Plant Performance

The power plant performance summary is shown in Table 21. The table compared DOE Case S2A, S2B, and Case S2B membrane. In the noncapture case, 653 MW gross power is generated, resulting in a net power production of 545 MW. For Case S2B, the gross power is

Table 21. Power Plant Performance Summary

POWER SUMMARY, Gross Power at Generator Terminals, kWe	**Case S2A**	**Case S2B**	**Case S2B Membrane**
Gas Turbine Power	419,100	426,400	442,100
Steam Turbine Power	233,600	194,900	201,200
TOTAL POWER, kWe	**652,700**	**621,300**	**643,300**
AUXILIARY LOAD SUMMARY, kWe			
Coal Handling	500	510	510
Coal Crushing	690	730	730
Ash Handling	590	630	630
Coal Dryer Circulation Blower	2420	2560	2560
Air Separation Unit Auxiliaries	1000	1000	1000
Air Separation Unit Main Air Compressor	48,130	53,710	53,710
Oxygen Compressor	6160	6600	6600
Nitrogen Compressors	26,380	30,060	30,060
CO_2 Compressor		28,290	7720
Boiler Feedwater Pumps	3840	3960	3960
Condensate Pump	210	240	240
Syngas Recycle Compressors	1440	1550	1550
Circulating Water Pump	1920	2020	2020
Ground Water Pumps	190	280	280
Cooling Tower Fans	1250	1320	1320
Air-Cooled Condenser Fans	2730	2230	2230
Acid Gas Removal	740	16,480	740
Gas Turbine Auxiliaries	1000	1000	1000
Steam Turbine Auxiliaries	100	100	100
Claus Plant/TGTU[1] Auxiliaries	250	250	250
Claus Plant TG Recycle Compressor	2470	1600	2470
Miscellaneous Balance of Plant[2]	3000	3000	3000
Transformer Losses	2270	2330	2330
TOTAL AUXILIARIES, kWe	**107,280**	**160,450**	**125,010**
NET POWER, kWe	**545,420**	**460,850**	**518,290**
Net Plant Efficiency, % (HHV)	39.9%	31.8%	35.7%
Net Plant Heat Rate, kJ/kWh (Btu/kWh)	9032 (8560)	11,331 (10,740)	10,124 (9595)
CONDENSER COOLING DUTY GJ/hr, 10^6 Btu/hr	**1224 (1160)**	**992 (940)**	**1018 (965)**
CONSUMABLES			
As-Received Coal Feed, kg/hr (lb/hr)	247,297 (545,197)	262,150 (577,946)	262,150 (577,946)
Thermal Input, kWt	1,368,368	1,450,564	1,450,564
Raw Water Withdrawal, m^3/min (gpm)	7.7 (2045)	11.3 (2989)	11.3 (2989)
Raw Water Consumption, m^3/min (gpm)	6.0 (1598)	9.5 (2517)	9.5 (2517)

[1] Tail gas treatment unit.

[2] Includes plant control systems, lighting, HVAC, and miscellaneous low-voltage loads.

reduced because of additional process steam required for WGS and other auxiliary components. The gross power production is 621 MW, and the net power production is 461 MW. This represents a reduction of 84 MW over the noncapture case, while feeding an additional 32,750 lb/hr of coal. The overall thermal efficiency is reduced from 39.9% to 31.8% from Case S2A to Case S2B. For the membrane case, the thermal efficiency is increased to 35.7%, a significant improvement over Case S2B. The gross power generation is increased to 643MW. This comes from increased turbine power generation that results from higher-temperature gas entering the combustion section, as well as slightly increased steam power because of higher turbine exit temperatures. The auxiliary load is decreased significantly because of two main factors. The first contributor is lower compression power required because the CO_2 remains at system pressure through the membrane. The second contributor is the reduction of auxiliary load that was needed for operating the Selexol system in Case S2B. These factors combine to reduce the auxiliary load from 160 to 125 MW. Overall plant heat rate is improved over Case S2B from 10,700 to 9600 Btu/kWh.

Modeling Conclusions

Two high-level assumptions were made in the present modeling effort that will significantly impact the overall plant performance if the criteria cannot be met. The first assumption was that the TRIG can achieve 1% methane concentration at the exit from optimization of operating temperature and process conditions. The second assumption was that the membrane operation was optimized for an IGCC setting and that 95% hydrogen recovery could be achieved with a countercurrent nitrogen sweep. The necessity of the first assumption shows that the TRIG is probably not the best choice of systems for a hydrogen separation membrane. An entrained-flow gasifier does not produce significant amounts of methane and would likely be a better choice. Additionally, an entrained-flow system would likely be operated at higher pressure, providing additional performance benefits to the membrane. Overall, if these assumptions can be met, hydrogen separation membranes have the potential to significantly improve the efficiency of an IGCC system with CO_2 capture over conventional technology.

CONCLUSIONS AND RECOMMENDATIONS

Approximately 470 hours of operation was completed on the TRDU gasifier, and over 260 hours of operation was conducted on the membrane. In spite of being a newly installed system, the WGS reactor, syngas compressor, and sulfur removal beds operated relatively well during the testing. Challenges with the candle filter operation periodically interupted operation of the membrane, but ultimately, the originally proposed testing goals were met.

Coal from the Antelope Mine in Wyoming was successfully gasified for the majority of the test campaign. Hydrogen concentrations leaving the gasifier were as high as 15% and were further increased to 20% on a dry basis after the WGS reactor. It was determined that operation of the sour shift catalyst near 400°C provided the highest level of shift when a low-sulfur coal was fired, and CO was able to be reduced below 1%. Periodic additions of hydrogen were able to push the hydrogen concentration to over 25% on a wet basis for specific tests. High-sodium Freedom lignite from North Dakota was also tested on the unit, and it was found that the fuel could be fired successfully with the addition of kaolin as a sodium-gettering agent.

The regenerable RVS-1 sulfur sorbent was shown to be able to reduce sulfur concentrations from nearly 4000 to below 5 ppm in one reactor. The sorbent was regenerated with oxygen and sulfur levels returned to below 5 ppm at the reactor exit. Sulfur levels were typically below 1 ppm when the Antelope coal was fired and were in the 1–4-ppm range when the North Dakota lignite was tested.

A hot-side sygnas compressor was successfully demonstrated to raise the pressure of the syngas from 120 to over 450 psi while maintaining the temperature above 450°F. This enabled the test system to operate similarly to a commercial demonstration by maintaining the moisure, tars, ammonia, and chlorine in the syngas feed to the membrane. The membrane was exposed to a wide variety of contaminants found in syngas.

The membrane was operated on syngas over two separate test campaigns. Initial flux on the membrane was lower than expected during the first campaign, but the flux did not significantly deteriorate through the test campaign. A bottle gas test was performed at the end of the campaign to see if higher hydrogen partial pressure would improve flux, but no significant improvement was noted. The system was dissassembled after the first campaign, and the membrane tubes were changed out with backup tubes. One tube failure was noted, but it was believed to have occurred during dissassembly of the vessel, since no process data indicated there had been a failure. The tubes were sent to Praxair for further analysis.

The second set of tubes was tested during the second campaign on both Antelope PRB coal and North Dakota lignite. The testing started with a bottle gas test, but lower-than-expected flux numbers were still observed. Significant parametrics were performed during the second campaign, and correlations for flux and permeance versus temperature, pressure, and flow were reported. As expected, the membrane flux was maximized when the highest partial pressure of hydrogen was delivered to the system at high flow conditions and 425°C. Membrane performance did not appear to signficantly change with time during the second campaign.

A bottle gas test was performed at the conclusion of the campaign to determine if the flux levels would return to the levels observed at Praxair if no contaminants were included in the feed stream. A 1-hour test followed by an 8-hour hydrogen soak and an additional 1-hour test were performed. The permeance of the membrane improved slightly during the bottle gas tests, but the performance did not return to the levels that were observed at Praxair. The tubes were removed at the conclusion of the testing and sent to Praxair for analysis.

Initial designs and data have been developed for a modular membrane technology that could be easily scaled up for a demonstration test. Prior to moving on to scale-up, the root cause of the low flux numbers needs to be determined. If there is found to be sulfur on the surface of the membrane, a polishing bed could easily be installed to remove sulfur down to a few parts per billion in the gas stream, thereby alleviating any sulfur issues. Control methods are available for other syngas contaminants that could also be inhibiting flux. Ideally, warm contaminant removal technologies would need to be used in order to take advantage of the thermal efficiency benefits provided by hydrogen separation membranes.

DESCRIPTION OF BUSINESS PLAN FOR COMMERCIALIZATION

Successful demonstration of hydrogen separation membranes on coal-derived syngas at the 100-lb/day scale will result in justification for scale-up to a demonstration-scale system. The EERC is working closely with Praxair to evaluate the detailed design of a demonstration-scale system. Praxair will be working with DOE to develop the exact details of the commercialization plan, including investment opportunities, demonstration sites, and securing suppliers for the necessary materials. The expertise provided by the EERC enables successful membrane integration with a syngas stream from a commercial-scale gasifier. The testing performed in this program enables the EERC to advise the membrane providers on the syngas cleanliness required to be achieved before membrane separation. The inputs from the demonstration-scale system will be used to design a full-scale membrane system that could either replace a physical solvent in an existing unit or be constructed as part of a grassroots plant. The data gathered and lessons learned through this project, including testing with Freedom lignite, provides key information that could be used to develop a highly efficient power system or polygeneration plant in North Dakota. Additional testing with Australian brown coals would be required in order to gather the necessary data to site a plant in that region.

REFERENCES

1. Kluiters, S.C.A. *Status Review on Membrane Systems for Hydrogen Separation*; Dec 2004.

2. U.S. Department of Energy. *Effects of a Transition to a Hydrogen Economy on Employment in the United States, Report to Congress;* July 2008.

3. Ellis, S. Honda Fuel Cell Vehicle Progress. Presented at the Advancing the Hydrogen Economy Action Summit II; Grand Forks, ND; Sept 4, 2008.

4. Holmes, M. Coal-to-Hydrogen. Presented at the Advancing the Hydrogen Economy Action Summit II; Grand Forks, ND; Sept 4, 2008.

5. National Energy Technology Laboratory. *Cost and Performance Baseline for Fossil Energy Plants, Volume 1: Bituminous Coal and Natural Gas to Electricity; Revision 2*; DOE/NETL-2010/1397; 2010.

6. Gerdes, K. *Current and Future Technologies for Gasification Based Power Generation, Volume 2: Carbon Capture, Revision 1*; DOE/NETL-2009/1389; 2010.

7. Klara, J.M. IGCC: Coals Pathway to the Future. Presented at the Gasification Technologies Conference; Oct 4, 2006.

8. Sondreal, E.; Swanson, M.; Benson, S.; Holmes, M.; Jensen, M. *A Review of Gasification Technology for Coproduction of Power, Synfuels, and Hydrogen from Low-Rank Coals*. In Proceedings of the 20th Symposium on Western Fuels; Marriott Denver Tech Center, Denver, CO; Oct 24–26, 2006.

9. Gerdes, K. The Potential of Advanced Gasification Pathways to Reduce CO_2 Capture Costs. Presented at the Gasification Technologies Conference, Colorado Springs, CO; Oct 2009.

10. Hoffman, J. Cost and Performance for Low-Rank Coal Power Plants. Presented at the Gasification Technologies Conference, Colorado Springs CO, Oct 2009.

11. Plunkett, J. Performance & Cost Comparisons of Alternate IGCC Based Carbon Capture Technologies. Presented at the Gasification Technologies Conference, Colorado Springs, CO, Oct 2009.

12. Stanislowski, J.; Laumb, J. Gasification of Lignites to Produce Liquid Fuels, Hydrogen, and Power. Presented at the Pittsburgh Coal Conference, Sept 2009.

13. Stocker, J.; Whysall, M.; Miller, G. *30 years of PSA Technology for Hydrogen Purification*; UOP LLC; 1998.

14. Adhikari, S.; Fernando, S. Hydrogen Membrane Separation Techniques. *Industrial & Engineering Chemistry Research* ***2006***.

15. DOE Hydrogen Program. *FY2008 Annual Progress Report*; www.hydrogen. energy.gov/ index.html; Dec 2008.

16. Ockwig, N.; Nenoff, T. Membranes for Hydrogen Separation. *Chemical Review* ***2007***.

17. Rothenberger, K.; Howard, B.; Killmeyer, R.; Ciocco, M.; Morreale, B.; Enick, R. Palladium-Copper Alloy Membrane Performance under Continuous H_2S Exposure. Presented at the National Hydrogen Association, Washington, DC, March 2005.

18. Morreale, B.; Ciocco, M.; Howard, B.; Killmeyer, R.; Cugini, A.; Enick, R. Effect of Hydrogen-Sulfide on the Hydrogen Permanence of Palladium-Copper Alloys at Elevated Temperatures. *Journal of Membrane Science* ***2004****, 241*, 219–224.

19. Subramanian, P.; Laughlin, D. Binary Alloy Phase Diagrams, 2nd, ed.; Massalski, T., ed.; ASM International; 1990; pp 1454–1456.

20. Volkov, A.; Kazantsev, V.; Kourov, N.; Kruglikov, N. Formation of the Structure and Properties of Cu-Pd Alloys During the A1-B2 Phase Transitions. *The Physics of Metals and Metallography* ***2008***.

21. Kamakoti, P.; Sholl, D. Ab Initio Lattice-Gas Modeling of Interstitial Hydrogen Diffusion in CuPd Alloys. *Physical Review B* ***2005****, 71*, 014301.

22. Sholl, D. Using Density Functional Theory to Study Hydrogen Diffusion in Metals: A Brief Overview. *Journal of Alloys and Compounds* ***2007***, 446–447, 462–468.

23. Kamakoti, P.; Sholl, D. A Comparison of Hydrogen Diffusivities in Pd and CuPd Alloys Using Density Functional Theory. *Journal of Membrane Science* ***2003****, 225*, 145–154.

24. Kamakoti, P.; Sholl, D. Towards First Principles-Based Identification of Ternary Alloys for Hydrogen Purification Membranes. *Journal of Membrane Science* ***2006****, 279*, 94–99.

25. Hao, S.; Sholl, D. Selection of Dopants to Enhance Hydrogen Diffusion Rates in MgH2 and $NaMgH_3$. *Applied Physics Letters* ***2009****, 94*, 171909.

26. Hao, S.; Sholl, D. Comparison of First Principles Calculations and Experiments for Hydrogen Permeation through Amorphous ZrNi and ZrNiNb Films. *Journal of Membrane Science* ***2010****, 350*, 402.

27. Hao, S.; Sholl, D. The Role of Interstitial H2 in Hydrogen Diffusion in Light Metal Borohydrides. *Phys. Chem. Chem. Phys.* ***2009****, 11*, 11106.

28. O'Brien, C. Sulfur Poisoning of Pd and PdCu Alloy Hydrogen Separation Membranes; Doctoral Thesis; Carnegie Mellon University; 2011.

29. Gabitto, J.; Tsouris, C. Sulfur Poisoning of Metal Membranes for Hydrogen Separation. *International Review of Chemical Engineering* **2009**, *1*(5), 394–411.

30. Ma, Y.; Pomerantz, N.; Chen, C. *Sulfur-Tolerant Pd/Cu and Pd/Au Alloy Membranes for Hydrogen Separation with High Pressure CO_2 Sequestration*; Periodic Progress Report, 2007.

31. Yang, J.; Nishimura, C.; Komaki, M. Hydrogen Permeation of Pd60Cu40 Alloy Covered V-15Ni Composite Membrane in Mixed Gases Containing H_2S. *Journal of Membrane Science* ***2008****, 309*, 246–250.

32. National Energy Technology Laboratory. *Cost and Performance Baseline for Fossil Energy Plants, Volume 3a: Low Rank Coal to Electricity: IGCC Cases*; DOE/NETL-2010/1399; May 2011.

33. Gupta, R.; Turk, B.; Lesemann, M.; Schlather, J.; Denton, D. Status of RTI/Eastman Warm Gas Clean-Up Technology and Commercialization Plans. Presented at the Gasification Technologies Conference, Washington, DC, Oct 8, 2008.